Relaxation Dispersion NMR spectroscopy

Andrea C. Sauerwein and D. Flemming Hansen*

Institute of Structural and Molecular Biology, Division of Biosciences, University College London, Gower Street, London, WC1E 6BT, United Kingdom.

Keywords: NMR, Protein dynamics, Relaxation dispersion, low-populated states.

1 Introduction

Relaxation dispersion nuclear magnetic resonance (NMR) spectroscopy has been developed since the 1950s and has now evolved into a very sensitive and versatile tool to study chemical and conformational exchange processes on the micro- to milliseconds (μs-ms) time scale. While relaxation dispersion NMR was originally designed with small molecules in mind it has become a very attractive tool also to study the dynamics of biological macromolecules, after major advances had been made in hardware, experimental design, and isotope labelling.

Many functional aspects of proteins can be derived from their time-averaged three-dimensional structure. However, in order to fully understand the inherently flexible protein molecules it is imperative to quantify their dynamics, since such dynamics reflect on functional mechanisms that often cannot be understood solely from time-averaged structures (Boehr, Dyson, & Wright, 2006; Henzler-Wildman & Kern, 2007). The three-dimensional structures of macromolecules, such as proteins, fluctuate in a time-dependent manner and populate several microstates that differ in their structure and free energy. Often there is one major populated structure, *the ground state*, in addition to one or more transiently and low populated structures that, despite their low population and short lifetime, often play crucial roles in protein folding (Korzhnev, Salvatella, et al., 2004; Sugase, Dyson, & Wright, 2007), ligand binding (Sugase et al., 2007), ligand recognition (Boehr, McElheny, Dyson, & Wright, 2006), allostery, and enzyme catalysis (Eisenmesser et al., 2005; Eisenmesser, Bosco, Akke, & Kern, 2002; Henzler-Wildman et al., 2007; Wolf-Watz et al., 2004). Currently, relaxation dispersion NMR is the foremost technique used to gain versatile information on these low populated structures, even when they cannot be characterised and detected by traditional structural and biophysical methods.

The general principle of obtaining information about the low populated states, their life-times and their populations, is to quantify the change in chemical shifts and line broadenings of NMR signals due to exchange events between the ground state and the low populated state(s). For this purpose two classes of NMR experiments have emerged, that is, the Carr-Purcell-Meiboom-Gill (CPMG) type experiments, which allow a quantification of the apparent transverse relaxation rates, $R_{2,\mathrm{eff}}$, as a function of the delay between successive refocusing pulses, and rotating frame relaxation rate measurements, $R_{1\rho}$, in which the relaxation is observed in the rotating frame and as a function of strength and/or offset of an applied radio frequency field.

A historical perspective that highlights the milestones in the development of relaxation dispersion spectroscopy will first be given, followed by an introduction to chemical exchange including an introduction to the two major classes of relaxation dispersion measurements. Subsequently, relaxation dispersion pulse schemes are discussed putting an emphasis on a qualitative explanation and a

description of when to use what specific experimental setup. This section also discusses appropriate isotope labelling schemes and the reader is advised to take them into account, as correct isotope labelling is critical to the success of the relaxation dispersion experiments. Finally, various recent applications of relaxation dispersion NMR will be discussed to illustrate the wealth and breath of information relaxation dispersion NMR can provide on biological systems.

1.1 History — Development of relaxation dispersion NMR

The Hahn echo: Basic principles of relaxation dispersion NMR were established in the early years of NMR spectroscopy. Erwin Hahn (Hahn, 1950) discovered the spin-echo experiment, which turned out to be one of the most versatile tools in NMR spectroscopy, already soon after the first successful NMR experiments had been carried out independently by Purcell, Torrey and Pound (Purcell, Torrey, & Pound, 1946) and Bloch, Hansen and Packard (Bloch, Hansen, & Packard, 1946). Hahn designed his experiment to allow for a determination of the transverse relaxation time, T_2, without the interference from an inhomogeneous external magnetic field, B_0. Hahn's spin-echo sequence can be written as

$$90^{\circ}_{x} - \tau - 90^{\circ}_{x} - \tau - echo \tag{1}$$

and assumes that the evolution time, τ, is sufficiently large for the transverse magnetisation to dephase completely before the refocusing 90°_{x} pulse is applied. To determine T_2 the Hahn echo sequence is repeated several times with varying evolution times, τ, and T_2 is derived from the exponential decay of the echo amplitudes, $A(\tau) = A(0)\exp(-\tau/T_2)$. However, Hahn noticed that the experiment is sensitive to molecular diffusion, which is explained by one of the fundamental assumptions of all spin-echo experiments: "The single magnetic moments, which make up the macroscopic magnetisation move in the same sense and at exactly the same rate before and after the refocusing pulse." In the case of macroscopic motion, here diffusion, this timekeeping is disturbed and individual magnetic moments lose their identity, thus blurring the refocusing.

Carr and Purcell echo: In the Hahn echo, only 50% of the initial magnetisation is observed — the rest is displaced during the pulse sequence. In 1954 Carr and Purcell (Carr & Purcell, 1954) suggested a modification to Hahn's spin-echo sequence in order to refocus all available magnetisation and to eliminate the effect of molecular diffusion on measurements of the transverse relaxation time T_2. To refocus the entire magnetisation the second 90° pulse of the Hahn spin-echo was replaced by a 180° pulse leading to:

$$90^{\circ}_{x} - \left\{\tau - 180^{\circ}_{x} - \tau\right\}_{N} - echo \tag{2}$$

with $N = 1,2,3, \ldots$. At first, equilibrium magnetisation along the +*z*-axis (Figure 1a) is rotated around the *x*-axis onto the –*y*-axis (Figure 1b), followed by an evolution period τ during which magnetisation dephases in the transverse plane (Figure 1c). At the end of this first evolution period the transverse magnetisation is again rotated around the *x*-axis (Figure 1d) and left to evolve for a second duration τ before it refocuses along the *y*-axis (Figure 1e). If $N = 2$ the refocused magnetisation is left to evolve in the transverse plane for another evolution time τ (Figure 1f) after which it is rotated by 180° around the *x*-axis (Figure 1g). During the subsequent evolution τ the magnetisation refocuses at the –*y*-axis (Figure 1h). It is noted that the sign of the observed magnetisation changes between +*y* and –*y* depending on whether *N* is odd or even. The absolute amplitude of successive echoes decreases exponentially with T_2.

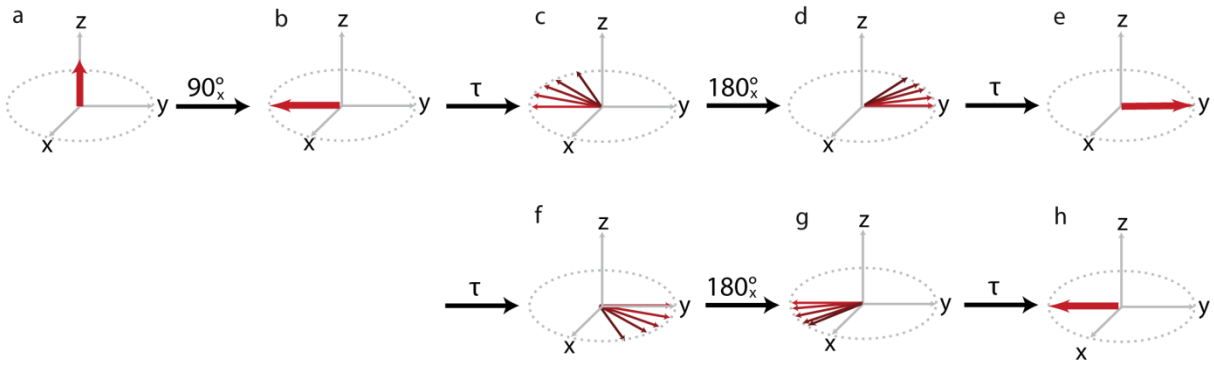

Figure 1: Schematic illustration of the Carr-Purcell spin-echo, assuming that the gyromagnetic ratio $\gamma > 0$. Details of the evolution of the magnetisation and the associated pulse sequence are described in the text.

To overcome diffusion effects on T_2 measurements Carr and Purcell (Carr & Purcell, 1954) suggested to apply a train of spin-echoes, $\{\tau - 180_x - \tau\}_N$, rather than increasing the length of τ. The cornerstone of their suggested pulse sequence is that if the repetition rate of the spin-echo train is sufficiently high, and thus τ is sufficiently short, then refocusing occurs before diffusion can cause a significant shift in the precession frequency of an individual magnetic moment.

The Carr-Purcell-Meiboom-Gill spin-echo: The major shortcoming of the Carr-Purcell spin-echo lies in the necessity for a very accurate calibration of the applied 180° pulses since a small error in the flip-angle adds up and becomes significant when a large number of pulses are applied — as needed to eliminate the effect of diffusion. This shortcoming, which result in a low reproducibility of the obtained transverse relation times, was addressed by Meiboom and Gill (Meiboom & Gill, 1958). Meiboom and Gill adapted the Carr-Purcell spin-echo (Carr & Purcell, 1954) to the measurement of long transverse relaxation times in liquids by introducing a 90° phase shift between the first and second pulse of their spin-echo sequence:

$$90^{\circ}_{x} - \left\{ \tau_{\mathrm{CPMG}} - 180^{\circ}_{y} - \tau_{\mathrm{CPMG}} \right\}_{N} - echo \tag{3}$$

with $N = 1,2,3, \ldots$. This spin-echo, which comprises the modifications suggested by Carr and Purcell (Carr & Purcell, 1954) and those suggested by Meiboom and Gill (Meiboom & Gill, 1958), is now known as the *Carr-Purcell-Meiboom-Gill spin-echo* and commonly referred to as *CPMG*. As illustrated in Figure 2 the CPMG experiment starts by applying a 90°_{x} pulse to rotate longitudinal magnetisation (Figure 2a) into the transverse plane and along the –*y*-axis (Figure 2b). During the subsequent evolution time, τ_{CPMG}, the transverse magnetisation de-phases (Figure 2c) and is subsequently rotated around the *y*-axis by a 180°_{y} refocusing pulse (Figure 2d), which allows transverse magnetisation to refocus along the –*y*-axis (Figure 2e) during the second evolution time, τ_{CPMG}. If a second echo train is applied (Figure 2f-g) magnetisation de-phases again and is rotated about the *y*-axis by a 180°_{y} pulse which is followed by another τ_{CPMG} during which magnetisation refocuses again along the –*y*-axis. This behaviour is identical to the one describe for the first echo train (Figure 2c-e).

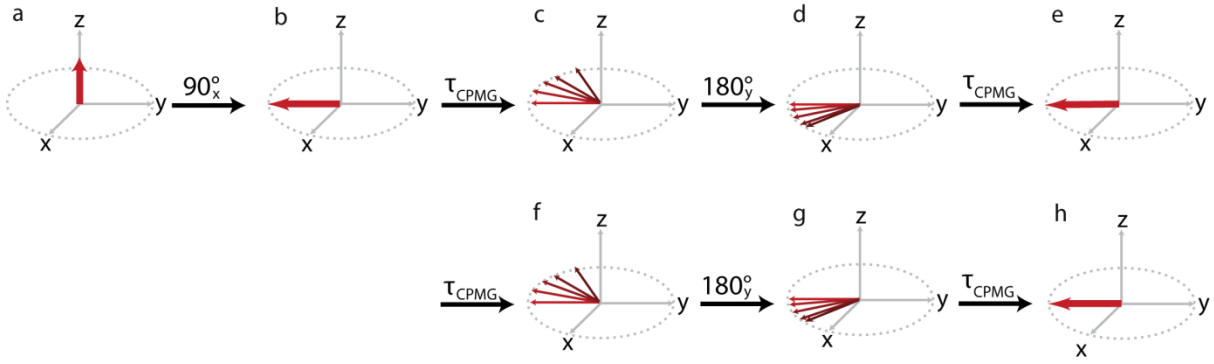

Figure 2: Illustration of the formation of the Carr-Purcell-Meiboom-Gill spin-echo assuming $\gamma > 0$. Details of the magnetisation evolution and the associated pulse sequence are described in the text.

It should be noted that, in contrast to the Carr-Purcell spin-echo, all echoes in the CPMG experiment have the same phase. Due to the shift in phase between the excitation pulse and the refocusing pulses any mis-calibrations of the latter will be compensated for, to a first order of approximation, for even numbers of N. This is illustrated and compared to a Carr-Purcell spin-echo in Figure 3.

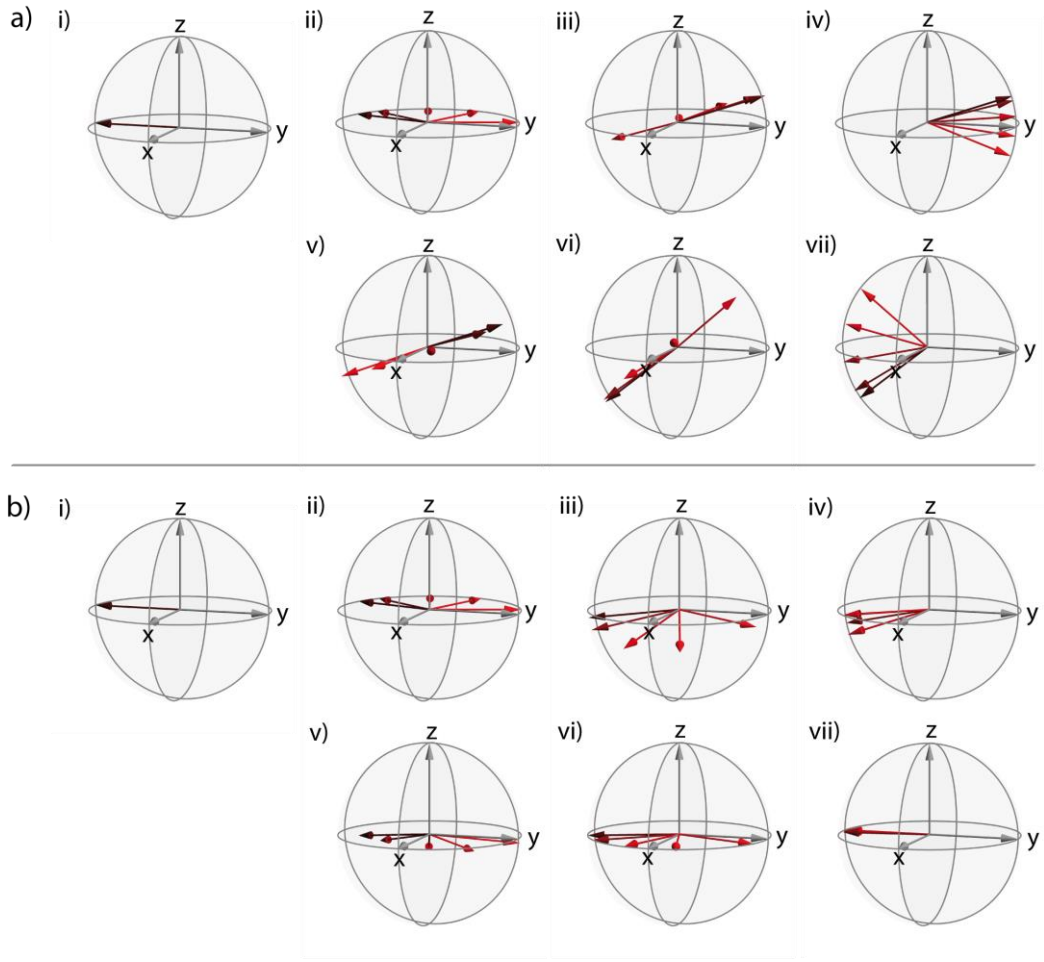

Figure 3: Visualisation of the impact of inaccurate 180° pulse calibrations and off-resonance effects on (a) a Carr-Purcell spin-echo and (b) on a CPMG experiment. As previously, the illustration assumes positive γ. The refocusing pulse used here has been mis-calibrated such that it causes a rotation of 200° rather than the desired 180°. The spins depicted have off-resonance frequencies of 500 Hz, 1500 Hz, 2500 Hz, 3500 Hz and 4500 Hz which corresponds to offsets between 0.6 and 5.5 ppm assuming a proton frequency of 800 MHz. Calculations and design of this graphic were done in Mathematica 9.0 employing the SpinDynamica code for Mathematica, programmed by Malcolm H. Levitt, Jyrki Rantaharju and Andreas Brinkmann, available at *www.SpinDynamica.soton.ac.uk*.

Dependence of relaxation dispersion on chemical exchange: Soon after the CPMG experiment was established it was applied to the study of chemical exchange and the theoretical framework for the CPMG experiment in the context of chemical exchange was expanded. An important contribution was made in 1963 where Luz and Meiboom (Luz & Meiboom, 1963) used the CPMG experiment to determine the number of water molecules involved in the proton transfer reaction between a trimethylammonium ion and trimethylamine in aqueous solution:

$$(CH_3)_3NH^+ + \begin{matrix} H \\ O\,H \end{matrix} + N(CH_3)_3 \overset{k}{\Rightarrow} (CH_3)_3N + \begin{matrix} H \\ H\,O \end{matrix} + H^+N(CH_3)_3 \quad (4)$$

To identify the number of protons involved in the reaction Luz and Meiboom measured proton exchange rates using CPMG frequencies, $\nu_{\mathrm{CPMG}} = 1/(4\tau_{\mathrm{CPMG}})$, between 1-300 Hz. Additionally, they derived a theoretical framework assuming fast exchange (McConnell, 1958; see below), which shows the dependence of the observed spin-echo decay on the repetition rate ν_{CPMG} of the $180°$ pulse. The result of Luz and Meiboom's theoretical work is essentially the expression given below in Eq. (15), which is still often used to explain CPMG relaxation dispersion curves near the fast-exchange regime. A very important remark made by Luz and Meiboom is that in order to probe the chemical exchange event with the CPMG relaxation dispersion experiment the CPMG pulsing rates used need to be comparable with the chemical exchange rate. In favourable cases and when the chemical exchange rate is related to a second-order rate constant, as in the study by Luz and Meiboom, the effective pseudo first-order rate constant can be altered by varying the concentration of the reacting species and brought into the window that is accessible by the CPMG experiments. Luz and Meiboom concluded from their CPMG relaxation dispersion experiments that only one water molecule is involved in the reaction, Eq. (4), and thus there is no evidence for proton transfer through a network of hydrogen-bonded water molecules.

It was then just a few years after Luz and Meiboom's first application of the CPMG experiment to study chemical exchange that Allerhand, Chen, Gutowsky and Wells (Allerhand, Chen, & Gutowsky, 1965; Allerhand & Gutowsky, 1964, 1965; Wells & Gutowsky, 1965) conducted several spin-echo studies of chemical exchange and derived methods for calculating the exchange rate from the observed dependence of the apparent transverse relaxation $R_{2,\mathrm{eff}}$ on the delay τ_{CPMG}. Their research started with the study of two chemically exchanging sites, A and B, which are associated with the respective populations p_{A} and p_{B}. Both sites were assumed to have equivalent intrinsic transverse relaxation rates $R_2 = 1/T_2$ in the absence of exchange and calculations indicated that the decay of the echo amplitudes is exponential or nearly exponential in all cases (Allerhand & Gutowsky, 1964), thus allowing for an interpretation of the chemical exchange via the apparent first-order transverse relaxation rate $R_{2,\mathrm{eff}}$. It turned out that the observed effective relaxation rate, $R_{2,\mathrm{eff}} = R_2 + R_{\mathrm{ex}}$, depends on the intrinsic transverse relaxation rate, the population of sites A and B, the chemical shift difference, $\Delta\omega = \omega_{\mathrm{B}} - \omega_{\mathrm{A}}$, between the two sites, the lifetime of the two states, and on the separation between two successive refocusing pulses $2\tau_{\mathrm{CPMG}}$. It was also shown that in the absence of chemical exchange the effective relaxation rate, $R_{2,\mathrm{eff}}$, is independent of the spacing between the refocusing pulses. Based on those results Allerhand and Gutowsky derived closed analytical expressions for the

previously observed cases (Allerhand & Gutowsky, 1965). The applicability of the closed expressions and the suitability of the spin-echo experiment to quantify chemical exchange were tested and exchange parameters were obtained for the chair-chair isomerisation of cyclohexane and d_{11}-cyclohexane (Allerhand et al., 1965). In particular, it was demonstrated that the spin-echo method could be used to measure exchange rates over five orders of magnitude and rates between 0.5 s^{-1} and $4 \cdot 10^4$ s^{-1} were observed over a large temperature range for d_{11}-cyclohexane. The homonuclear J_{HH} scalar couplings did influence and modulate the spin-echo decays, while no effect on the spin-echo decays was observed for the heteronuclear J_{HD} scalar coupling in d_{11}-cyclohexane. However, for the homonuclear case only those decays were analysed that allowed the scalar coupling to be ignored during analysis. So far the spin-systems considered, when analysing spin-echo decays, assumed no coupling and therefore a separate study was conducted on the dependence of the refocusing pulse separation for a coupled pair of spin ½ nuclei in a liquid assuming both weak and strong coupling (Wells & Gutowsky, 1965). It was shown that the scalar coupling modulates the observed intensities in both cases and that this modulation does change only in degree, but not in kind. The modulation of the intensities during the spin-echo train depends on the coupling constant between the involved spins and their chemical shift separation $\Delta\omega$ and varies with the pulse separation 2τ (see below).

Spin-lock relaxation dispersion: Another relaxation dispersion technique to determine exchange rate constants was introduced in 1970 by Deverell et al. (Deverell, Morgan, & Strange, 1970) and is based on the observation of the longitudinal relaxation time, $T_{1\rho}$, in the rotating frame. To obtain exchange parameters, rotating frame relaxation rates, $R_{1\rho} = 1/T_{1\rho}$, are measured as a function of the amplitude of the applied spin-lock field and when chemical exchange is present, the rotating frame relaxation times depend on this amplitude allowing a quantification of the underlying exchange parameters. Compared to CPMG experiments rotating frame relaxation measurements enable the measurement of faster exchange rates, since larger effective fields can be applied (Deverell et al., 1970).

Early applications to biological systems: It took more than two decades before the early developments of CPMG relaxation dispersion spectroscopy were applied to biological systems. During those years major advances were made in the field of NMR spectroscopy, such as the introduction of pulsed NMR and digital fast Fourier transform. NMR methods were developed to study proteins and the introduction of isotope labelling of proteins, and subsequently heteronuclear 2D correlation spectra, allowed a rapid expansion of the field. Specifically, in the early 1990s several studies of NMR relaxation were carried out on uniformly ^{15}N labelled proteins (Clore, Driscoll, Wingfield, & Gronenborn, 1990; Kay, Torchia, & Bax, 1989; Koerdel, Skelton, Akke, Palmer III, & Chazin, 1992; Stone, Chandrasekhar, Holmgren, Wright, & Dyson, 1993; Szyperski, Luginbühl, Otting, Güntert, & Wüthrich, 1993). These studies were motivated by work of Kay et al. who introduced 2D-heteronuclear sequences for the measurement of the heteronuclear nuclear Overhauser

effect (NOE), longitudinal, T_1, and transverse, T_2, relaxation times of individual nuclei in uniformly ^{15}N labelled proteins (Kay et al., 1989). Although all of the above studies realised the increase of transverse relaxation rates in the presence of chemical exchange Orekhov et al. demonstrated in 1994 how this enhancement of transverse relaxation can be used to derive chemical or conformational exchange parameters (Orekhov, Pervushin, & Arseniev, 1994).

Orekov et al. studied the backbone dynamics of a U-^{15}N-(1-71) fragment of bacteriorhodopsin using 2D ^{1}H-^{15}N NMR spectroscopy (Orekhov et al., 1994). The measured relaxation rates, $R_{2,\mathrm{eff}} = R_2 + R_{\mathrm{ex}}$, consist of two contributions: R_2, the intrinsic transverse relaxation rate that contains contributions from dipole-dipole and CSA relaxation mechanisms and depends on the pico- to nanosecond time scales, and R_{ex} which contains information about the chemical or conformational exchange on the millisecond time scale. Using a set of CPMG experiments $R_{2,\mathrm{eff}}$ was measured for different inter-pulse delays in the CPMG evolution period τ_{CPMG} — it then became possible to extract both R_2 and the R_{ex} parameter that depends on k_{ex} and $\Delta\omega$. Here k_{ex} is the exchange rate constant between the two exchanging states and $\Delta\omega$ is the chemical shift difference between those states. It was shown that cooperative motions on the millisecond timescale are present in the (1-71) fragment of bacteriorhodopsin and that they are characterised by a ^{15}N chemical shift dispersion of approximately 1 ppm (Orekhov et al., 1994). However, Orekhov at al. (Orekhov et al., 1994) based their analysis on the assumption that only R_{ex} depends on the CPMG pulse rate, which is true under their experimental conditions, but it in general requires that $\tau_{\mathrm{CPMG}} \ll \frac{1}{(4J_{\mathrm{NH}})}$, where J_{NH} is the scalar coupling constant between ^{1}H and ^{15}N.

Relaxation compensated CPMG: It was not until Loria et al. (Loria, Rance, & Palmer III, 1999a) introduced their innovative relaxation compensated CMPG experiment in 1999 that problems associated with pulsing rates comparable to the one-bond J_{NH} scalar coupling were overcome and measurements of accurate chemical and conformational exchange rates between 100 s^{-1} and 2000 s^{-1} became possible. In the same year Loria et al. (Loria, Rance, & Palmer III, 1999b) implemented TROSY (Transverse Relaxation Optimized Spectroscopy) selection (Pervushin, Riek, Wider, & Wüthrich, 1997) into their relaxation compensated CPMG pulse sequence (Loria et al., 1999a) to allow for measurement of exchange line broadenings to the narrower component of the ^{1}H-^{15}N scalar coupled doublet. This modification allows relaxation measurement of larger macromolecules, which were previously not amenable to chemical exchange measurements due to the fast decay of their transverse relaxation. The TROSY-based CPMG pulse sequence was demonstrated on a sample of U-98%-^{15}N labelled basic pancreatic inhibitor and a 54 kDa homodimer of triosephosphate isomerase, 83% deuterated and 98% ^{15}N labelled (Loria et al., 1999b). Both sequences are pioneering for modern relaxation dispersion NMR and they are discussed in detail in section 2.

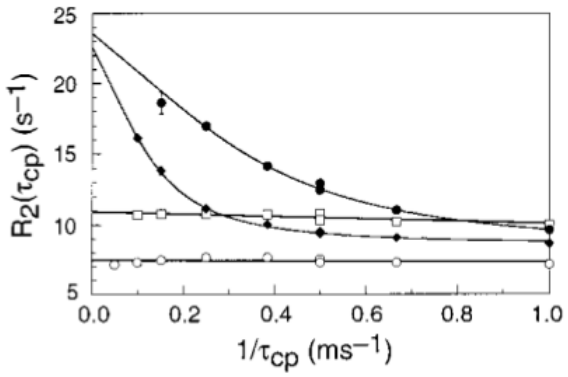

Figure 4: First relaxation compensated relaxation dispersion curve by Loria et al. (Loria et al., 1999a). The ^{15}N relaxation dispersions curves of four residues of BPTI is shown; C14 (□), Q31 (O), C38 (◆), and R39 (•). Solid lines for C38 and R39 are the best fits to Eq. 15. The relaxation dispersions for residues C38 and R39 show a clear dependence of the transverse relaxation rate R_2 on the delay τ_{CPMG}, thus revealing that these residues are involved in a chemical exchange. Reproduced from (Loria et al., 1999a) with permission from …

Subsequent developments of biological relaxation dispersion experiments included the extension of methods suitable for ^{15}N labelled proteins to ^{13}C CPMG relaxation dispersion experiments suitable for observing chemical exchange in nucleic acids (Boisbouvier, Brutscher, Simorre, & Marion, 1999). Furthermore, the relaxation compensated CPMG experiment (Loria et al., 1999a) was modified for measurements of $^{13}C_\alpha$ relaxation dispersion and applications were demonstrated (Hill, Bracken, DeGrado, & Palmer III, 2000). However, to avoid interference from the homonuclear J_{CC} scalar couplings — as present in uniformly ^{13}C labelled samples — this study was conducted on a 4.5 kDa synthetic peptide in which four leucines were selectively labelled in the C_α position. This synthetic peptide, α2D, is a de novo designed dimeric four-helix bundle with a native-like three-dimensional structure. Chemical exchange line broadening was observed for all labelled leucine residues and was subsequently used to describe protein folding based on the extracted folding and unfolding rate constants.

The constant-time relaxation dispersion experiment: So far relaxation dispersion spectroscopy of proteins had focussed on their backbone dynamics. However, backbone dynamics can be different from the protein side-chain dynamics, which often probe the hydrophobic core and can give insight into molecular recognition and protein stability. This inspired the development of relaxation dispersion experiments to measure the micro- to millisecond protein side-chain dynamics of $^{15}NH_2$ groups in asparagine and glutamine (Mulder, Skrynnikov, Hon, Dahlquist, & Kay, 2001) and those of $^{13}CH_3$ groups in methionine (Skrynnikov, Mulder, Hon, Dahlquist, & Kay, 2001). Both side-chain probes deviate from the classical AX spin system employed for backbone relaxation dispersion measurements, and it therefore became necessary to adapt the pulse sequences for AX_2 and AX_3 spin-systems. Multiple spin systems had been previously shown to suffer from contributions from scalar

couplings and dipole-dipole cross correlated spin relaxation (Kay et al., 1992) making the extraction of accurate exchange parameters difficult. These difficulties were overcome by introducing a *constant-time CPMG* interval, which renders the contributions from effects not related to chemical exchange insignificant, as long as they are independent of ν_{CPMG}. Both methods were demonstrated on a L99A mutant of T4 lysozyme and exchange parameters were obtained for the side-chain amide groups of asparagines and glutamines and the methyl groups of methionine. Although Kay and co-workers (Mulder, Skrynnikov, et al., 2001; Skrynnikov et al., 2001) originally introduced the constant-time relaxation dispersion experiment to enable the determination of exchange parameters in AX_2 and AX_3 spin-systems it is now routinely used for AX spin-systems, since it dramatically reduces the time required to obtain a full set of high-resolution relaxation dispersion data.

Henceforth, relaxation compensated constant time CPMG became a standard method and was subsequently extended for the determination of chemical exchange on other than the established sites/groups. Among the new sites considered were amide protons in the protein backbone (Ishima & Torchia, 2003). The relaxation dispersion profiles of amide protons suffer from contributions from homonuclear $^3J_{\mathrm{NH\text{-}H\alpha}}$ scalar couplings, which can be overcome by substituting the 180° pulse used for relaxation compensation with a selective pulse (e.g. a REBURP) or by perdeuteration of none-exchanging protons. Both approaches and their feasibility for the extraction of exchange parameters were demonstrated by applications to ^{1}H-^{15}N-ubiquitin or ^{1}H-^{15}N-perdeuterated HIV-1 protease. In the case of the HIV-1 protease it was shown that the combination of proton and nitrogen backbone dynamics would yield a more comprehensive picture of the slow backbone dynamics than either of them on their own (Ishima & Torchia, 2003).

Having introduced relaxation dispersion measurements on the amide group (^{1}H and ^{15}N) and on the C_α of the protein backbone there is only one protein backbone site that has not been considered — the carbonyl site. The main obstacle for obtaining carbonyl dispersion profiles is their modulation by the large $J_{\mathrm{C_\alpha C'}}$ scalar coupling (~55 Hz) which makes extraction of reliable exchange parameters more difficult. In order to suppress contributions from $J_{\mathrm{C_\alpha C'}}$ scalar couplings Ishima et al. introduced frequency selective pulses that only invert the carbonyl carbon into the CPMG element (Ishima, Baber, Louis, & Torchia, 2004) and demonstrated carbonyl dispersion measurements of inhibitor bound HIV-1 protease.

Beyond two-site chemical exchange: So far, the biological relaxation dispersions were analysed assuming a two-site chemical exchange model and it was the work of Grey et al. that showed that also three-site exchange of biological systems is accessible to modern relaxation dispersion experiments (Grey, Wang, & Palmer III, 2003). Their work was based on the disulfide-bridge isomerisation of the basic pancreatic trypsin inhibitor (BPTI), which had previously been investigated by relaxation dispersion spectroscopy. Those measurements revealed an isomerisation of the C14-C38 disulfide

bond characterised by the rotation of its C38 χ_1 dihedral angle from $+60°$ to $-60°$. However, line broadening of residues C14, K15, C38 and R39 suggested an additional faster exchange process affecting C14 and K15. To determine the kinetic, thermodynamic, and structural properties of the additional exchange process Grey et al. (Grey et al., 2003) acquired relaxation dispersion data using a modified relaxation compensated CPMG experiment (Wang, Grey, & Palmer III, 2001). Furthermore, they derived an analytical closed expression to analyse three-site exchange in the fast exchange limit; other cases require a numerical solution. Their formalism was successfully used to demonstrate that the C14-C38 disulfide bond in BPTI undergoes an additional isomerisation resulting from a rotation of the C14 χ_1 dihedral angle from $-60°$ to $+60°$. Moreover, in 2004 Korzhnev et al. showed that two mutants of Fyn SH3 fold via a low-populated folding intermediate. Thus, by recording CPMG relaxation dispersion experiments of mutants of Fyn SH3, Korzhnev et al. (Korzhnev, Salvatella, et al., 2004) identified two low-populated states and thus a three-site exchange system; all exchange parameters were extracted employing a numerical integration of the underlying Bloch-McConnell equations.

Multiple-quantum relaxation dispersion: Complementing single-quantum CPMG type relaxation dispersion experiments of ^{15}N and ^{1}H magnetisation with (i) ^{1}H-^{15}N double- and zero-quantum dispersion experiments (Orekhov, Korzhnev, & Kay, 2004) and (ii) ^{1}H-^{15}N multiple-quantum dispersions experiments (Korzhnev, Kloiber, & Kay, 2004) turned out to be the next significant advancement in relaxation dispersion. The extension of the relaxation dispersion method to all four coherences allows a more quantitative description of the protein dynamics and more reliable extraction of the underlying exchange parameters, in particular for three-site exchanging systems. In their work Orekhov et al. (Orekhov et al., 2004) introduced a constant-time TROSY based CPMG experiment which measures the decay of double- and zero-quantum ^{1}H and ^{15}N coherences as a function of the applied ν_{CPMG} frequency. They demonstrated the aptitude of their experiment by analysing the exchange between the folded and unfolded conformers of the G48M mutant of the Fyn SH3 domain. Additionally, the comparison of the multiple-quantum decay rates allows one to determine the relative signs of $\Delta\omega_{\mathrm{H}}$ and $\Delta\omega_{\mathrm{N}}$. However, a disadvantage of the introduced methodology is the requirement of a highly deuterated sample to extract accurate exchange parameters, since ^{1}H-^{1}H transverse cross relaxation and homonuclear scalar coupling transfer of magnetisation from ^{1}H-amide to aliphatic protons complicate this extraction in protonated samples. Backbone ^{1}H-^{15}N multiple-quantum dispersion experiments were presented by Korzhnev et al. for applications on either ^{1}H or ^{15}N spins (Korzhnev, Kloiber, et al., 2004). It has been shown that the multiple-quantum dispersion experiment often has a different functional dependence on the applied radio frequency field when compared to single-, zero- and double-quantum relaxation dispersion experiments, a fact that can be exploited to improve the reliability of the extracted exchange parameters. Other than the zero- and double-quantum experiments presented by Orekhov et al.

(Orekhov et al., 2004) the multiple-quantum experiments suggested could also be applied to protonated samples. This was demonstrated by extracting exchange parameters for the folding and unfolding of the G48M mutant of the Fyn SH3 domain in perdeuterated and protonated ^{15}N-labeled samples (Korzhnev, Kloiber, et al., 2004).

Vector-orientations in low-populated state: All relaxation dispersion techniques discussed so far were carried out in isotropic media and therefore solely based on the chemical shift difference between the exchanging states. This makes it impossible to detect any line broadening and therefore chemical exchange if the chemical shift difference between exchanging states is very close to zero. In those cases chemical exchange can be measured in alignment/anisotropic media, which prevent the averaging of anisotropic interactions such as dipolar couplings and anisotropic chemical shifts. In 2007 Ingumenova et al. (Igumenova, Brath, Akke, & Palmer III, 2007) demonstrated that differences in residual dipolar couplings (RDCs) can be obtained from N,N-dimethyltrichloroacetamide (DMTCA) using relaxation dispersion experiments. More precisely, they used constant time CPMG experiments (Loria et al., 1999a; Skrynnikov et al., 2001) at different temperatures to study $^{13}C_2$-methyl DMTCA under anisotropic conditions. The newly introduced dependence of the relaxation dispersion curves on ^{1}H-^{13}C-RDCs allowed insights into the chemical exchange of DMTCA in the slow and fast exchange regimes and ΔD_{CH} was quantified using the Carver-Richards equation (Carver & Richards, 1972).

In the same year it was shown (Vallurupalli, Hansen, Stollar, Meirovitch, & Kay, 2007) how relaxation dispersion measurements in aligned media enable the determination of RDCs and therefore bond vector orientations of transient low populated protein structures. In contrast to the above experiments in aligned media (Igumenova et al., 2007) the experiments presented by Vallurupalli et al. make use of the ^{1}H-^{15}N-RDCs in the protein backbone and employ TROSY, anti-TROSY and ^{1}H CW decoupled CPMG measurements. First the authors obtained relaxation dispersion data for the binding of a target protein to the SH3 domain from yeast Abp1p, the bound population was 6.8%. For this two-site exchange, populations, exchange rates, chemical shifts, and RDCs can be extracted; RDCs for the minor/ligand bound state were calculated according to: $D_{\mathrm{NH}}^{\mathrm{minor}} = \Delta D_{\mathrm{NH}} + D_{\mathrm{NH}}^{\mathrm{major}}$, where $D_{\mathrm{NH}}^{\mathrm{major}}$ is the residual dipolar coupling of the major state measured using conventional IPAP style experiments (Ottiger, Delaglio, & Bax, 1998). Similar experiments were also conducted to obtain information on the low populated unfolding state of the G48M Fyn SH3 domain. Together with methods to probe other vector orientations (Baldwin, Hansen, Vallurupalli, & Kay, 2009; D. F. Hansen, Vallurupalli, & Kay, 2008b; Vallurupalli, Hansen, & Kay, 2008a) in low populated states it was now possible to determine long-range restraints for structure determinations of low-populated states (Vallurupalli, Hansen, & Kay, 2008b) and to detect chemical exchange in systems with almost zero difference in the isotropic chemical shift (Igumenova et al., 2007).

Application of relaxation dispersion experiments to nucleic acids: Most of developments of relaxation dispersion NMR that we have discussed so far have focussed on CPMG experiments for protein samples. In 2000 Pardi and co-workers (Hoogstraten, Wank, & Pardi, 2000) showed an elegant application of relaxation dispersion to probe the micro-millisecond dynamics of residues in the active site of the lead-dependent ribozyme. In particular, Hoogstraten et al. obtained $R_{1\rho}$ rates at different spin-lock strengths to probe the dynamics between the ground state and the excited state and showed strong evidence for a dynamic network of hydrogen bonds that stabilise a GAAA tetraloop motif. In 2009 Hansen et al. (A. L. Hansen, Nikolova, Casiano-Negroni, & Al-Hashimi, 2009) adapted a ^{15}N off-resonance $R_{1\rho}$ experiment, which was originally designed by Kay and co-workers (Korzhnev, Orekhov, & Kay, 2005), to obtain off-resonance $R_{1\rho}$ rates for protonated carbons in uniformly labelled and unlabelled nucleic acids. The experiments employ a selective Hartmann-Hahn transfer to excite the spins of interest and record data in a 1D fashion, which allows the data acquisition on unlabelled samples. The feasibility of the presented relaxation dispersion measurement was demonstrated on the A-site of RNA — a classical example for the importance of conformational dynamics in RNA function — and on unlabelled duplex DNA containing a 1,N6-ethenoadenine lesion (A. L. Hansen et al., 2009). The significance of this experiment for observing conformational exchange in nucleic acids is further illustrated by several applications, some of which are discussed in detail in the applications below.

1.2 Theoretical aspects of chemical exchange

In order to study chemical or conformational exchange by NMR spectroscopy it is a prerequisite that the nucleus in question exchanges between at least two distinct environments, that is, the nucleus experiences a different local magnetic field at the different sites and thus evolves with different frequencies. The simplest model of chemical exchange, that of a (distinct) two-site chemical exchange, can generally be written as:

$$A \underset{k_{BA}}{\overset{k_{AB}}{\rightleftharpoons}} B \tag{5}$$

where k_{AB} and k_{BA} are the first-order forward and reverse reaction rates between the two states A and B; the overall reaction rate is denoted $k_{ex} = k_{AB} + k_{BA}$ and the corresponding life-times of the two states are $\tau_A = 1/k_{AB}$ and $\tau_B = 1/k_{BA}$, respectively. The chemical shifts (in ppm) of the chemically exchanging states are ϖ_A for state A and ϖ_B for state B, with the difference $\Delta\varpi = \varpi_B - \varpi_A$. We will below use the symbol ω to denote the offset from the RF-carrier in rad/sec, and ϖ denotes the offset in units of ppm. The populations of the states are denoted p_A for state A and p_B for state B, where $p_A + p_B = 1$ and $p_A / p_B = k_{BA}/k_{AB}$. Thus, the exchange can equivalently be

described by either (*i*) the two first-order micro-kinetic rate constants, k_{AB} and k_{BA}, or (*ii*) by the overall exchange rate k_{ex} and the population of one of states, e.g. p_B.

The Bloch-McConnell equations: In 1958 Harden McConnell modified the original Bloch equations to also include chemical exchange; the Bloch equations with McConnell's modifications often form the basis for analyses of chemical exchange by NMR spectroscopy and these are referred to as the *Bloch-McConnell equations* (McConnell, 1958). The basic crux of the Bloch-McConnell equations is that the time-derivative of the magnetisations in state *A* and *B* are described by a set of coupled first-order differential equations. As an example, the Bloch-McConnell equations describing the time-evolution of the transverse magnetisation of the two-state chemical exchange given in Eq. (5) are

$$\frac{\mathrm{d}}{\mathrm{d}t}M_A^+ = -\big(R_{2,A} - i\omega_A\big)M_A^+ - k_{AB}M_A^+ + k_{BA}M_B^+ \tag{6}$$

$$\frac{\mathrm{d}}{\mathrm{d}t}M_B^+ = -\big(R_{2,B} - i\omega_B\big)M_B^+ - k_{BA}M_B^+ + k_{AB}M_A^+ \tag{7}$$

in the absence of RF-fields. Here, $M_j^+ = M_{x,j} + iM_{y,j}$, is the complex transverse magnetisation of site $j = A, B$, i is the imaginary unit, and $R_{2,j}$ is the corresponding intrinsic transverse relaxation rate of site *j*, in the absence of exchange. The intrinsic transverse relaxation rate could, for example, stem from chemical shift anisotropy, dipole-dipole, or quadruple relaxation mechanisms. The solution to the set of coupled differential equations, Eqs. (6)-(7), that describe the evolution of the magnetisations during free precession can easily be obtained from the corresponding matrix-form of the homogeneous differential equations

$$\frac{d}{dt}\begin{pmatrix}M_A^+\\M_B^+\end{pmatrix} = -\begin{pmatrix}R_{2,A} - i\omega_A & 0\\0 & R_{2,B} - i\omega_B\end{pmatrix}\begin{pmatrix}M_A^+\\M_B^+\end{pmatrix} + \begin{pmatrix}-k_{AB} & k_{BA}\\k_{AB} & -k_{BA}\end{pmatrix}\begin{pmatrix}M_A^+\\M_B^+\end{pmatrix} \tag{8}$$

$$\frac{d}{dt}\mathbf{M}^+ = -\mathbf{\Gamma}\mathbf{M}^+ + \mathbf{K}\mathbf{M}^+ = (-\mathbf{\Gamma} + \mathbf{K})\mathbf{M}^+ \tag{9}$$

$$\mathbf{M}^+(t) = e^{(-\mathbf{\Gamma}+\mathbf{K})t}\mathbf{M}^+(t=0) \tag{10}$$

where $\mathbf{M}^+$ is the vector $\{M_A^+, M_B^+\}$, $\mathbf{\Gamma}$ is the Liouvillian accounting for intrinsic transverse relaxation and chemical shift evolution, and $\mathbf{K}$ is the exchange matrix. In general, a Fourier transformation of the resulting free induction decay gives rise to two Lorentzian signals *A'* and *B'*, which in the limit of $k_{ex} \to 0$ approach *A* and *B*, respectively. Of particular interest here is the line-width and chemical shift of the resulting exchange-average signals *A'* and *B'*, which are given by the complex eigenvalues of the $(-\mathbf{\Gamma} + \mathbf{K})$ Liouvillian matrix in Eq. (10),

$$-R_{2,A'} + i\omega_{A'} = \frac{1}{2}\left\{-\left(k_{2,AB} + k_{2,BA}\right) + \sqrt{\left(k_{2,AB} - k_{2,BA}\right)^2 + 4k_{AB}k_{BA}}\right\}, \quad (11)$$

$$-R_{2,B'} + i\omega_{B'} = \frac{1}{2}\left\{-\left(k_{2,AB} + k_{2,BA}\right) - \sqrt{\left(k_{2,AB} - k_{2,BA}\right)^2 + 4k_{AB}k_{BA}}\right\} \quad (12)$$

when $R_{2,B} > R_{2,A}$ and where $k_{2,AB} = k_{AB} + R_{2,A} - i\omega_A$ and $k_{2,BA} = k_{BA} + R_{2,B} - i\omega_B$ (D. F. Hansen & Led, 2003). The intensities of the two exchange-averaged signals are given by the initial intensities, $\mathbf{M}(t = 0)$, multiplied by the eigenvectors of the $(-\mathbf{\Gamma} + \mathbf{K})$ matrix. The dependence of the observed line-widths $(R_{2,A'}, R_{2,B'})$ and peak-positions $(\omega_{A'}, \omega_{B'})$ on the exchange parameters, k_{ex} and p_B, is not directly transparent from Eqs. (11)-(12) and many approximations to these equations have therefore been derived to provide a simpler explanation of the observed NMR parameters under many different conditions, such as, highly skewed populations $p_A \gg p_B$, 'slow exchange', and 'fast-exchange'.

The fast-exchange regime: Only one exchange-average signal is observed in the NMR spectrum at an intermediate chemical shift, if the overall exchange rate constant is much larger than the difference in chemical shift between the two sites; this situation is referred to as the *fast-exchange regime*. More specifically, when $k_{ex} \gg |\Delta R_2 + i\Delta\omega|$, then (D. F. Hansen & Led, 2003)

$$\omega_{A'} \approx p_A\omega_A + p_B\omega_B, \quad (13)$$

$$R_{2,A'} \approx p_A R_{2,A} + p_B R_{2,B} + \frac{p_B(1-p_B)}{k_{ex}}(\Delta\omega^2 - \Delta R_2^2). \quad (14)$$

Often it is assumed that $\Delta R_2 = R_{2,B} - R_{2,A}$ is small compared to $\Delta\omega$, thus simplifying Eq. (14) and making the dependence of the line-width and chemical shift on the exchange parameters easily accessible. As discussed above, the application of a CPMG element decreases the effective transverse relaxation rate of the exchange-average signals as compared to free-precession. More specifically, if the fast-exchange condition applies, the dependence of the transverse relaxation rate on the CPMG frequency is given by (Luz & Meiboom, 1963)

$$R_{2,A'}(\tau_{CPMG}) \approx p_A R_{2,A} + p_B R_{2,B} + \frac{p_B(1-p_B)\Delta\omega^2}{k_{ex}}\left(1 - \frac{2}{k_{ex}\tau_{CPMG}}\tanh\left(\frac{k_{ex}\tau_{CPMG}}{2}\right)\right), \quad (15)$$

with all parameters as defined above. As compared to the free-precession scenario, the application of a CPMG sequence modulates the chemical exchange contribution with a factor of $1 - 2\tanh(k_{ex}\tau_{CPMG}/2)/(k_{ex}\tau_{CPMG})$. Moreover, in the fast-exchange regime, the exchange contribution to the transverse relaxation rate of the observed signal is proportional to $\Delta\omega^2$, this implies that additional information about the chemical exchange is provided when the relaxation dispersion

curves, $R_{2,A'}(\tau_{CPMG})\ vs.\ \tau_{CPMG}$, are obtained at multiple spectrometer frequencies. Even for nuclei outside the fast-exchange regime, the relaxation dispersion curve will depend on the spectrometer frequency, and relaxation dispersions are therefore most-often obtained at multiple fields in order to derive the most accurate parameters. Carver and Richards (Carver & Richards, 1972) showed that the decay of transverse magnetisation can be approximated by a single exponential during the application of a CPMG sequence, both in the case of fast and intermediate exchange, and they derived elaborate analytical expressions for such cases (Carver & Richards, 1972; Davis, Perlman, & London, 1994). Yet, the Carver-Richards equations are not applicable for nuclei in the slow-exchange regime and other approximate equations have been derived for the study of such nuclei.

The slow-exchange regime: The nucleus of interest is in the *slow-exchange regime,* when the overall exchange rate constant is slow compared to the chemical shift difference between its two states, $k_{ex} \ll |\Delta R_2 + i\Delta\omega|$. For nuclei in the slow-exchange regime two separate signals are observed in the NMR spectrum and their intensities are nearly proportional to the populations of the two states. If one of the exchanging states is significantly less populated than the other state, the corresponding NMR signal will be of very low intensity effectively resulting in the observation of only a single signal, despite the fact that the nucleus of interest is in the slow-exchange regime. Thus, the observation of a single signal, versus the observation of two separate signals, cannot be used as a tangible measure for the specific exchange regime. In the slow-exchange regime, and to a first order of approximation, the chemical shifts of the observed signals are those of the intrinsic states, $\omega_{A'} \approx \omega_A$, and $\omega_{B'} \approx \omega_B$. Small chemical-exchange induced shifts do occur (Skrynnikov, Dahlquist, & Kay, 2002) and these can in some cases be used to derive the position of a low-populated state (see below). A line-broadening effect will be observed in the slow-exchange regime corresponding to the inverse of the lifetime of the observed state. Thus, during free-precession,

$$R_{2,A'} \approx R_{2,A} + k_{AB}, \tag{16}$$

$$R_{2,B'} \approx R_{2,B} + k_{BA} \tag{17}$$

The effective transverse relaxation rate is also altered for nuclei in the slow-exchange regime by the application of a CPMG sequence. Specifically, when the exchange rate is much slower than the rate of pulsing, $1/\tau_{CPMG} \gg k_{ex}$, Tollinger et al. (Tollinger, Skrynnikov, Mulder, Forman-Kay, & Kay, 2001) showed that

$$R_{2,\mathrm{A}'} \approx R_{2,A} + k_{AB}\left(1 - \frac{\mathrm{Sin}(\Delta\omega\tau_{\mathrm{CPMG}})}{\Delta\omega\tau_{\mathrm{CPMG}}}\right). \tag{18}$$

Thus, again the exchange contribution to the effective transverse relaxation rate has been modified as compared to the free precession, in the slow exchange by $1 - \mathrm{Sin}(\Delta\omega\tau_{\mathrm{CPMG}})/(\Delta\omega\tau_{\mathrm{CPMG}})$. For nuclei outside both the slow-exchange and the fast-exchange regimes, the dependence of the transverse relaxation rates on the chemical exchange parameters becomes significantly more complicated. Although several analytical expressions have been derived to tackle many of such scenarios (Carver & Richards, 1972), a numerical solution of the underlying Bloch-McConnell equations is often the preferable choice, since such solutions are made without approximations and are generally generated very fast using modern computers and standard software packages.

Extracting the effective transverse relaxation rate, $R_{2,eff}$: In the constant-time CPMG experiment the effective relaxation rate, $R_{2,\mathrm{eff}}$, of the exchange-average signal is calculated as a function of the CPMG frequency:

$$\nu_{\mathrm{CPMG}} = \frac{1}{4\tau_{\mathrm{CPMG}}} \tag{19}$$

where τ_{CPMG} is the evolution time in the CPMG element, $\{\tau_{\mathrm{CPMG}} - 180° - \tau_{\mathrm{CPMG}}\}_N$. Thus, the frequency ν_{CPMG} refers to the frequency of application of the element $\tau_{\mathrm{CPMG}} - 180° - 2\tau_{CPMG} - 180° - \tau_{CPMG}$. In the constant-time relaxation dispersion experiment, the effective relaxation rate used to extract the chemical exchange parameters can be calculated from the intensity of the NMR signal in two spectra, one with the CPMG element and one reference spectrum:

$$R_{2,eff} = -\frac{1}{T_{relax}} \ln \frac{I(\nu_{CPMG})}{I_0} \tag{20}$$

where $I(\nu_{CPMG})$ is the intensity of the signal at a given CPMG frequency ν_{CPMG} and I_0 is the intensity in a reference spectrum recorded without a CPMG element. The lowest value of ν_{CPMG} is determined by the length of the constant time delay T_{relax} and the highest value of ν_{CPMG} is dictated by the hardware specifications *i.e.* the number of 180° pulses that can be given in the time T_{relax}. Moreover, during the constant-time relaxation delay, T_{relax}, the inter-pulse delay $2\tau_{CPMG}$ is adjusted so that $2N\tau_{CPMG} = T_{relax}$.

As mentioned earlier the 180° pulses in the CPMG sequence refocus chemical shift evolution and reduce the effective chemical shift difference between the exchanging sites. Thus, the chemical exchange contribution to the transverse relaxation rate is reduced when the CPMG frequency, ν_{CPMG}, increases and depending on the frequency at which the 180° pulses are applied the chemical exchange can be moved from the slow-exchange regime to the fast-exchange regime.

Spin-lock relaxation dispersions: Another method used to obtain the chemical-exchange parameters is the spin-lock experiment, where the effective transverse relaxation rate is derived from the corresponding relaxation rate in the rotating frame, $R_{1\rho}$ (Palmer III & Massi, 2006). As with the CPMG relaxation dispersion experiment described above, the obtained relaxation rate, $R_{1\rho}$, depends on the chemical exchange parameters and the strength of an applied (spin-lock) field. In the case of a low-populated state, $p_A \gg p_B$, Trott and Palmer derived analytical expressions for the relationship between the measured relaxation rate and the exchange parameters:

$$R_{1\rho} = R_1 \cos^2\theta + R_2 \sin^2\theta + \frac{p_B(1-p_B)\,\Delta\omega^2 k_{ex} \sin^2\theta}{k_{ex}^2 + \omega_1^2 + \omega_B^2} \tag{21}$$

where $\tan\theta = \omega_1/(p_A\omega_A + p_B\omega_B)$, ω_1 is the field strength (rad/s) of the spin-lock field that is applied along the *x*-axis of the rotating frame, and $p_A\omega_A + p_B\omega_B$ is the population-average offset of the nucleus from the RF carrier. Moreover, $\omega_{eff} = \sqrt{\omega_1^2 + \omega_B^2}$ is the effective field, and in accordance with the CPMG relaxation dispersion experiment described above, the exchange-contribution to the $R_{1\rho}$ rate is suppressed when the effective strength of the spin-lock, ω_{eff}, is increased. In particular, the exchange contribution is efficiently quenched when the spin-lock field strength is much larger than the overall rate constant, *i.e.*, when $k_{ex}/(k_{ex}^2 + \omega_1^2 + \omega_B^2)$ in Eq. (21) becomes small. The dependence of $R_{1\rho}$ on the spin-lock field strength ω_1 and on the offset, ω_B, can be used to derive 'relaxation dispersion curves' in the form of $R_{1\rho}(\omega_1, \omega_B)$, that can be used to extract chemical exchange parameters (Korzhnev, Orekhov, et al., 2005; Massi, Grey, & Palmer III, 2005). As for the CPMG relaxation dispersion experiment described above, experiments at multiple spectrometer frequencies are in general necessary to break the correlation between the obtained parameters, in particular, the correlation between $\Delta\omega$ and p_B.

Three-state exchange and beyond: The developments of new and more sensitive CPMG pulse sequences, new isotope labelling schemes, theoretical frameworks, and improved fitting procedures over the last decade have allowed the elucidation of systems that exchange between more than two distinct sites (Eisenmesser et al., 2002; Grey et al., 2003; Hass, Hansen, Christensen, Led, & Kay, 2008; Korzhnev, Neudecker, Mittermaier, Orekhov, & Kay, 2005; Vallurupalli & Kay, 2006). Analytical expressions describing the CPMG and $R_{1\rho}$ relaxation dispersion curves for multiple-site exchange have been derived for special cases (Grey et al., 2003), however, the most common approach for the analysis of multiple-site exchange is a numerical solution, in conjunction with a least-squares fit, of the underlying Bloch-McConnell equations. In that regard, it is straightforward to show that Eqs. (9)-(10) can be generalised to describe the evolution of magnetisations during multiple-site chemical exchanges,

$$\frac{d}{dt}\mathbf{M}^{+} = (-\mathbf{\Gamma} + \mathbf{K})\mathbf{M}^{+} \tag{22}$$

where, $\mathbf{M}^{+} = \{M_A^{+}, \dots, M_i^{+}, \dots, M_j^{+}, \dots M_N^{+}\}$, is the vector holding the time-dependent transverse magnetisations of the chemically exchanging sites, $(\mathbf{\Gamma})_{ij} = \delta_{ij}(R_{2,i} - i\omega_i)$, is a diagonal matrix giving the intrinsic transverse relaxation rates and chemical shifts, $(\mathbf{K})_{ij}$ $(i \neq j)$ is the Markovian (first-order) rate constant between site *i* and *j*, with the diagonal element given by

$$\mathbf{K}_{ii} = -\sum_{j \neq i} k_{ij} \tag{23}$$

As for the two-site chemically exchanging system, the solution to Eq. (22) is given by $\mathbf{M}^{+}(t) = e^{(-\mathbf{\Gamma}+\mathbf{K})t}\mathbf{M}^{+}(t=0)$, which can be obtained numerically using standard mathematic software or standard libraries.

2 Relaxation dispersion experiments

2.1 Nitrogen based relaxation dispersion experiments

Relaxation dispersions in two-spin systems, exemplified by the protein backbone NH spin-system: The basic CPMG element, $\{\tau_{CPMG} - 180° - \tau_{CPMG}\}_N$, was originally designed for accurate measurements of transverse relaxation rates by refocusing the magnetisation of interest during a relaxation delay and thereby removing artefacts due to magnetic field inhomogeneity. It soon became apparent (Luz & Meiboom, 1963), however, that the contribution from micro-millisecond chemical exchange processes to the derived transverse relaxation rates is depend on the frequency at which the refocusing 180° pulses are applied, $\nu_{CPMG} = 1/(4\tau_{CPMG})$. Quantitatively, the contribution to the transverse relaxation from a chemical exchange processes is suppressed, when the frequency of applied 180° pulses is increased, and numerous of equations describing the effective transverse relaxation rate, $R_{2,eff}$, as a function of the exchange parameters and ν_{CPMG} have been derived, as described above. For several decades scalar couplings acting on the nucleus of interest were a major hindrance for the application of the CPMG relaxation dispersion experiment to the quantification of chemical exchange parameters. For example, in applications that involve the amide nitrogen spin in protein backbones, the scalar coupling between the nitrogen and the amide proton would often obscure the information about the chemical exchange process. Some applications alleviate this problem by choosing the inter-pulse delay, $2\tau_{CPMG}$, so that an integer number of proton decoupling cycles could be applied in each $2\tau_{CPMG}$ delay (Kristensen, Siegal, Sankar, & Driscoll, 2000).

It was the elegant sequence of Palmer and co-workers (Loria et al., 1999a) and their introduction of the relaxation-compensated CPMG element that marked a new era in the applications of CPMG relaxation dispersion to the study of low-populated states of macromolecules, since it allowed a quantitative determination of the exchange parameters. The cornerstone of the relaxation-compensated CPMG element and applications to two-spin systems, such as the ^{15}N-^{1}H spin system, is that the magnetisation of interest spends an equal amount of time as in-phase and as anti-phase with the coupled nucleus. For the amide ^{15}N-^{1}H spin-pair, this means that the magnetisation of interest spends *exactly* the same time as $2H_zN_{x,y}$ and as $N_{x,y}$. The previous troublesome modulation of the derived relaxation rates by the scalar coupling, which effectively exchanges anti-phase and in-phase magnetisation, is thereby eliminated. The relaxation-compensated CPMG sequence and the P-element are depicted below in Figure 5.

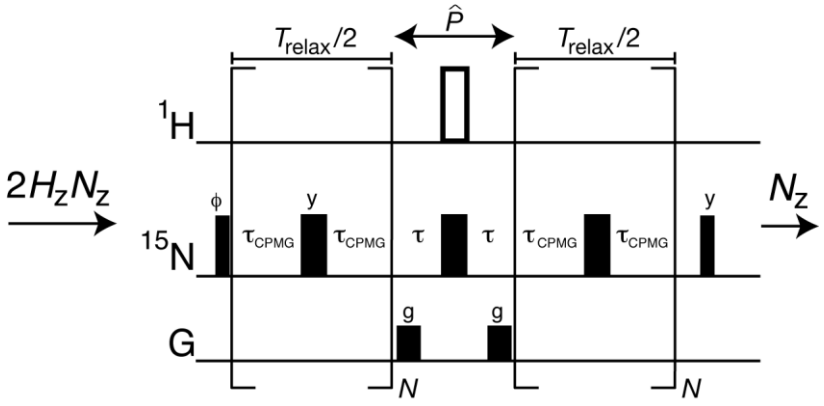

Figure 5: The relaxation compensated CPMG-element introduced by Loria et al. (Loria et al., 1999a). Narrow black bars represent 90° pulses; wider black bars represent 180° pulses, while the open rectangle represents a composite proton inversion pulse ($90_x180_y90_x$). The P-element ($\hat{P}$, an INEPT) converts anti-phase magnetisation, in this case $2H_zN_y$, to in-phase magnetisation, N_x; and visa versa. Overall, the design of the relaxation-compensated relaxation dispersion experiment ensures that the magnetisation of interest spends equal time as anti-phase and in-phase magnetisation irrespectively of length of the inter-pulse delay $2\tau_{CPMG}$ and the number of applied refocusing pulses. The phase cycle is $\phi = \{x, -x\}$, with the receiver $\phi_{rec} = \{x, -x\}$.

In order to keep off-resonance effects to a minimum an even number of refocusing pulses must be applied on each side of the P-element in the relaxation-compensated sequence, in line with the originally proposed idea by Carr, Purcell, Meiboom, and Gill (Carr & Purcell, 1954; Meiboom & Gill, 1958), Figure 2. Yet, with this constrain and as detailed below the introduction of the relaxation-compensated relaxation dispersion experiment allowed for many new and exciting applications to macromolecules.

Constant-time CPMG: The introduction of the relaxation-compensated CPMG experiment opened up the possibility of obtaining well-defined relaxation dispersion curves, that is, $R_{2,eff}(\nu_{CPMG})$ *vs.*

ν_{CPMG}, which according to the discussions above in the theoretical section contains the critical information about the chemical exchange processes. However, with the original relaxation-compensated CPMG experiment (Loria et al., 1999a) a series of 2D spectra are recorded with varying T_{relax} for each given constant ν_{CPMG} in order to determine the rates $R_{2,eff}$ from fits of single-exponential decays, $I_0 exp(-R_{2,eff}T_{relax})$ to the observed decay; $I(T_{relax})$ *vs.* T_{relax}. For application to N-H spin systems of proteins, this approach requires that a pseudo 3D spectrum {^{15}N, ^{1}H, T_{relax}} is recorded for each value of ν_{CPMG}, which effectively prevents a high-resolution $R_{2,eff}(\nu_{CPMG})$ relaxation dispersion curve to be obtained. It was the introduction of the constant-time relaxation-compensated CPMG relaxation dispersion by Kay and co-workers (Mulder, Skrynnikov, et al., 2001) that alleviated this problem. In the constant-time CPMG experiment the relaxation delay T_{relax} is kept constant and only the number of applied refocusing pulses is varied. A reference spectrum is recorded with $T_{relax} = 0\ \mathrm{s}^{-1}$ and each of the effective relaxation rates are subsequently calculated from $R_{2,eff}\ (\nu_{CPMG}) = -1/T_{relax}\ \ln(I(\nu_{CPMG})/I_0)$, where $I(\nu_{CPMG})$ is the intensity in the 2D spectrum with ν_{CPMG}, and I_0 is the intensity in the reference spectrum. Even though each of the relaxation rates are estimated from only two experimental data points using this constant-time approach, it is our experience that the constant-time approach does allow for a much higher resolution of the corresponding relaxation dispersion curves and thus a significant more accurate quantification of the underlying chemical exchange processes. Another advantage of the constant-time relaxation dispersion experiment is that minor artefacts that occur due to cross-correlated relaxation mechanisms, etc., tend to cancel in the analysis of chemical exchange parameters because these effects are often 'absorbed' in the fitted intrinsic transverse relaxation rate, $R_{2,0}$. The relaxation of transverse carbon magnetisation in $^{13}C^{1}H_3$ groups is complicated by cross-correlated relaxations between pairs of dipolar coupled spins of the methyl group (Kay et al., 1992). Consequently, the apparent relaxation of the transverse ^{13}C magnetisation is multi-exponential and extraction of a first-order 'intrinsic' relaxation rate from a standard decay curve, $I(\tau)\ vs.\ \tau$, becomes problematic. The cancelation of modulations caused to cross-correlated relaxations in the constant-time CPMG relaxation experiments therefore becomes particularly important in the analysis of methyl $^{13}C^{1}H_3$ relaxation dispersions (Skrynnikov et al., 2001).

TROSY-based relaxation dispersion: The intrinsic relaxation of the coherences used to probe the chemical exchange in Figure 5 relaxes, on average, as ($R_2(N_x)$+ $R_2(2H_zN_x)$)/2, which for medium-to-large proteins (>30 kDa) prevents a quantification of the chemical exchange contributions to the transverse relaxation rate. The introduction of the TROSY-based CPMG by Loria et al (Loria et al., 1999b), Figure 6, which for the N-H spin system probes the effective transverse relaxation of the TROSY component $R_2(2H^{|\beta\rangle}N_x)$, allows a quantification of relaxation dispersions of larger proteins. The improvements for larger proteins are due to a reduced intrinsic transverse relaxation during the

T_{relax} delay and also by providing a better spectral resolution in spectra, since the relaxation dispersions are encoded in a TROSY-based correlation map $\{\omega_{\square}(2H^{|\beta>}N_{x,y}), \omega_{\square}(2H_{x,y}N^{|\beta>})\}$ as opposed to the in-phase correlation map of the conventional experiment; $\{\omega_{\square}(N_{x,y}), \omega_{\square}(H_{x,y})\}$.

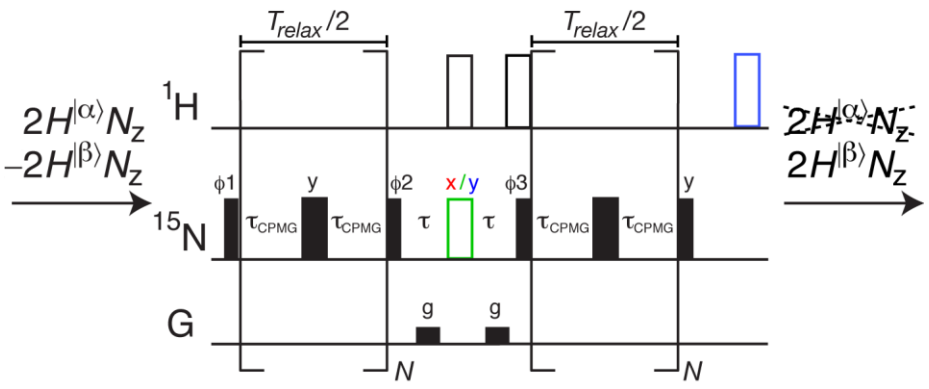

Figure 6: The TROSY/anti-TROSY CPMG sequence. As above, narrow bars represent 90° pulses, wider bars represent 180° pulses and open rectangles represent composite 180° pulses. The TROSY version of this sequence, (black and red) originally proposed by Loria et al. (Loria et al., 1999b), was recently modified to allow also for the measurement of anti-TROSY (black and blue) relaxation dispersions (Vallurupalli, Hansen, et al., 2007). The green 180° is applied both in the TROSY and in the anti-TROSY experiment, however with a different phase. The element between the two CPMG blocks is designed so that the intensity of the TROSY component is inverted relative to the intensity of the anti-TROSY component to compensate for cross-correlated relaxation between the two components that is caused by amide-proton spin-flips. The pulses with phase ϕ_2 and ϕ_3 serve to allow for measurements in partly aligned samples where the ^{15}N-^{1}H couplings vary in a site-specific manner due to residual dipolar couplings. Moreover, the phases are chosen in such a way that both even and odd numbers of refocusing pulses N can be applied for both TROSY and anti-TROSY experiments. The remainder of the full sequence is designed so that the TROSY component, $2H^{|\beta>}N_x$, is selected. The phase cycle is: $\phi_1=\{x, -x\}$, $\phi_2=\{y, y, -y, -y\}$, $\phi_3=\{x, x, -x, -x\}$.

In the product-operator basis (Sorensen, Eich, Levitt, Bodenhausen, & Ernst, 1983) consisting of the transverse TROSY $2N_{x,y}H^{\beta}$ coherences and the anti-TROSY $2N_{x,y}H^{\alpha}$ coherences, the time evolutions in the absence of chemical exchange are governed by the following differential equation:

$$\frac{d}{dt}\begin{pmatrix} 2N_xH^{\alpha} \\ 2N_yH^{\alpha} \\ 2N_xH^{\beta} \\ 2N_yH^{\beta} \end{pmatrix} = -\begin{pmatrix} R_2+\eta_{xy}+\mu & \Omega+\pi J_{NH} & -\mu & 0 \\ -(\Omega+\pi J_{NH}) & R_2+\eta_{xy}+\mu & 0 & -\mu \\ -\mu & 0 & R_2-\eta_{xy}+\mu & \Omega-\pi J_{NH} \\ 0 & -\mu & -(\Omega-\pi J_{NH}) & R_2-\eta_{xy}+\mu \end{pmatrix}\begin{pmatrix} 2N_xH^{\alpha} \\ 2N_yH^{\alpha} \\ 2N_xH^{\beta} \\ 2N_yH^{\beta} \end{pmatrix} \quad (24)$$

$=$ $\mathbf{v}$

following the idea by Allard et al. (Allard, Helgstrand, & Hard, 1997, 1998; D. F. Hansen, Vallurupalli, Lundström, Neudecker, & Kay, 2008). Here, $\mathbf{v}$ is the vector $\mathbf{v}$ ={$2N_xH^\alpha$, $2N_yH^\alpha$, $2N_xH^\beta$, $2N_yH^\beta$}, $\mathbf{\Gamma}$ is the matrix representation of the Liouvillian, η_{xy} is the ^{1}H-^{15}N dipole-dipole/^{15}N CSA cross-correlated relaxation rate, $\mu = R_1(^1\text{H})/2$ is the cross-correlated relaxation between the TROSY and anti-TROSY components, Ω is the difference between the radio frequency (RF) transmitter and the resonance frequency of the nitrogen under consideration, $R_2 + \mu$ is the intrinsic average transverse relaxation rate of the in-phase and anti-phase coherences, i.e., $R_2 \approx R_2(N_x)$. The solution to the homogeneous set of differential equations in Eq. (24) during free precession is $\mathbf{v}(t) = \exp(-\mathbf{\Gamma}t)\mathbf{v}(0)$, while the application of the, here assumed infinitely short and perfect, ^{15}N 180°_x refocusing pulse in Figure 6 can be represented by the matrix operator

$$\widehat{180^\circ_x} = \begin{pmatrix} 1 & 0 & 0 & 0 \\ 0 & -1 & 0 & 0 \\ 0 & 0 & 1 & 0 \\ 0 & 0 & 0 & -1 \end{pmatrix} \tag{25}$$

The matrix representation of the proton 180°(^{1}H) inversion pulse, which effectively interchanges TROSY magnetisation with anti-TROSY magnetisation, is given by:

$$\widehat{180^\circ_H} = \begin{pmatrix} 0 & 0 & 1 & 0 \\ 0 & 0 & 0 & 1 \\ 1 & 0 & 0 & 0 \\ 0 & 1 & 0 & 0 \end{pmatrix}. \tag{26}$$

For isotropic samples with $^1J_{NH}=1/(4\tau)$ and neglecting off-resonance effects, we can ignore the $90^\circ\,\phi_2$ and $90^\circ\,\phi_3$ pulses in Figure 6 and calculate the evolution of the magnetisations during the sequence. Starting after the $90^\circ\phi_1$ ($\phi_1 = x$) pulse and with initial magnetisation of $\mathbf{v}(0)=\{0,1,0,-1\}$, the final magnetisation is given by $\mathbf{v}_{CPMG} = \hat{\mathbf{C}}_\mathbf{x}\hat{\mathbf{P}}_\mathbf{T}\hat{\mathbf{C}}_\mathbf{y}\mathbf{v}(0)$, where $\hat{\mathbf{C}}_\mathbf{y}$ is the matrix-operator corresponding to the first CPMG block, $\hat{\mathbf{P}}_\mathbf{T}$ is the modified P-element in the middle of the sequence, and $\hat{\mathbf{C}}_\mathbf{x}$ is the second CPMG block. Specifically,

$$\hat{\mathbf{C}}_\mathbf{y} = \left[\exp(-\mathbf{\Gamma}\tau_{\text{CPMG}})\,\widehat{180^\circ_y}\exp(-\mathbf{\Gamma}\tau_{\text{CPMG}})\right]^N \tag{27}$$

Qualitatively, the proton longitudinal relaxation acts as an exchange between the TROSY and anti-TROSY magnetisation, since a proton spin-flip, $^1\text{H}^{|\alpha\rangle} \leftrightarrow {}^1\text{H}^{|\beta\rangle}$, effectively inter-converts the two spin states $2N_xH^\alpha$ and $2N_xH^\beta$. This exchange phenomena is also evident from Eq. (24) that resamples the evolution matrix of a two-site chemical exchange system, with $k_{ex} = R_1(^1\text{H})$, $p_B = 0.5$, and $\Delta\omega = 2\pi J_{HN}$. For most cases involving proteins $R_1(^1\text{H}) \ll 2\pi {}^1J_{HN}$, thus the exchange between the TROSY and anti-TROSY components, caused by proton spin-flips, is in the 'slow-exchange regime' (see above). Using the equations derived previously for slow-exchanging systems (Tollinger et al.,

2001), we can calculate the effective relaxation rate of the TROSY coherence during the first CPMG block:

$$R_{2,eff}^{TROSY} \approx R_2 - \eta_{xy} + \frac{1}{2}R_1(^1\mathrm{H})\left(1 - \frac{\mathrm{Sin}(2\pi J_{\mathrm{HN}}\tau_{\mathrm{CPMG}})}{2\pi J_{\mathrm{HN}}\tau_{\mathrm{CPMG}}}\right). \quad (28)$$

As seen from Eq. (28) the proton spin-flips, and thus the exchange between the TROSY and the anti-TROSY components, cause the effective relaxation rate of the TROSY component to depend on the CPMG inter-pulse delay, τ_{CPMG}, even in the absence of a genuine chemical exchange process. Particularly, in this situation, the effective relaxation rate of the TROSY component increases as the CPMG frequency, $\nu_{CPMG} = 1/(4\tau_{CPMG})$, is increased, which would lead to inaccurately derived chemical exchange parameters. The insertion of the modified $\mathbf{P_T}$-element between the two CPMG blocks, Figure 6, has the effect of inverting the TROSY intensity relative to the anti-TROSY intensity half-way through the sequence, thus, to a first-order of approximation eliminating the τ_{CPMG} dependence of the $R_{2,eff}^{TROSY}$ rate caused by proton spin-flips. The CPMG relaxation dispersion resulting from the sequence $\hat{\mathbf{C}}_\mathbf{x}\hat{\mathbf{P}}_\mathbf{T}\hat{\mathbf{C}}_\mathbf{y}$ therefore only reports on genuine chemical exchange processes. The flow of magnetisation through the TROSY CPMG relaxation dispersion experiment is shown schematically in Figure 7. Finally, as explained previously (Vallurupalli, Hansen, et al., 2007), the TROSY CPMG element, Figure 6, provides an additional advantage over the traditional relaxation-compensated sequence in that odd numbers of *N* can also be used without compromising on RF pulse imperfections (off-resonance effects). Thus, the TROSY experiment is most often the preferable experiment for applications involving medium to large proteins.

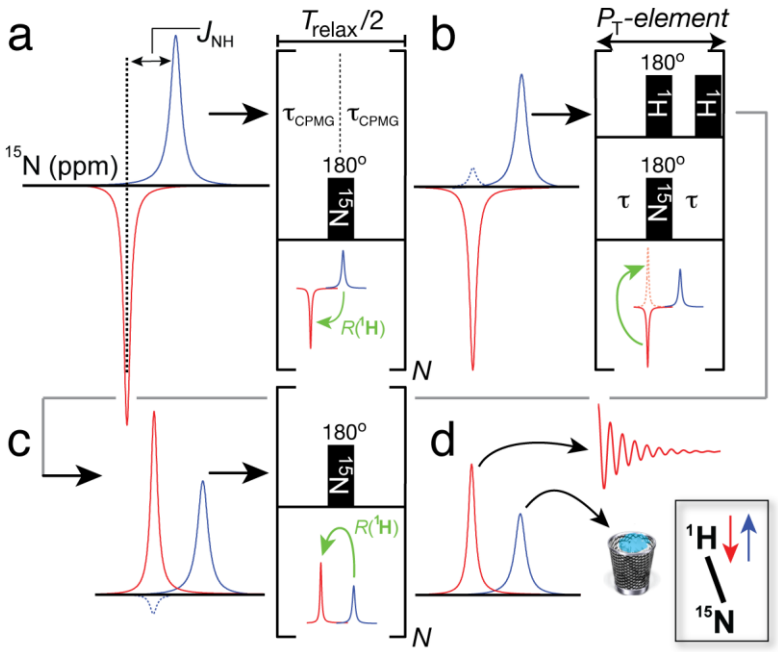

Figure 7: Schematic representation of the TROSY CPMG relaxation dispersion experiment and its compensation for proton spin-flips. (a) The first CPMG block is applied to anti-phase magnetisation. Magnetisation is transferred between the TROSY and anti-TROSY components by the proton spin-flips as indicated with green arrows. (b) As indicated with the dashed blue peak, magnetisation has been transferred from the anti-TROSY component to the TROSY component via the proton spin-flip during the first CPMG block. The modified P-element, $\mathbf{P_T}$, in (b) and between the two CPMG blocks serves to invert the intensity of the TROSY component. (c) Consequently the effect of the proton spin-flips is inverted for the second half of the sequence, to a first order of approximation. (d) The TROSY component is finally selected and labelled with the $2N_xH^\beta$ chemical shift (t_1) and $2N^\beta H_x$ chemical shift (t_2), respectively for detection.

Probing relaxation dispersions of in-phase magnetisation: The CPMG experiments described above involve the quantification of chemical exchange from coherences that have contributions from the amide proton longitudinal relaxation to the intrinsic relaxation rate. For example, the relaxation-compensated CPMG experiment in Figure 5 probe the average transverse relaxation of N_{xy} and $2N_{xy}H_z$ coherences; and also the TROSY relaxation is enhanced by amide proton longitudinal relaxation. The effect of proton relaxation becomes particularly pronounced for medium sized [U-^{1}H^{15}N] isotope labelled proteins, where the aliphatic protons relax the amide proton very effectively. Moreover, for amide sites that are solvent-exposed and where the amide proton exchanges rapidly with the bulk solvent, large contributions are observed in the relaxation dispersions to the intrinsic relaxation rate. The in-phase CPMG relaxation experiment (D. F. Hansen, Vallurupalli, & Kay, 2008a), Figure 8, eliminates the losses of sensitivity associated with fast amide proton longitudinal relaxation and proton exchange with the bulk solvent, since the relaxation dispersion is probed through the in-phase coherence, N_{xy}, while decoupling the scalar nitrogen-proton interaction with a specially designed scheme. The sequence in Figure 8 also benefits from a self-compensation detailed below that allows

both odd and even values of *N*, without introducing an error due to off-resonance effects or pulse-imperfections. This self-compensation is achieved by the 180° ϕ_3 pulse (Figure 8), which is sandwiched between two identical blocks of CPMG elements, and thus creates a 'mirror plane' and symmetry of the sequence.

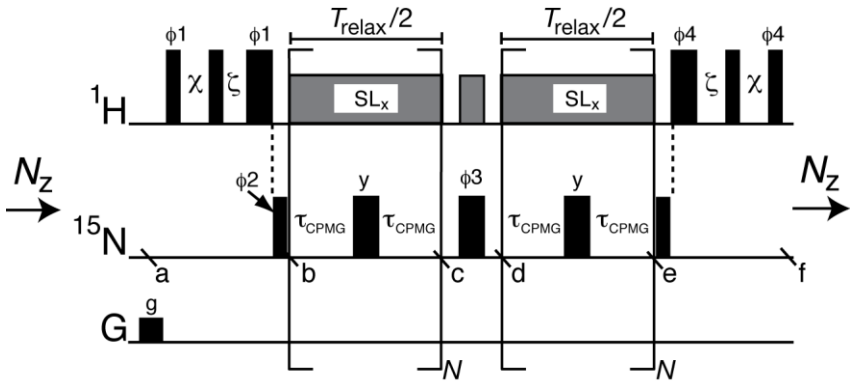

Figure 8: The in-phase CPMG-element (D. F. Hansen, Vallurupalli, & Kay, 2008a), which probes the relaxation dispersion via the in-phase N_{xy} coherence. The strength of the continuous wave (CW) decoupling field applied on ^{1}H is, $\nu_{CW}=2k\,\nu_{CPMG}$, where *k* is an integer. The elements before and after the CPMG element serve to align the H_2O magnetisation along the applied spin-lock field (D. F. Hansen & Kay, 2007), SL_x, in order to reduce magnetisation losses due to saturation of the H_2O magnetisation; the delays of this element are $\chi = 1/(2\pi\nu_{CW}) - 4pw/\pi$ and $\zeta = pwn - 2pw/\pi$, where pw (pwn) is the ^{1}H (^{15}N) high-power 90^o pulse-width. The phase-cycle is $\phi1=\{y, y, -y, -y\}$, $\phi2=\{x, -x\}$, $\phi3=\{x, x, -x, -x\}$, $\phi4=\{-y, -y, y, y\}$, and $\phi_{rec}=\{x, -x, x, -x\}$.

The evolution of magnetisation during the in-phase CPMG experiment can be described using the following set of differential equations:

$$\frac{d}{dt}\begin{pmatrix} N_x \\ N_y \\ N_z \end{pmatrix} = -\begin{pmatrix} R_2 & \Omega & -\omega_{1y} \\ -\Omega & R_2 & \omega_{1x} \\ \omega_{1y} & -\omega_{1x} & R_1 \end{pmatrix}\begin{pmatrix} N_x \\ N_y \\ N_z \end{pmatrix}, \tag{29}$$

taking into account nitrogen off-resonance effect and assuming that the nitrogen-proton scalar coupling evolution is completely eliminated by the proton decoupling field (see below). Here, ω_{1x} (ω_{1y}) is the angular frequency of the applied ^{15}N pulsing field along *x* (*y*) for the refocusing pulses; $\omega_{1x} = \omega_{1y} = 0$ for free precession. Integration of Eq. (29) is similar to integration of Eq. (24), since both equations are homogeneous and linear differential equations. Thus, the evolution of magnetisation between *b* and *c* of the sequence in Figure 8 is given by:

$$M_c = [\exp(\mathbf{\Gamma_f}\tau_{CPMG})\exp(\mathbf{\Gamma_{py}}\tau_p)\exp(\mathbf{\Gamma_f}\tau_{CPMG})]^N N_y = \hat{\mathbf{R}}N_y, \tag{30}$$

where M_c is the magnetisation at point *c*, τ_p is the length of the 180^o refocusing pulse, and $\mathbf{\Gamma_f}$ is the matrix representation of the Liouvillian that describes free precession, that is, the matrix of Eq. (29)

with $\omega_{1x} = \omega_{1y} = 0$. The Liouvillians describing the evolution during the application of an *x*-pulse or *y*-pulse are represented by $\mathbf{\Gamma_{px}}$ or $\mathbf{\Gamma_{py}}$, respectively, and are given by

$$\mathbf{\Gamma_{px}} \approx -\begin{pmatrix} 0 & \Omega & 0 \\ -\Omega & 0 & \omega_{1x} \\ 0 & -\omega_{1x} & 0 \end{pmatrix}, \tag{31}$$

$$\mathbf{\Gamma_{py}} \approx -\begin{pmatrix} 0 & \Omega & -\omega_{1y} \\ -\Omega & 0 & 0 \\ \omega_{1y} & 0 & 0 \end{pmatrix}, \tag{32}$$

where relaxation during the application of the pulse has been neglected, since in general $R_1\tau_p < R_2\tau_p \ll 1$, however, pulse-imperfections and off-resonance effects are included. The $180^{o}_{\phi 3}$ pulse between *c* and *d* is phase cycled, $\phi 3 = \{x, x, -x, -x\}$, and this pulse is thus assumed to be 'perfect'. Under this set of conditions the total evolution of magnetisation between *b* and *e* is given by:

$$M_e = \hat{\mathbf{K}} M_d \begin{pmatrix} 1 & 0 & 0 \\ 0 & -1 & 0 \\ 0 & 0 & -1 \end{pmatrix} \hat{\mathbf{K}} N_y = \hat{\mathbf{K}} \hat{\pi}_x \hat{\mathbf{K}} N_y. \tag{33}$$

We see from the definitions above that,

$$\hat{\pi}_x \exp(\mathbf{\Gamma_f} \tau_{CPMG}) = [\exp(\mathbf{\Gamma_f} \tau_{CPMG})]^{\dagger} \hat{\pi}_x, \tag{34}$$

$$\hat{\pi}_x \exp(\mathbf{\Gamma_{py}} \tau_p) = [\exp(\mathbf{\Gamma_{py}} \tau_p)]^{\dagger} \hat{\pi}_x \tag{35}$$

where † denotes Hermite-conjugation of the matrix operator. Since $\exp(\mathbf{\Gamma_{py}} \tau_p)$ describes a pure rotation in three-dimensional space it is a unitary operator and thus,

$$\exp(\mathbf{\Gamma_{py}} \tau_p)[\exp(\mathbf{\Gamma_{py}} \tau_p)]^{\dagger} = \begin{pmatrix} 1 & 0 & 0 \\ 0 & 1 & 0 \\ 0 & 0 & 1 \end{pmatrix}. \tag{36}$$

Furthermore, $\mathbf{\Gamma_f}$ is block-diagonal and $\exp(\mathbf{\Gamma_f} \tau_{CPMG})$ can therefore simply be solved by a quadratic equation, leading to:

$$\begin{aligned} &\exp(\mathbf{\Gamma_f} \tau_{CPMG})[\exp(\mathbf{\Gamma_f} \tau_{CPMG})]^{\dagger} \\ &= \begin{pmatrix} \exp(-2R_2\tau_{CPMG}) & 0 & 0 \\ 0 & \exp(-2R_2\tau_{CPMG}) & 0 \\ 0 & 0 & \exp(-2R_1\tau_{CPMG}) \end{pmatrix}, \end{aligned} \tag{37}$$

Combining Eqs. (34)

(35), and (37) with Eq. (33) allows us to integrate the evolution through the entire CPMG pulse sequence from point *a* to *f*; the π pulse forming the mirror plane is coloured red,

$$\hat{\mathbf{K}}\hat{\pi}_{\mathrm{x}}\exp(\boldsymbol{\Gamma}_{\mathbf{f}}\tau_{\mathrm{CPMG}})\exp(\boldsymbol{\Gamma}_{\mathbf{py}}\tau_{\mathrm{p}})\exp(\boldsymbol{\Gamma}_{\mathbf{f}}\tau_{\mathrm{CPMG}})[\exp(\boldsymbol{\Gamma}_{\mathbf{f}}\tau_{\mathrm{CPMG}})\exp(\boldsymbol{\Gamma}_{\mathbf{py}}\tau_{\mathrm{p}})\exp(\boldsymbol{\Gamma}_{\mathbf{f}}\tau_{\mathrm{CPMG}})]^{N-1} =$$
$$[\exp(\boldsymbol{\Gamma}_{\mathbf{f}}\tau_{\mathrm{CPMG}})\exp(\boldsymbol{\Gamma}_{\mathbf{py}}\tau_{\mathrm{p}})\exp(\boldsymbol{\Gamma}_{\mathbf{f}}\tau_{\mathrm{CPMG}})]^{N-1}\exp(\boldsymbol{\Gamma}_{\mathbf{f}}\tau_{\mathrm{CPMG}})\exp(\boldsymbol{\Gamma}_{\mathbf{py}}\tau_{\mathrm{p}})\exp(\boldsymbol{\Gamma}_{\mathbf{f}}\tau_{\mathrm{CPMG}}) \quad (38)$$
$$\exp(\boldsymbol{\Gamma}_{\mathbf{f}}\tau_{\mathrm{CPMG}})^{\dagger}\exp(\boldsymbol{\Gamma}_{\mathbf{py}}\tau_{\mathrm{p}})^{\dagger}\exp(\boldsymbol{\Gamma}_{\mathbf{f}}\tau_{\mathrm{CPMG}})^{\dagger}\hat{\pi}_{\mathrm{x}}[\exp(\boldsymbol{\Gamma}_{\mathbf{f}}\tau_{\mathrm{CPMG}})\exp(\boldsymbol{\Gamma}_{\mathbf{py}}\tau_{\mathrm{p}})\exp(\boldsymbol{\Gamma}_{\mathbf{f}}\tau_{\mathrm{CPMG}})]^{N-1}$$

In the limit where $(R_2 - R_1)\tau_{CPMG}$ is small, the diagonal matrix of Eq. (37) commutes with $\exp(\boldsymbol{\Gamma}_{\mathbf{py}}\tau_{\mathrm{p}})$ and Eq. (38) can be written as:

$$[\exp(\boldsymbol{\Gamma}_{\mathbf{f}}\tau_{\mathrm{CPMG}})\exp(\boldsymbol{\Gamma}_{\mathbf{py}}\tau_{\mathrm{p}})\exp(\boldsymbol{\Gamma}_{\mathbf{f}}\tau_{\mathrm{CPMG}})]^{N-1} \times$$

$$\begin{pmatrix} \exp(-4R_2\tau_{\mathrm{CPMG}}) & 0 & 0 \\ 0 & \exp(-4R_2\tau_{\mathrm{CPMG}}) & 0 \\ 0 & 0 & \exp(-4R_1\tau_{\mathrm{CPMG}}) \end{pmatrix} \times$$

$$\hat{\pi}_{\mathrm{x}}[\exp(\boldsymbol{\Gamma}_{\mathbf{f}}\tau_{\mathrm{CPMG}})\exp(\boldsymbol{\Gamma}_{\mathbf{py}}\tau_{\mathrm{p}})\exp(\boldsymbol{\Gamma}_{\mathbf{f}}\tau_{\mathrm{CPMG}})]^{N-1} \quad (39)$$

Thus, it is now straightforward to follow the same strategy through the remaining N–1 blocks between *a* and *e* to obtain:

$$\hat{\mathbf{K}}\hat{\pi}_{\mathrm{x}}\hat{\mathbf{K}}N_{\mathrm{y}} \approx$$
$$\begin{pmatrix} \exp(-4NR_2\tau_{\mathrm{CPMG}}) & 0 & 0 \\ 0 & \exp(-4NR_2\tau_{\mathrm{CPMG}}) & 0 \\ 0 & 0 & \exp(-4NR_1\tau_{\mathrm{CPMG}}) \end{pmatrix}\hat{\pi}_{\mathrm{x}}N_{\mathrm{y}} \quad (40)$$
$$= -\exp(-4R_2N\tau_{\mathrm{CPMG}})\,N_{\mathrm{y}}$$

The in-phase CPMG relaxation dispersion experiment in Figure 8 therefore very efficiently compensates for off-resonance effects and pulse-imperfections. The in-phase sequence, however, does not compensate for the fact that the magnetisation spends more time along the *z*-axis (R_1 relaxation) for higher CPMG ν_{CPMG} frequency, which is evident from the assumption made above, that is $(R_2 - R_1)\tau_{CPMG}$ is small. For medium sized proteins, ~10-15 kDa, the error introduced in the relaxation dispersion due to $R_2 - R_1 \neq 0$ is normally on the order of 1 s^{-1} (D. F. Hansen, Vallurupalli, & Kay, 2008a) and can easily be taken into account in the analysis of the data (D. F. Hansen, Vallurupalli, Lundström, et al., 2008).

The in-phase relaxation dispersion CPMG experiment relies on accurate decoupling of the nitrogen-proton scalar coupling during the constant-time CPMG element. Prior to the introduction of the relaxation-compensated CPMG experiment such decoupling was achieved by adjusting τ_{CPMG} so that an integer number of, e.g. WALTZ, decoupling cycles would fit into each inter-pulse delay of length $2\tau_{CPMG}$. The in-phase CPMG sequence employs a similar strategy with the exception that a continuous-wave field is applied, such that $\nu_{CW} = 2k\nu_{CPMG}$, where k is an integer and ν_{CW} is the field strength (in Hz) of the proton decoupling. This choice of ν_{CW} means, if the CW field is seen as a series of 180° pulses back-to-back (Vallurupalli, Scott, Williamson, & Kay, 2007), that an even number of 180° decoupling pulses are applied between each pair of 180° nitrogen refocusing pulse.

The main advantage of using a CW decoupling, as compared to e.g. a WALTZ decoupling, is that higher ν_{CPMG} (smaller τ_{CPMG}) can be employed.

2.2 Carbon and proton based relaxation dispersion experiments

Relaxation dispersions of ^{15}N nuclei in proteins offer a wealth of information about chemical exchange processes, in particular, the ^{15}N-based experiments allow for extraction of chemical exchange parameters such as p_B and k_{ex}, that have now been determined for many biochemical events, such as, protein folding, enzyme catalysis, and ligand binding. However, the ^{15}N chemical shift that is obtained for the low-populated states from these experiment contains limited information about the structure (Le & Oldfield, 1994), in particular, limited information about the secondary structure of these states. In contrast, the chemical shift of backbone carbon nuclei, such as, $^{13}C'$ and $^{13}C_\alpha$, are faithful reporters on the secondary structure of the protein. Thus, it has been known for a long time that being able to probe carbon chemical shifts of low-populated states is critical for characterising the structure of these states.

Alpha-carbon relaxation dispersions: The $^{13}C_\alpha$ chemical shifts of low-populated states can be obtained using an in-phase CPMG relaxation dispersion experiment similar to the one shown above for ^{15}N, (D. F. Hansen, Vallurupalli, Lundström, et al., 2008) with proton decoupling of the $^{1}H_\alpha$-$^{13}C_\alpha$ scalar coupling adjusted to match the CPMG frequency and with benefit from the self-compensation provided by the 180º in the centre of the sequence. The major difference between the proposed method to obtain $^{13}C_\alpha$ relaxation dispersions, as compared to the ^{15}N dispersions, is that selective isotope labelling of $^{13}C_\alpha$ is imperative in order to eliminate homonuclear ^{13}C-^{13}C scalar coupling evolutions during the CPMG element. If allowed to evolve, such homonuclear ^{13}C-^{13}C couplings would cause modulations of the relaxation dispersion profile and consequently obscure the information about the chemical exchange process. Selective $^{13}C_\alpha$ labelling can be achieved either by adding selectively labelled amino acids to the growth media (Hill et al., 2000) or by using [2-^{13}C]-glucose as the sole carbon source (Lundström, Teilum, et al., 2007). A maximum of 50% enrichment of the C_α positions can be achieved using [2-^{13}C]-glucose since effectively two molecules of 3-phosphoglycerate (one labelled and one unlabelled) are produced from each glucose molecule. Moreover, the C_α position of isoleucine and valine cannot be probed because of simultaneous labelling of C_α and C_β, while C_α of leucine is not enriched. Yet, relaxation dispersions of 17 of the 20 amino-acids can be obtained using this method. An improvement that was added to the recently published $^{13}C_\alpha$ pulse scheme (D. F. Hansen, Vallurupalli, Lundström, et al., 2008) is that the transfer of magnetisation from in-phase ^{1}H to in-phase ^{13}C is achieved using a hetCP DIPSI transfer (Brown & Sanctuary, 1991; Zuiderweg, 1990) that, when applied at a sufficient high field, minimizes the relaxation due to chemical exchange during the transfer.

Relaxation dispersions of carbonyl carbon in proteins: One major challenge for characterising ^{13}C' relaxation dispersions of uniformly ^{13}C-labelled samples is that the homonuclear scalar coupling between ^{13}C' and $^{13}C_{\alpha}$ hampers accurate quantification of the chemical exchange parameters, since this coupling modulates the relaxation dispersion profile; unless special care is taken. Ishima and Torchia (Ishima et al., 2004) suggested two different approaches to suppress the scalar ^{13}C'-$^{13}C_{\alpha}$ coupling evolution during the relaxation dispersion experiment, that is, (*i*) employing specific [^{13}C',U-^{12}C,^{15}N] labelling or (*ii*) applying selective $180°$ refusing pulses during the CPMG elements, such that the scalar $^{13}C_{\alpha}$-^{13}C' coupling is refocused in each $\{\tau_{CPMG} - 180° - \tau_{CPMG}\}$ step.

A series of ^{13}C' CPMG relaxation pulse-sequences were later developed for ^{13}C' specific labelled samples (D. F. Hansen, Vallurupalli, Lundström, et al., 2008), which utilizes the $90°$ phase-shifted $180°$ pulse in the middle of the CPMG sequence to self-compensate for pulse-imperfections and off-resonance effects, such that odd numbers of N can be used.

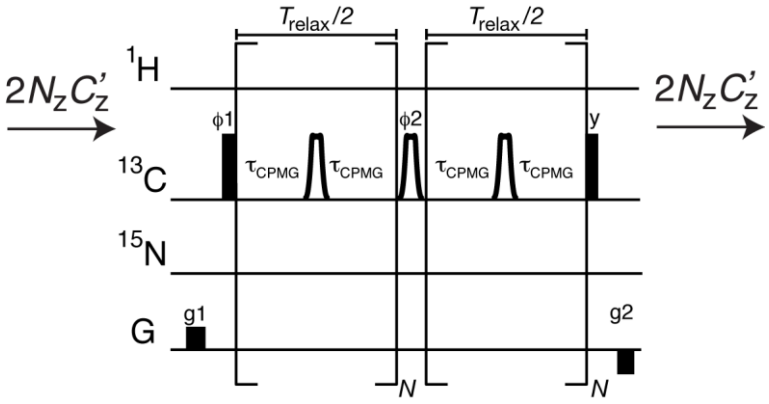

Figure 9: Magnetisation transfer from ^{15}N to ^{13}C' occurs prior to the sequence shown, where in particular ^{15}N magnetisation is refocused with respect to ^{1}H and de-phased with respect to ^{13}C' to generate a coherence of the form $2N_zC'_z$. The shaped ^{13}C' selective pulses during the CPMG element are either of RE-BURP shaped (Geen & Freeman, 1991), Gaussian shaped, or an optimised ^{13}C' selective shaped pulse (Lundström, Hansen, & Kay, 2008). The ^{13}C' selective pulse is typically applied at 177 ppm with a bandwidth of ~10 ppm, in order to refocus the ^{13}C', while not perturbing the residual aliphatic ^{13}C spin. The phase cycle is: $\phi_1=\{y, -y, y, -y\}$, $\phi_2=\{y, y, -y, -y\}$, $\phi_{rec}=\{x, -x, x, -x\}$.

Figure 9 shows the central part of the ^{13}C' constant-time relaxation dispersion pulse scheme for measuring millisecond time-scale dynamics in ^{15}N-, ^{13}C'-selectively labelled proteins (D. F. Hansen, Vallurupalli, Lundström, et al., 2008). The use of ^{13}C'-selective pulses during the CPMG element refocuses small (two or more bond) C'-aliphatic carbon couplings that arise from the labelling scheme employed. The evolution of the ^{13}C'-^{15}N scalar coupling is in this sequence only refocused by the ^{13}C' pulses and consequently the ratio of anti-phase $2C'_{xy}N_z$ and in-phase C'_{xy} magnetisation will depend on

the specific CPMG frequency ν_{CPMG}. The difference in intrinsic relaxation rate of the $2C'_{xy}N_z$ anti-phase and C'_{xy} in-phase coherences is in general very small and can in most cases be ignored or taken explicitly into account in the further analysis of the resulting relaxation dispersion curves. Evolution of the ^{13}C'-^{1}H$_N$ scalar coupling (~4 Hz) would lead to the creation of anti-phase coherences that relax significantly faster, $2C'_{xy}H_z$ and $4C'_{xy}N_zH_z$, however, the small ^{13}C'-^{1}H$_N$ scalar coupling constant limits this evolution, which furthermore is refocused by the $180°$ ^{13}C' refocusing pulses. In some cases the evolution of the ^{13}C'-^{1}H$_N$ coupling due to the through-space residual dipolar couplings has been exploited for structure determinations of low-populated states and sequences similar to the one shown in Figure 9 that probe the $4C'_{xy}N_zH^{|\alpha>}$ and $4C'_{xy}N_zH^{|\beta>}$ relaxation dispersions separately have been designed for these purposes (D. F. Hansen, Vallurupalli, & Kay, 2008b).

The sequence shown in Figure 9 requires specific ^{13}C' labelled proteins. Briefly, specific ^{13}C' labelling can be achieved either from adding specifically isotope-labelled amino acids to the growth media or by supplementing the growth media with [1-^{13}C]-pyruvate and H$^{13}CO_3^-$ (Lundström et al., 2008). While adding specifically labelled amino acids can lead to high enrichments, such an approach is often very expensive and thus not practical for quantifying secondary structures of low-populated states. ^{13}C' labelling via supplementing the growth media (Lundström et al., 2008) with [1-^{13}C]-pyruvate unfortunately also has some shortcomings: The ^{13}C' of leucine and histidine are not enriched and amino acids that are derived from the precursors oxaloacetate or α-ketoglutarate are only enriched to approximately 25-33%. The relatively poor enrichment of ^{13}C' using these methods results in loss of sensitivity, in particular for protein samples that are not amenable to higher concentrations. Alternative approaches for quantifying the ^{13}C' relaxation dispersions from uniformly ^{13}C labelled proteins have therefore been developed (Lundström et al., 2008).

Methods to probe the ^{13}C' relaxation dispersion in uniformly ^{13}C labelled samples heavily rely on the application of selective pulses throughout the pulse scheme; Figure 10.

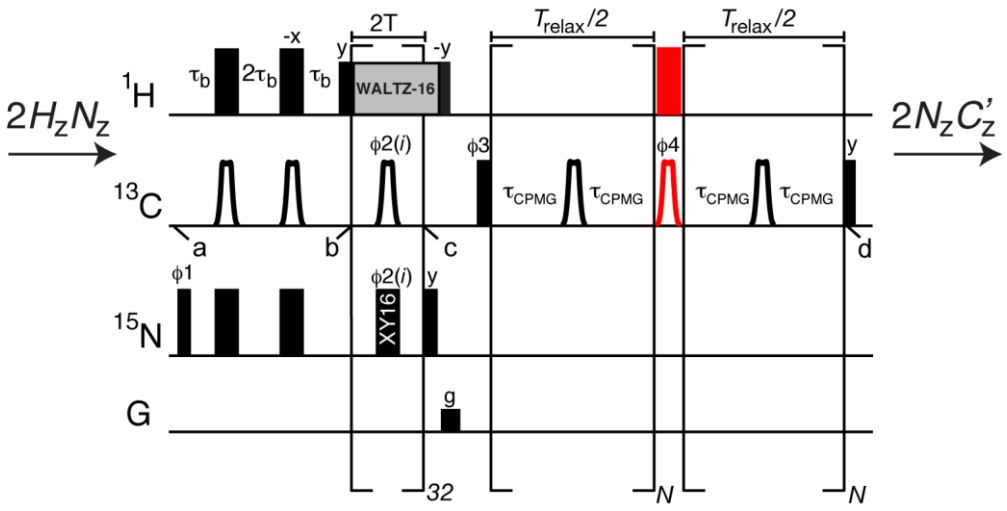

Figure 10: The central part of the pulse scheme for quantifying ^{13}C' CPMG relaxation dispersions in U-[^{13}C,^{15}N] isotope labelled proteins (Lundström et al., 2008). ^{1}H, ^{13}C and ^{15}N 90° (180°) pulses are shown as narrow (wide) bars. The ^{1}H carrier is placed on the water signal, the ^{15}N RF carrier at 119 ppm, while the ^{13}C carrier is centred at 176 ppm. Pulse phases are assumed *x*, unless otherwise stated. The 90° ^{13}C pulses are made ^{13}C' selective by applying at a field strength of $\Delta\Omega/\sqrt{15}$, $\Delta\Omega$ = 118 ppm. The selective pulses applied to ^{13}C' during the N –> C' transfer (*a*-to-*c*) and during the CPMG periods (*c*-*d*) are of a duration of {450 μs, 450 μs, 380 μs} at {500 MHz, 600 MHz, 800 MHz}, respectively. These pulses are specifically optimised not to excite the magnetisation of aliphatic carbons and also have a very flat excitation profile around the ^{13}C' chemical shifts (176 ±10 ppm). From *a* to *b* the ^{15}N magnetisation is refocused with respect to the ^1H_N and initial defocussing with respect the ^{13}C' takes place, which continues from *b* to *c*. From *b* to *c* the application of simultaneous ^{13}C and ^{15}N pulses at a frequency of, in this case 800 Hz, partially quenches the chemical exchange that occurs on the millisecond time scale (Mulder, Spronk, Slijper, Kaptein, & Boelens, 1996). The simultaneous pulses applied have phases $\phi2(i)=2\{x, y, x, y, y, x, y, x, -x, -y, -x, -y, -y, -x, -y, -x\}$ so as to minimise off-resonance effects and pulse imperfections. ^{1}H WALTZ decoupling is applied to avoid the evolution of the ^{1}H-^{15}N scalar coupling during the ^{15}N –> ^{13}C' transfers. The delays are, τ_b= 1.38 ms, T = 10 ms. The gradient g is applied with a strength of ~ 7 G/cm for 1 ms. The refocusing pulses shown in red serve the same purpose as the central 90° shifted 180° pulse of the in-phase relaxation dispersion experiment described above, i.e., that of minimizing off-resonance effects and pulse-imperfections. These central 180° pulses can be exchanged for an element that partially suppresses ^{13}C'-^{13}CO couplings, which becomes significant for Asp and Asn residues, where the scalar coupling between the backbone ^{13}C' and the side-chain ^{13}CO can deteriorate the relaxation dispersion profile.

The ability to obtain accurate ^{13}C' relaxation dispersion profiles in [U-^{13}C, ^{15}N] labelled proteins becomes particular important when investigating the structure of low-populated states, since the ^{13}C' relaxation dispersions can be obtained from the same sample as the ^{15}N dispersions. Ideally, a [U-^{13}C, U-^{15}N, U-^{2}H,^1H_N] isotope labelled sample is generated, which can be used to derive the ^{13}C', ^{15}N, and ^1H_N relaxation dispersion profiles (Lundström, Vallurupalli, Hansen, & Kay, 2009).

Proton relaxation dispersions: The chemical shifts of ^{1}H amide protons, derived from the samples mentioned above and using relaxation compensated pulse sequences (Ishima & Torchia, 2003), depend in a complex manner on the specific protein structure. For example, the amide proton chemical shifts are sensitive to both hydrogen bond-length, solvent accessibilities, and backbone ϕ_i/ψ_{i-1} dihedral angles (Shen & Bax, 2007; Xu & Case, 2002). On the other hand the $^{1}H_{\alpha}$ chemical shift is a very specific reporter on the secondary structure, since it is mainly predicted from the ϕ_i/ψ_i dihedral angles (Ando, Saito, Tabeta, Shoji, & Ozaki, 1984; Spera & Bax, 1991; Wishart & Case, 2001). Although the $^{1}H_{\alpha}$ chemical shift also can depend on aromatic ring-current (Neal, Nip, Zhang, & Wishart, 2003; Wishart & Case, 2001), these chemical shift are very valuable in general, and in particular for low-populated states where $^{1}H_{\alpha}$ chemical shift becomes particularity important in order to quantify their secondary structures.

Probing alpha-proton chemical shifts of low-populated states: Accurate reporters of the secondary structure of proteins are $^{13}C_{\alpha}$ and $^{1}H_{\alpha}$, whose chemical shifts have been used to predict the secondary structure of proteins over the last ~two decades (Wishart & Sykes, 1994). Thus, having access to the chemical shift of $^{1}H_{\alpha}$, in addition to the $^{13}C_{\alpha}$ chemical shifts, of low-populated states adds significantly to the accuracy by which the structure of these states can be determined. Pulse sequences and isotope labelling schemes have therefore been developed to allow for accurate measurements of such chemical shifts (Lundström, Hansen, Vallurupalli, & Kay, 2009).

The main obstacle for obtaining accurate chemical exchange parameters of $^{1}H_{\alpha}$ in protonated proteins is that of scalar couplings with other protons in the immediate vicinity of the $^{1}H_{\alpha}$ nuclei of interest. For example, the scalar $^{1}H_{\alpha}$-$^{1}H_{\beta}$ and $^{1}H_{\alpha}$-$^{1}H_{N}$ couplings are not (completely) refocused by the application of 180° pulses and, moreover, the transfer of magnetisations between the $^{1}H_{\alpha}$ of interest and other proton spins depend on their chemical shift differences and on ν_{CPMG}, which further complicates the situation. The $^{1}H_{\alpha}$-$^{1}H_{N}$ scalar coupling can in most instances be removed by dissolving the protein in D_2O and thus the substitution of the amide protons for deuterons will remove this homonuclear coupling. However, the $^{1}H_{\alpha}$-$^{1}H_{\beta}$ scalar coupling and couplings with other aliphatic protons will still cause a modulation of the relaxation dispersion curve that, in turn, prevents the extraction of accurate chemical exchange parameters. Currently, the most efficient method to suppress the effect of $^{1}H_{\alpha}$-$^{1}H_{\beta}$ scalar couplings on relaxation dispersion profiles is fractionate deuteration of the $^{1}H_{\beta}$ positions by overexpression in a 50%/50% H_2O/D_2O minimal medium using $^{13}C_6D_7$-deuterated glucose. Depending on residue type, deuteration levels of 50%-80% can be achieved for $^{1}H_{\beta}$. Residual homonuclear couplings that arise from protonated non-$^{1}H_{\alpha}$ spins can be further suppressed by the *J*-refocusing filter depicted in Figure 11, this follows the idea discussed above in Figure 7.

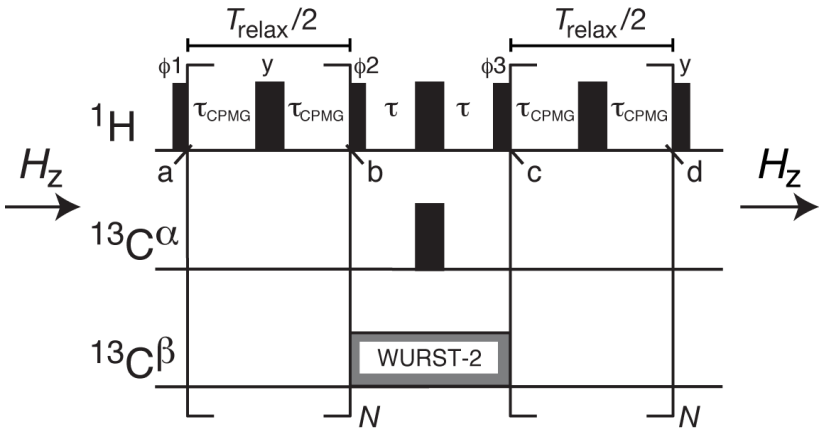

Figure 11: The central part of the pulse scheme used to obtain $^1H_\alpha$ CPMG relaxation dispersions in [U-^{13}C, U-^2H_N, 50%/50% ^{2}H/^{1}H] labelled proteins (Lundström, Hansen, et al., 2009). 90° (180°) RF pulses are shown as narrow (wide) black bars. The ^{1}H RF-carrier is placed on the water (4.77 ppm) and the ^{13}C RF-carrier is at 58 ppm, which is in the middle of the $^{13}C_\alpha$ region. All pulse phases are assumed to be *x* unless indicated otherwise. The element between the two CPMG blocks suppresses the J_{H_α,H_β} scalar coupling evolutions, where $\tau = 1/(2\,J_{H_\alpha C_\alpha})$ ~ 3.52 ms. $^{13}C_\beta$ decoupling is achieved with a WURST-2 (Kupce & Freeman, 1995) centred at 27.5 ppm and with a bandwidth of 25 ppm, max(rms) field strength of 1.22(0.69) kHz. The $^{13}C_\beta$ of threonine and serine are not decoupled using this scheme and these residues are therefore unavailable for analysis. The phase cycle is: $\phi 1 = \{x, -x\}, \phi 2 = \{x, x, -x, -x\}, \phi 3 = \{-x, -x, x, x\}, \phi_{rec} = \{x, -x, x, -x\}$.

The element that is present between the two CPMG blocks in Figure 11 is required to refocus the $^1H_\alpha$-$^1H_\beta$ scalar couplings, and has been designed both in the limit of slow pulsing (weak coupled spins) and in the limit of fast pulsing (~ strongly coupled spins). As an example, we consider here the slow pulsing regime and thus weakly coupled spins; a similar analysis for the fast pulsing regime is given elsewhere (Lundström, Hansen, et al., 2009). During the first CPMG block of length $T_{relax}/2$, and with focus on the homonuclear $^1H_\alpha$-$^1H_\beta$ coupling, the in-phase $^1H_\alpha$ magnetisation evolve according to,

$$H_z^\alpha \xrightarrow{90_x} -H_y^\alpha \xrightarrow{N\times\{\tau_{\mathrm{CPMG}}-180_y-\tau_{\mathrm{CPMG}}\}}$$

$$-H_y^\alpha \cos\left(\pi J_{H_\alpha H_\beta} T_{\mathrm{relax}}/2\right) + 2H_x^\alpha H_z^\beta \sin\left(\pi J_{H_\alpha H_\beta} T_{\mathrm{relax}}/2\right) \qquad (41)$$

where we have neglected pulse-imperfections and off-resonance effects, such that the 180° proton pulse refocuses both $^1H_\alpha$ and $^1H_\beta$ spins. The purpose of the *J*-refocusing element is to invert the $^1H_\alpha$-$^1H_\beta$ scalar coupling evolutions during the second half of the CPMG experiment. This refocusing is achieved by inverting the H_y^α coherence, while conserving the $2H_x^\alpha H_z^\beta$ coherence. Critical to the element is the selective $^{13}C_\beta$ decoupling, which allows a selective inversion of the $^1H_\beta$ magnetisation relative to the $^1H_\alpha$ magnetisation. In particular, the $^{13}C_\beta$ decoupling suppresses the evolution of the $^1H_\beta$ coherences due to the $^1H_\beta$-$^{13}C_\beta$ scalar coupling, where in contrast, transverse $^1H_\alpha$ coherences can

selectively evolve with the $^1H_\alpha$-$^{13}C_\alpha$ scalar coupling, thus driving the selective inversion of these spins. The action of the element on the in-phase and anti-phase coherences is as follows:

$$H_y^\alpha \xrightarrow{90_x} H_z^\alpha \xrightarrow{\tau-180_x(C_\alpha)-180_y-\tau} -H_z^\alpha \xrightarrow{90_{-x}} -H_y^\alpha ,$$

$$2H_x^\alpha H_z^\beta \xrightarrow{90_x} -2H_x^\alpha H_y^\beta \xrightarrow{\tau-180_x(C_\alpha)-180_y-\tau} -2H_x^\alpha H_y^\beta \xrightarrow{90_{-x}} 2H_x^\alpha H_z^\beta . \quad (42)$$

It is now straightforward to see that the effect of the homonuclear $^1H_\alpha$-$^1H_\beta$ scalar coupling has been refocused and evolution of these homonuclear couplings during the second CPMG block will cancel the evolution that took place during the first CPMG block. A combination of the homonuclear *J*-refocusing and fractional deuteration allows accurate chemical shifts of $^1H_\alpha$ to be obtained in low-populated states (Lundström, Hansen, et al., 2009).

It should be noted that the $^1H_\alpha$ relaxation dispersions of serine and threonine cannot be obtained using the approach described above, because the $^{13}C_\beta$ chemical shifts of these residues are outside the typical range; the C_β decoupling applied during the *J*-refocusing element will therefore not decouple the $^{13}C_\beta$ of threonine and serine residues. Moreover, even though there are no H_β nuclei present in glycine residues, the fact that the two $^1H_\alpha$ protons are scalar coupled to the same $^{13}C_\beta$ and scalar coupled to each other, deteriorates the resulting relaxation dispersions. Specific glycine-$^1H_\alpha$ relaxation dispersion experiments have therefore been developed (Vallurupalli, Hansen, Lundström, & Kay, 2009).

Relaxation dispersions of methyl-groups and applications to large proteins: Methyl-groups provide unique probes of the hydrophobic core of proteins and thus offer a unique opportunity to probe the structure and dynamics of the hydrophobic core of low-populated states. Most CPMG relaxation dispersion experiments designed for probing millisecond dynamics of methyl-groups rely on $^{13}C^1H_3$-selective isotope labelling of the protein of interest; we will therefore only discuss experiments that have been designed for such selectively labelled samples.

One of the first NMR pulse sequences to quantify methyl-carbon chemical shifts of low-populated states utilised initial magnetisation from in-phase ^{13}C polarizations (Skrynnikov et al., 2001); and a flow of magnetisation that can be summarised by ^{13}C –> CPMG –> $t_1(^{13}C)$ –> $t_2(^1H)$. Compared to the isolated two-spin system ^{15}N-^1H discussed above, the energy levels and the corresponding cross-correlated relaxations pathways present within the $^{13}C^1H_3$ methyl group are significantly more complex. Yet, Skrynnikov et al. (Skrynnikov et al., 2001) showed that an element very similar to the *P*-element (Figure 5) combined with a constant-time CPMG relaxation dispersion experiments allows for extraction of accurate methyl carbon chemical shifts of low-populated states. It was later shown that significant increases in sensitivity of the single-quantum methyl relaxation dispersions can be achieved by using initial proton polarisation and a flow of magnetisation summarised by

magnetisation ^{1}H –> ^{13}C –> CPMG –> $t_1(^{13}C)$ –> $t_2(^{1}H)$ (Lundström, Vallurupalli, Religa, Dahlquist, & Kay, 2007). Several other single-quantum methyl-CPMG relaxation dispersion experiments have been developed over the last years based on these original ideas. These include, CPMG experiments probing the dispersion of the individual components of the ^{13}C quartet (Kontaxis & Bax, 2001) in order to derive residual dipolar couplings (Baldwin et al., 2009) or pico-nanosecond dynamics (D. F. Hansen, Vallurupalli, & Kay, 2009) of the low-populated state. Moreover, advanced labelling schemes now allow selective labelling of methyl-groups isotopermers such as, $^{13}CD_2H$, allowing the application of sequences originally developed for two-spin systems (Baldwin, Religa, Hansen, Bouvignies, & Kay, 2010).

Methyl-groups are also unique in the sense that they allow for a probing of both the structure (D. F. Hansen & Kay, 2011) and the dynamics (Baldwin et al., 2010; Sprangers & Kay, 2007; Tzeng & Kalodimos, 2009) of super-molecular machines. Obtaining relaxation dispersions of these machines opened up the possibility for characterisations that, until recently, were considered just a dream. It was the joint effort of both new isotope-labelling schemes and new CPMG relaxation dispersion pulse sequences that were developed over the last decade that have now made this dream come true. The cornerstone of these experiments is specific [U-^{2}H, $^{13}C^{1}H_3$-] labelling, exploitation of the methyl-TROSY effect, and quantification of multi-quantum coherences, whose relaxations are not affected by spin-spin relaxation mechanism ($J(0)$ terms do not appear in the relaxation of multi-quantum coherences). The CPMG relaxation dispersion experiment for probing large molecules therefore probes the relaxation dispersion of ^{13}C-^{1}H multi-quantum coherence. Since the chemical shift evolution of multi-quantum coherences depend on two chemical shifts, *i.e.*, that of the proton and the carbon, the resulting relaxation dispersion profile does not always have the same shape as those seen for single-quantum relaxation dispersions. Yet, the multi-quantum dispersions often give indispensable information about the low-populated states (Sprangers & Kay, 2007).

Spin-locking relaxation dispersion experiments: Qualitatively, a CPMG relaxation dispersion and thus a decrease in $R_{2,eff}$ with increasing ν_{CPMG}, is observed because the effective and 'time-average' chemical shift difference between the two chemically exchanging sites is suppressed. A similar decrease in the effective chemical shift difference can be obtained using a constant-power spin-lock as opposed to a series of high-power 180° pulses. The similarity between the spin-lock experiment and the CPMG experiment becomes even more apparent in the limit of very high ν_{CPMG}, where the 180° pulses are applied nearly back-to-back. Spin-lock relaxation dispersions curves, $R_{1\rho}$ *vs.* ω_1, that are very similar to CPMG relaxation dispersion curves have been obtained (Korzhnev, Orekhov, et al., 2005) and chemical exchange parameters such as k_{ex}, p_B and $\Delta\omega$ can be derived from these curves in a similar manner that parameters are derived from CPMG relaxation dispersions curves. One advantage of using spin-lock experiments, as compared to CPMG relaxation, is that much larger

effective fields, ω_{eff}, can be applied to the spin in questions by exploiting off-resonance spin-locking where the spin-lock field together with the chemical shift offset from the carrier both adds to the effective field (Lundström & Akke, 2005; Massi et al., 2005).

2.3 Deriving the sign of $\Delta\omega$

The CPMG relaxation dispersion experiments discussed above generally report on the *absolute chemical shift difference* between chemically exchanging states. In order to use the chemical shifts of a low-populated state for secondary structure predictions and structure calculations using chemical shift-based computational approaches (Cavalli, Salvatella, Dobson, & Vendruscolo, 2007; Shen et al., 2008; Shen, Delaglio, Cornilescu, & Bax, 2009), the chemical shift of the low-populated state and consequently the *signed chemical shift difference* between the two states needs to be determined. Several approaches have therefore been developed to determine the sign of the chemical shift difference, $\Delta\omega$. One approach for determining the sign of $\Delta\omega$ relies on the fact that the nucleus of interest is in the intermediate exchange regime. In the fast exchange regime the major peak is observed at a population average position, $p_A\omega_A + p_B\omega_B$, while in the slow exchange regime the major peak is observed at the high-populated state's chemical shift, ω_A. For intermediate exchange the major peak will thus be observed somewhere between $p_A\omega_A + p_B\omega_B$ and ω_A and moving the exchange regime by changing $\Delta\omega$ (in Hz) moves the position (in ppm) of the major peak. In practise this means that a correlation spectrum is recorded at two different magnetic field strengths, for example 11.7 T (500 MHz) and 18.8 T (800 MHz), and the chemical shift of the observed state will in many cases move slightly. The shifts observed between two magnetic fields are in general smaller than the line-width of the nucleus in question; yet, the resulting derived signs are very accurate.

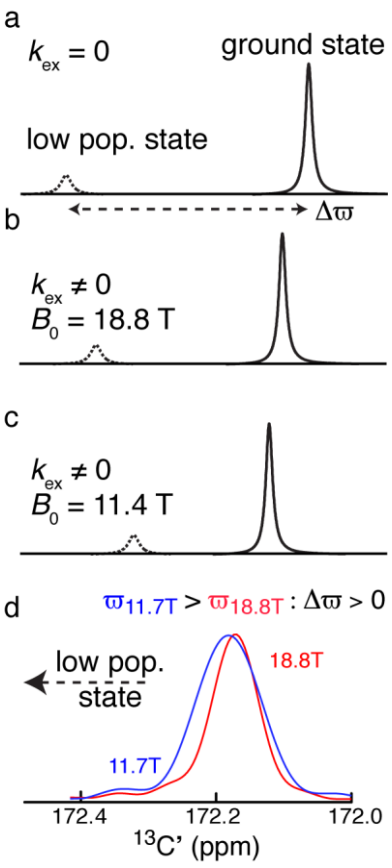

Figure 12: Recording a spectrum at two different magnetic field strengths can in many cases, even when $p_B \ll 1$, allow for a determination of the sign of $\Delta\omega$. In the above example, the sign of chemical shift difference is obtained by the method of Skrynnikov et al. (Bouvignies et al., 2010; Skrynnikov et al., 2002) that compares peak positions of ^{1}H, ^{15}N, and ^{13}C' in correlation spectra recorded at different magnetic fields. The top three panels show the ground state and the low populated state chemical shifts (a) in the absence of chemical exchange (b) at high magnetic fields, e.g. 18.8 T, and (c) at a lower magnetic field, e.g. 11.4 T. (d) Cross-peaks of the major state are closer to correlations in the low populated state at lower magnetic field and hence $\Delta\omega > 0$ in the example provided.

Alternative approaches for obtaining the sign of $\Delta\omega$ have been developed recently and rely on a $R_{1\rho}$ type experiment (Auer et al., 2009; Korzhnev, Orekhov, et al., 2005). In line with a saturation-transfer experiment, $R_{1\rho}$ rates are measured off-resonance of the major peak in questions and the resulting rates from each side of the observed resonance are compared to derive the sign. For example, if the $R_{1\rho}$ rate on the upfield side of the major peak is faster than the corresponding rate on the downfield side, then the low-populated state chemical shift is upfield of the major peak.

Alternative approaches for obtaining the chemical shifts of low-populated states: Saturation transfer experiments have long been used to probe 'invisible' and low-populated states. Some of the early applications involved the determination of chemical shifts of paramagnetic blue copper proteins,

where the interaction between the nuclei of interest and an unpaired electron hindered the direct observation of the hyperfine shifted nuclei (Bertini, Lucinat, & Parigi, 2001). The specific chemical shift of such nuclei in the immediate vicinity of a paramagnetic site can prove very valuable in the investigation of the structure of paramagnetic proteins (Bertini et al., 1999; D. F. Hansen et al., 2012). Bertini and co-workers (Bertini et al., 1999) therefore developed an approach where a saturation field was applied 'in the blind' to the invisible paramagnetic signals of the blue copper protein plastocyanin, and transfer of saturation was observed for the corresponding diamagnetic signals. The saturation transfer had in this case become possible because a mixed sample of diamagnetic (Cu(I)) and paramagnetic (Cu(II)) protein was produced and the electron self-exchange of plastocyanin provided the chemical exchange and thus the transfer of saturation from the paramagnetic to the diamagnetic site. Later the same method was used to obtain the line-width of the paramagnetic shifted signals (D. F. Hansen & Led, 2006). One obvious benefit of the saturation transfer method, as compared to the conventional CPMG approach, is that the chemical shifts and to some extent the line-widths of the low-populated/invisible state are direct outcomes of the experiment making additional sign-experiments unnecessary.

The saturation transfer approach was recently, and elegantly, taken one step further and applied to study the dynamics of amyloid fibres (Fawzi, Ying, Ghirlando, Torchia, & Clore, 2011). In particular, these experiments were designed with the main aim of deriving the line-widths that report on the dynamics of the low-populated state. More recently this idea was taken yet another step further by Vallurupalli et al. in the CEST experiments (Vallurupalli, Bouvignies, & Kay, 2012) and used to observe the chemical shift and transverse relaxation of low-populated folding intermediates through a saturation transfer technique. The advantage of the CEST experiments as compared to the CPMG relaxation dispersion experiments and the spin-lock experiments is that both the signed chemical shift and the line-width of the resonances corresponding to the low-populated state are directly assessable in the experiment. One current disadvantage of the CEST-type experiments is the more limited time-scale of chemical exchange processes that can be probed.

3 Overview of the different methods to probe chemical exchange

The time-scale of chemical exchange: The experimental setup and in particular the specific choice of pulse sequence to be used depends critically on the time-scale of the chemical exchange under investigation. For very slowly exchanging systems, $k_{ex} \approx 1\,s^{-1} - 10\,s^{-1}$, and when the NMR signals of all the exchanging sites can be observed directly, the longitudinal chemical exchange experiments can provide valuable information (Farrow, Zhang, Forman-Kay, & Kay, 1994; Morrison et al., 2012). Specifically, when a nucleus exchanges slowly between two distinct sites, and consequently gives rise to two discrete peaks in the NMR spectrum, the longitudinal chemical exchange experiment can give a direct link between the two peaks in form of an exchange cross-peak.

By introducing a variable delay, during which the chemical exchange is monitored via the intensity of the resulting exchange cross-peaks, allows a determination of the chemical exchange rate constants. For slightly faster exchange events, $k_{ex} \approx 10\ s^{-1} - 400\ s^{-1}$, the newly developed CEST experiment (Vallurupalli et al., 2012; Ward, Aletras, & Balaban, 2000) is a very sensitive method to directly derive the exchange rate constant, the populations of the exchanging sites, the signed-chemical shift difference between the exchanging sites, and in some cases also the intrinsic transverse relaxation rate of each of the exchanging sites (Fawzi et al., 2011). However, the CEST method currently only covers exchange rates k_{ex} in the range from approximately 10 s^{-1} to 400 s^{-1} (Vallurupalli et al., 2012). The CPMG relaxation dispersion, which is the main focus here, covers the broader range of chemical exchange events with k_{ex} from ~50 s^{-1} to 2500 s^{-1} (D. F. Hansen, Vallurupalli, Lundström, et al., 2008). When the exchange rate exceeds ~ 2500 s^{-1}, and thus when approaching the fast-exchange regime, the derived exchange parameters from the relaxation dispersion curves often get correlated. In particular, the chemical shift difference, $\Delta\omega$, and the population of the exchanging sites, p_B, are often strongly correlated in such cases, that only the product $p_B\Delta\omega^2$ can be obtained accurately. Recent developments, in particular the elegant combination of CPMG relaxation dispersions with exchange-induced chemical shift, allows processes with k_{ex} up to approximately 6000 s^{-1} to be probed, since the combination of the two measurements, exchange-induced shift and relaxation dispersion, to some extent breaks the correlation between the derived parameters. The spin-lock $R_{1\rho}$ relaxation experiment is currently the preferred experiment to probe fast exchange processes, where k_{ex} up to ~ $5 \times 10^4\ s^{-1}$ have been measured (Evenäs, Malmendal, & Akke, 2001; Palmer III & Massi, 2006). The advantage of the $R_{1\rho}$ relaxation dispersion experiment is that high spin-lock fields, (large ω_1), can be applied off-resonance of the nucleus in questions, (large ω_B), thereby modulating the term $k_{ex}^2 + \omega_B^2 + \omega_1^2$ in Eq. (21) even for large values of k_{ex}.

Information provided by the different experiments: Several relaxation dispersion pulse sequences, with associated isotope labelling schemes, have been developed over the last decade, some of which were described in detail above. The specific choice of method and pulse sequence to use will depend on many factors, such as, the specific scientific question in mind, stability of the samples used and the underlying nature of the chemical exchange event in question. Most of the initial applications of relaxation dispersions to probe chemical exchange of biomolecules were nitrogen relaxation dispersion experiments, using uniformly ^{15}N isotope labelled samples. Although these ^{15}N-based experiments are the most sensitive and were the forerunners for many applications to come, the resulting chemical shifts of the low-populated states provide only limited information about the structure of these states. Yet, based on their high sensitivity, the ^{15}N-based experiments are most often used when the underlying thermodynamics and/or kinetics of the chemical exchange event are sought after. CPMG relaxation dispersion experiments that probe the chemical exchange via other nuclei

must be employed, when a detailed structure of the low-populated state, and structural transitions between the ground state and the low-populated state are the focal point. It has long been known that carbon chemical shifts are accurate reporters on the local structure, and C_α and C' chemical shifts of low-populated states provide valuable insight into their secondary structure. Furthermore, when the carbon chemical shifts are combined with the chemical shift of H_α and to some extent H_N a good and reliable prediction of the local structure can be obtained using database-based tools such as TALOS+ (Shen et al., 2009). However, in order to determine an accurate overall structure, as opposed to just the local structure, structural restrains that report on the global structure are often desirable. Thus, when the overall structure and fold of the low-populated state are significantly different from the ground state, bond-vector orientations in the form of residual dipolar couplings (RDCs) and residual chemical shift anisotropies (RCSAs) can be obtained. Specifically, RDCs of the low-populated states can be obtained by performing two CPMG relaxation dispersion experiments, one for each of the two components of the doublet reporting on the RDC. As an example, for measurements of the ^{15}N-^{1}H RDCs, a CPMG relaxation dispersion curve is obtained for both the $2N_{xy}H^{|\alpha>}$ and the $2N_{xy}H^{|\beta>}$ transition of the ^{15}N-^{1}H doublet. Residual chemical shift anisotropies report on the orientation of the anisotropic part of the chemical shift tensor in the molecular frame and are in general obtained as the difference between the chemical shift in an isotropic media and the chemical shift in an anisotropic media. One such example is the C' RCSA, which can be obtained in low-populated states from two C' CPMG relaxation dispersion experiments, one performed in an isotropic media and one performed on a sample in an anisotropic media. The resulting C' RCSAs report on the orientation of the C' CSA tensors of the low-populated state and can be used as restraints in structure calculations.

4 Applications

In the following section we discuss several applications of various relaxation dispersion experiments with the aim to demonstrate the power and scope of relaxation dispersion NMR. Although the examples are structured around a particular biological problem they bring forward the strategy of obtaining structural, kinetic, and thermodynamic parameters of chemically exchanging systems. We will initially discuss applications to protein folding, where either folding into its native state or an aggregation prone state is studied, since many such studies have been used to establish the technique of CPMG relaxation dispersion.

Protein folding: There are numerous of examples with relaxation dispersion experiments in the context of protein folding (Korzhnev, Salvatella, et al., 2004; Meinhold & Wright, 2011; Neudecker, Zarrine-Afsar, Davidson, & Kay, 2007). Among them is the characterisation of the low-populated folding intermediates of mutants of the SH3 domain from the Fyn tyrosine kinase (Korzhnev, Salvatella, et al., 2004)**.** One of the scientific questions was that of the influence of protein-folding

intermediates on protein folding, the folding energy-landscape and thus the stability of protein-folding intermediates. To investigate this question, Korzhnev et al. performed ^{15}N CPMG relaxation dispersion experiments (Tollinger, Skrynnikov, Mulder, Forman-Kay, & Kay, 2001) at different magnetic fields and also at different temperature; some examples are shown for Ser41 and Thr44 of the G48M mutant of FynSH3 in Figure 13a, b. Global fitting of a three state exchange model,

$$\underset{\text{unfolded}}{U} \underset{k_{IU}}{\overset{k_{UI}}{\rightleftharpoons}} \underset{\text{intermediate}}{I} \underset{k_{FI}}{\overset{k_{IF}}{\rightleftharpoons}} \underset{\text{folded}}{F} \tag{43}$$

to the obtained data allowed a determination of the populations and exchange rates shown in Figure 13c, d which, in turn, showed that the population of the folding intermediate increases with temperature, while the population of the unfolded-state is comparatively temperature independent. The derived populations and exchange rates were then used to extract relative thermodynamic parameters for each of the states and mutants (inset Figure 13c). For the Fyn SH3 protein the free energy difference between the folded- and unfolded-state of mutant G48M, $\Delta G_{U-F} = 2.3$ kcal mol^{-1}, is higher than the same free energy difference for mutant G48V, $\Delta G_{U-F} = 1.8$ kcal mol^{-1}, thus G48M is more stable than G48V. Additional to the thermodynamic and kinetic information, low-resolution structural information is available from the obtained ^{15}N chemical shift differences between the different states, and these shifts suggested a more native like intermediate of G48V than of G48M. Subsequently, chemical shifts were used to calculate an ensemble of structures for both mutants (Korzhnev, Salvatella, et al., 2004). By deriving thermodynamic and kinetic parameters, as well as low-solution structures of low-populated states, the study of Fyn SH3 provided in many ways an avenue for the characterisation of low-populated states involved in biochemical reactions, in this case protein folding.

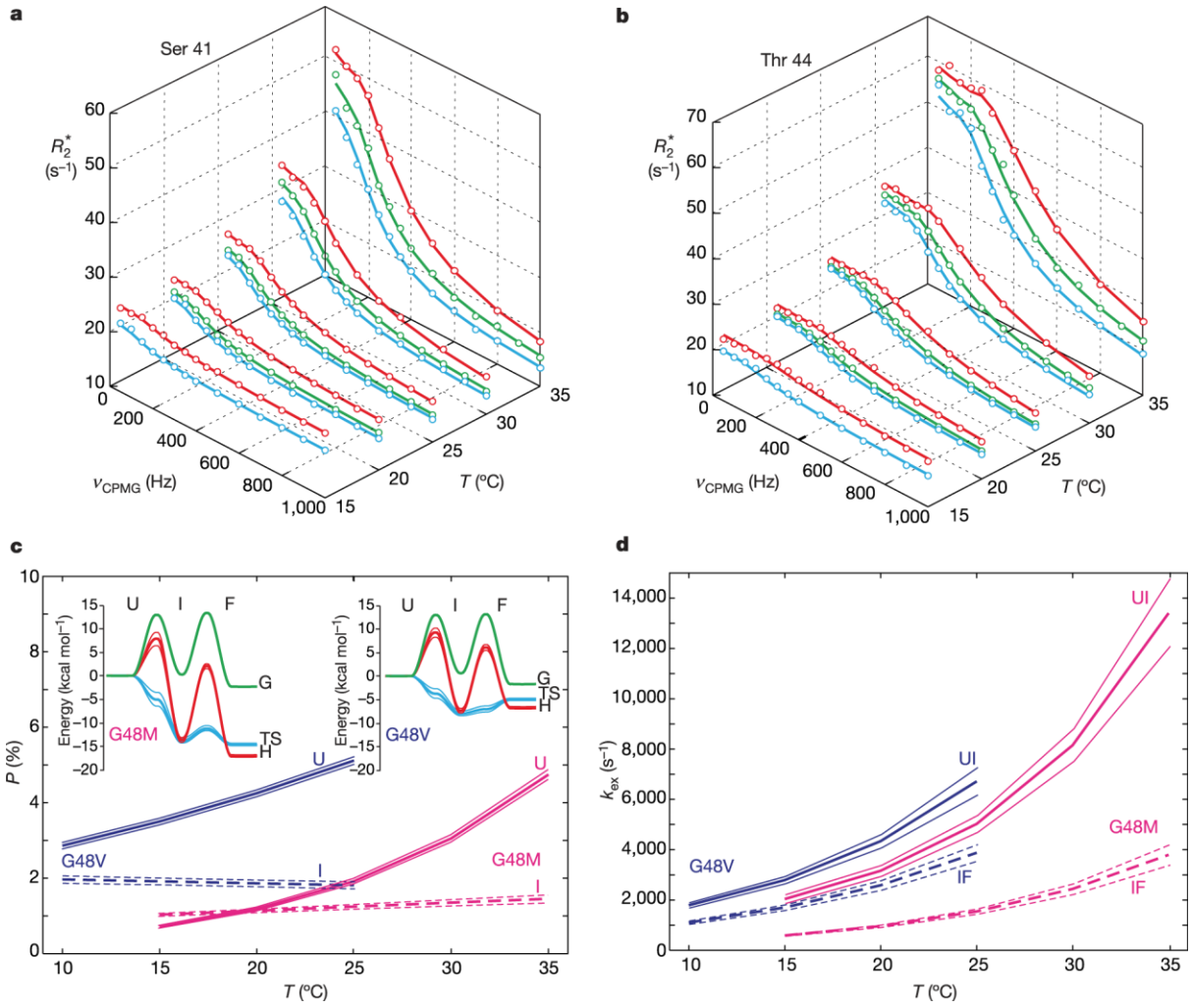

Figure 13: Relaxation dispersion data for G48M and G48V Fyn SH3. Typical relaxation dispersion curves of the G48M mutant are shown for (a) Ser42 and (b) Thr44. Data were acquired at different temperatures and different field strength (blue: 500 MHz, green: 600 MHz, red: 800 MHz) and subsequently fitted to a global three-state folding model, Eq. (43). The temperature dependence of the populations is shown in (c) for G48M and G48V along with energy diagrams for G48M at 25ºC and for G48V at 17.5ºC. For the same mutants temperature dependent exchange rates are shown in (d). Figure reproduced with permission from (Korzhnev, Salvatella, et al., 2004) (Figure 2).

Protein folding and aggregation: Relaxation dispersion experiments cannot only be used to learn how proteins fold into their native structure, but also to derive mechanisms that underlie protein misfolding and aggregation (Farber, Slager, & Mittermaier, 2012; Lim, Dyson, Kelly, & Wright, 2013; Neudecker et al., 2012). Since protein misfolding is a characteristic of several neurodegenerative diseases, such as Alzheimer's disease, it is of fundamental importance to understand its mechanism on a molecular level to allow for the development of more efficient treatments. In that regard, Neudecker et al. chose to determine the structure and aggregation properties of the transient intermediate of the A39V/N53P/V55L Fyn SH3 domain, a protein which is known to fold from an unfolded state (U) via an on-pathway, low populated (~2%) intermediate (I) into a native

β-sandwich fold (N) (Neudecker et al., 2012). However, structural restraints for the transiently populated states are not readily available and calculations of a high-resolution structure of the intermediate with replica exchange molecular dynamics require a sufficient number of experimental restraints. Neudecker et al. obtained those restraints exclusively from relaxation dispersion measurements of suitably isotope labelled samples in isotropic and aligned media. ^{15}N single-quantum CW CPMG (D. F. Hansen, Vallurupalli, & Kay, 2008a), ^{15}N TROSY/AntiTROSY CPMG (Vallurupalli, Hansen, et al., 2007), ^{1}HN SQ CPMG (Ishima & Torchia, 2003), ^{1}HN/^{15}N ZQ/DQ CPMG (Orekhov et al., 2004), ^{13}C' SQ CPMG (Lundström et al., 2008), $^{13}C_{\alpha}$ SQ CPMG (D. F. Hansen, Vallurupalli, Lundström, et al., 2008) and $^{1}H_{\alpha}$ SQ CPMG (Lundström, Hansen, et al., 2009) were combined with previously recorded methyl group ^{13}C SQ CPMG experiments (D. F. Hansen, Neudecker, & Kay, 2010; D. F. Hansen, Neudecker, Vallurupalli, Mulder, & Kay, 2010) to determine ^{15}N, $^{1}H_{N}$,^{13}C', $^{13}C_{\alpha}$ and $^{1}H_{\alpha}$ backbone chemical shifts, ^{15}N-^{1}HN backbone residual dipolar couplings (RDCs) and ^{13}C' residual chemical shift anisotropies (RCSAs) of the intermediate. Chemical shifts of a given nucleus X of the intermediate were calculated using $\varpi_{X,I} = \varpi_{X,N} + \Delta\varpi_{N\rightarrow I}$ where $\varpi_{X,N}$ is the chemical shift of nucleus X in the native state and $\Delta\varpi_{N\rightarrow I} = \varpi_{X,I} - \varpi_{X,N}$ is the chemical shift difference extracted from the respective relaxation dispersion measurements. Similar calculations were employed to calculate the RDCs and the RCSAs of the intermediate. The high resolution structure calculated from those restraints shows that the native five stranded incomplete anti-parallel β barrel fold of the A39V/N53P/V55L Fyn SH3 domain is native like in the intermediate except for the C-terminal β_5 strand which is unfolded. This implies that the interactions of the bulge Pro 57 of strand β5 with strand β1 are absent thus exposing its extremely hydrophobic amino acid sequence making it highly aggregation prone (Neudecker et al., 2012). Since aggregation of the intermediate is limited by its low population (~2%), a structural mimic of the intermediate, A39V/N53P/V55L/Δ57-60 Fyn SH3, was used to investigate the suspected aggregation. This truncated structure aggregates spontaneously under NMR conditions and aggregates were subsequently examined by circular dichroism and electron microscopy. The work of Neudecker et al. suggest that aggregation occurs via a locally unfolded state rather than via global unfolding (Neudecker et al., 2012).

An immediate disease related protein misfolding study was conducted on transthyretin (TTR) whose amyloid formation is linked to several degenerative diseases such as senile systemic amyloidosis, familial amyloid polyneuropathy, and familial amyloid cardiomyopathy (Lim et al., 2013). TTR is a homo-tetrameric protein whose monomers exhibit a β-sandwich structure and it is known that its amyloid formation involves a transition from the tetramer via a folded monomer into an assembly-prone amylogenic intermediate:

$$tetramer \rightleftharpoons folded\ monomer \rightleftharpoons aggregation\ prone\ monomer \rightleftharpoons amyloid \quad (44)$$

The authors chose to work with a monomeric mutant of TTR (F87M/L110M, M-TTR) allowing them to focus on conformational fluctuations between the natively folded TTR and the aggregation-prone monomer. ^{15}N constant-time CPMG experiments were acquired for both wild-type (WT) M-TTR and T119M M-TTR (a mutant that suppresses amyloid formation) at two static magnetic fields. The obtained relaxation rates show that, compared to WT M-TTR, fewer residues exhibit dispersion at a greatly reduced rate in the protective mutant (Figure 14). To reveal the residues and secondary structure elements involved in transient local unfolding, exchange rates for WT M-TTR and T119M M-TTR were mapped onto the crystal structure of M-TTR (Figure 14b and c).

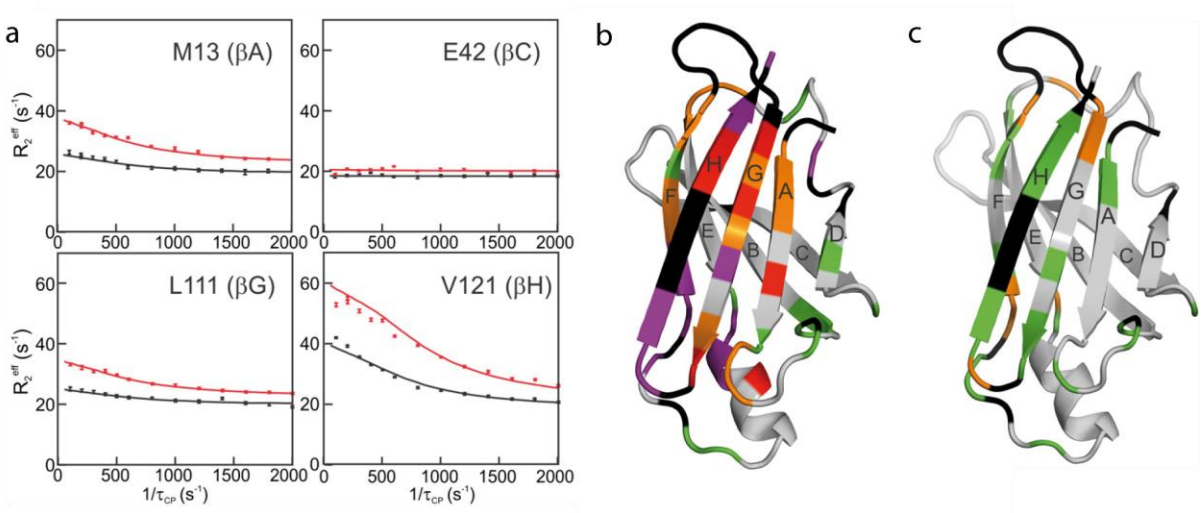

Figure 14 (a) Representative ^{15}N relaxation dispersion curves of M-TTR recorded at 18.8 T (red) and 11.7 T (black). The lines represent global fits with a two-site exchange model including all residues. (b) and (c) Conformational dynamics mapped onto the M-TTR x-ray structure (1GKO), (b) WT M-TTR and (c) T119M M-TTR. The colour scheme is as follows: red: $R_{ex} > 20\text{s}^{-1}$; orange: $10\ \text{s}^{-1} < R_{ex} < 20\text{s}^{-1}$; green: $3\ \text{s}^{-1} < R_{ex} < 10\text{s}^{-1}$; purple: the amide cross peak is not observed in WT M-TTR but in T119M M-TTR; black: prolines or cross peaks that are missing for both WT and T119M M-TTR. Figure reproduced with permission from (Lim et al., 2013) (Figure 2a and Figure 4).

More quantitative measures were obtained by fitting the dispersion data to a global two-site exchange model. In the model, an aggregation prone monomer is presented with populations of 3.5 ± 0.2% for WT M-TTR and 1.0 ± 0.1% for T119M M-TTR, and exchange rates that differ between the WT M-TTR ($k_{ex}^{WT} = 1700 \pm 50\ \text{s}^{-1}$) and T119M M-TTR ($k_{ex}^{T119M} = 2400 \pm 100\ \text{s}^{-1}$). These results support that the amyloidogenic intermediate of T119M M-TTR is less stable and returns to the ground state (folded monomer) faster than WT M-TTR — suppressing the intermediate suppresses amyloid formation.

Protein folding and ligand binding: Many eukaryotic proteins are disordered in their native environment and the mode of action, such as folding and binding, of those intrinsically disordered proteins is poorly understood. One intrinsically disordered protein was investigated by Sugase et al. (Sugase et al., 2007), whose study looked at the binding and folding of the intrinsically disordered phosphorylated kinase inducible activation domain (pKID) from the transcription factor CREB. In order to identify whether pKID folds before binding to the KIX domain of the CREB binding protein or on the surface of KIX (Figure 15a) Sugase et al. employed ^{1}H-^{15}N HSQC titrations and ^{15}N transverse relaxation dispersion experiments (Loria et al., 1999a; Mulder, Mittermaier, Hon, Dahlquist, & Kay, 2001; Tollinger et al., 2001).

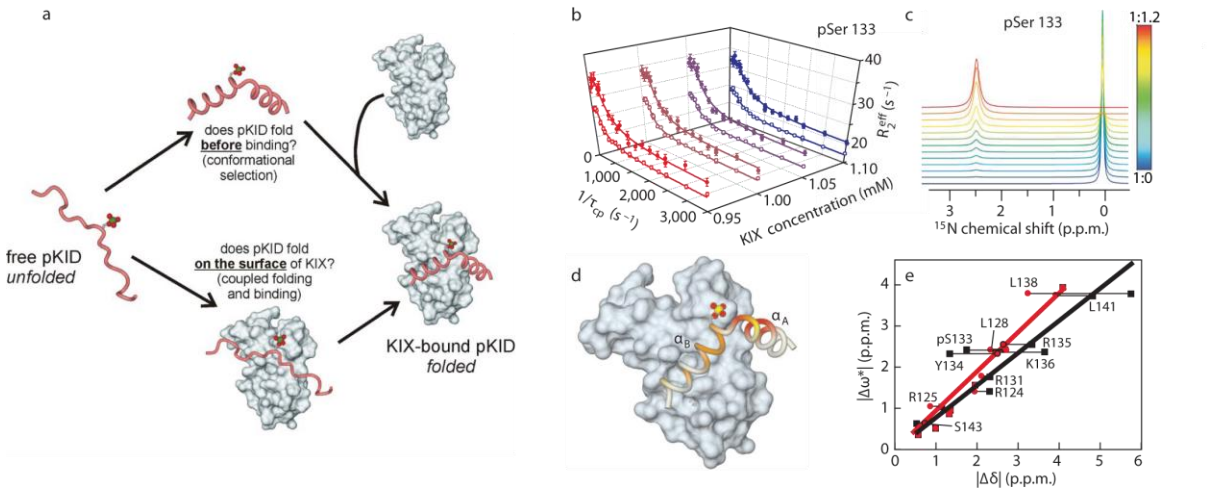

Figure 15: (a) Schematic diagram illustrating the folding before binding vs. folding upon binding question addressed by Sugase et al. (Sugase et al., 2007). (b) ^{15}N transverse relaxation dispersion profiles for the pKID phosphorylated serine (pSer 133). Data were acquired at 11.7 T and 18.8 T (filled and open circles, respectively). The dispersion profiles shown were obtained for 1 mM [^{15}N]-pKID in the presence of 0.95, 1.00, 1.05 and 1.10mM KIX. (c) ^{15}N NMR spectra of pSer 133 simulated at a ^{15}N resonance frequency of 81.1MHz employing the relaxation parameters previously obtained by fitting the dispersion curves to a three-site exchange model. Chemical shifts in the free form are set to zero. The gradient at the right shows the pKID:KIX concentration ratio. (d) The degree of folding in the intermediate is accessed by $\Delta\omega_{FI}/\Delta\omega^{*}$ ratios, which are colour coded onto the structure of the high-affinity complex: $\Delta\omega_{FI}/\Delta\omega^{*} > 0.9$ (red); $0.5 < \Delta\omega_{FI}/\Delta\omega^{*} < 0.9$ (orange); $\Delta\omega_{FI}/\Delta\omega^{*} < 0.5$ (yellow). (e) Correlation of experimental ^{15}N chemical shift differences ($\Delta\omega^{*}$) with equilibrium chemical shift differences ($\Delta\delta$), where $\Delta\delta_{FB}$ is the chemical shift difference between the free pKID and the fully bound state (black) and $\Delta\delta_{EB}$ is the chemical shift difference between the encounter complex and the fully bound state (red). Lines indicate the best fit. Figure reproduced and modified from (Sugase et al., 2007) Figures 3 and S1.

The ^{1}H-^{15}N HSQC titrations of KIX into pKID showed that binding of pKID occurs on two chemical shift timescales: (*i*) a fast exchange process during which pKID forms an ensemble of encounter complexes which are mainly stabilised by non-specific hydrophobic contacts on the surface of KIX and (*ii*) a slow exchange during which pKID binds to the primary high affinity site. To gain further insight into the coupled binding and folding effective relaxation dispersion rates, $R_{2,eff}$, were obtained at different pKID:KIX ratios and two spectrometer frequencies (Figure 15b). The resulting dispersion curves where subsequently fitted to a two- and three-site exchange model, however, the kinetic parameters obtained for the two-site exchange were physically unrealistic resulting in the choice of the three-site model

$$\underset{\text{free (F)}}{pKID + KIX} \quad \underset{k_{IF}}{\overset{k_{FI}}{\rightleftharpoons}} \quad \underset{\text{intermediate (I)}}{pKID : KIX^{*}} \quad \underset{k_{BI}}{\overset{k_{IB}}{\rightleftharpoons}} \quad \underset{\text{bound (B)}}{pKID : KIX} \tag{45}$$

for further analysis. The kinetic and structural parameters obtained by analysis with the three-site exchange model were used to simulate ^{15}N-NMR spectra, which show that although the rate of exchange between the bound and the intermediate state is fast, the overall exchange between the free and the bound state is slow (Figure 15c). The extend of the pKID folding in the intermediate was assessed by comparison of the chemical shift differences between the free and the intermediate state, $\Delta\omega_{FI}$, and the free and the bound state, $\Delta\omega^{*}$, where the bound shift is a population weighted average of the chemical shifts of the intermediate and bound state. Ratios of $\Delta\omega_{FI}/\Delta\omega^{*}$, as they are colour coded in Figure 15d, show that the α_A helix is almost completely formed in the intermediate, while the α_B helix is only partly folded. The NMR titrations mentioned earlier did suggest an additional intermediate, the encounter complex, which occurs before the intermediate forms. Figure 14e) correlates the observed chemical shift with chemical shifts differences between free pKID and the fully bound state ($\Delta\delta_{FB}$) and with chemical shift difference between the encounter complex and the fully bound state ($\Delta\delta_{EB}$). These plots show a significantly higher correlation of $\Delta\omega^{*}$ with $\Delta\delta_{EB}$ suggesting that the transient encounter complex is essential for productive binding and that the high-affinity complex evolves without dissociation from the encounter complex via the intermediate to the fully bound state (Sugase et al., 2007).

Ligand binding and enzyme kinetics: Many catalytic reactions occur on the micro- to milliseconds timescale and it is therefore realistic to assume a connection between enzyme dynamics and catalysis. To explore this link the structural motions of several enzymes, such as, cyclophilin A (Eisenmesser et al., 2005, 2002), and adenylate kinase (Henzler-Wildman et al., 2007; Wolf-Watz et al., 2004) have been studied during catalysis.

Cyclophilin A (CypA) is a member of the highly conserved cyclophylins, a class of enzymes found in many tissues and known to catalyse the cis-trans isomerisation of X-Pro peptide bonds where X is any

amino acid. The conformational exchange of CypA during catalysis was investigated by Eisenmesser et al. using ^{15}N relaxation dispersion in presence and absence of the substrate N-succinyl-Ala-Phe-Pro-Phe-p-nitroanilide (Eisenmesser et al., 2002). In the presence of substrate, CypA exists in a three state equilibrium between a free enzyme (E) and two substrate-bound states, of which one binds the cis-isomer (ES_{cis}) and the other the trans-isomer (ES_{trans}) of the substrate. The three-state model of CypA catalysis can be illustrated as:

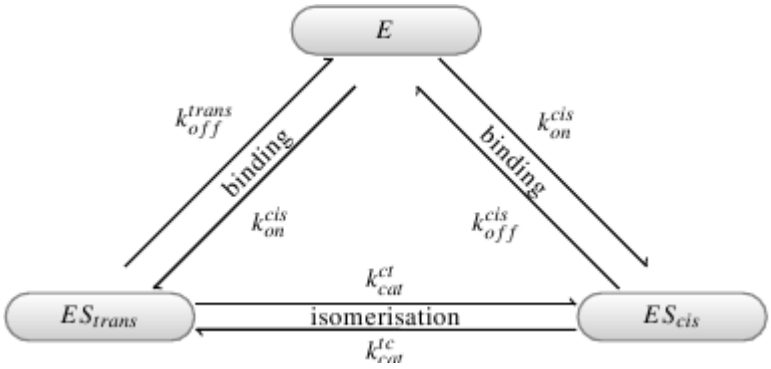

(46)

An increase in effective transverse relaxation rates was observed for 10 out of 160 backbone amides upon the addition of substrate and mapped onto the CypA crystal structure (Figure 16b). To identify whether the observed chemical exchange is based on binding, isomerisation or both, transverse relaxation rates were determined as a function of substrate concentration (Figure 16a). For most residues $R_{2,eff}$ is reported to increase with substrate concentration up to an intermediate concentration before it decreases again, *e.g.* residue K82 shown in Figure 16a. The authors interpret this pattern as binding-driven, assuming significant populations of all three states at intermediate substrate concentrations. The monotonic increase of $R_{2,eff}$ with increasing substrate concentrations as observed for residue R55 (Figure 16a) is ascribed to contributions from the inter-conversion between ES_{cis} and ES_{trans}. To determine how the observed changes correspond to substrate turnover the rate constants had to be determined and compared to previously known rate constants for the substrate isomerisation. If only binding contributes the observed relaxation rates, then relaxation dispersion data can be fitted to a two-state model according to $E \rightleftharpoons ES$ using the closed form analytical expression derived by Luz & Meiboom (Luz & Meiboom, 1963). For residues K82, L98, N102 and A103 this yields values of K_D^{obs} between 0.95 and 1.20 mM and values of k_{off} between 10,700 and 14,800 s^{-1}. In cases were data could not be adequately fitted by a two-state model, $R_{2,eff}$ was simulated for the full three-state model, Eq.(46); a fit to the data of R55 is shown in Figure 16a. The quantitative analysis confirmed the authors' qualitative assessment that the exchange observed for most residues is dominated by binding and only dispersion data for residues involved in isomerisation require a three-state model to achieve satisfactory fits.

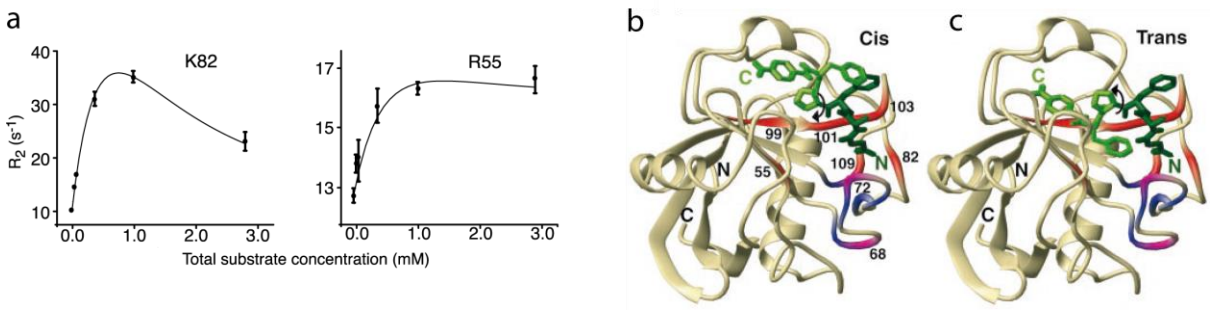

Figure 16: (a) Effective transverse relaxation plotted as a function of substrate concentration for CypA residues K82 and R55. (b) Chemical exchange mapped onto the CypA crystal structure (1RMH) containing the substrate (green) in cis-conformation. Cyp A residues which show exchange in the presence and absence of substrate are colour coded in blue. Those residues colour coded in red exhibit exchange only during substrate turnover and magenta residues show chemical exchange in the absence and presence of the substrate, but exchange increases in its presence. The black arrows in (b) and (c) combined with the substrate conformations in the two subfigures show the proposed isomerisation pathway obtained based on the enzyme dynamics. Figure reproduced with permission from (Eisenmesser et al., 2002) (Figure 3 and 4)

The results obtained by relaxation dispersion confirm the role of R55 in the catalysis and allow the authors to propose a reaction trajectory for the catalysis (Figure 16c). They suggest that during CypA catalyses the part COOH-terminal to the prolyl peptide bond is rotated by 180° to convert the cis-isomer of the substrate into its trans-isomer (Eisenmesser et al., 2002).

In 2002 Eisenmesser et al. (Eisenmesser et al., 2002) identified residues involved in the isomerisation reaction catalysed by Cyp A, however, they were not able to provide a detailed physical picture of the motions during catalysis. This prompted an advanced study, which compared the motions of free and substrate bound CypA (Eisenmesser et al., 2005). For this purpose ^{15}N-TROSY-CPMG measurements of amides (Loria et al., 1999b; Mulder, Mittermaier, et al., 2001) and ^{13}C-CPMG measurements of side-chain methyl groups (Mulder, Mittermaier, et al., 2001) were conducted on samples of free CypA and on N-succinyl-Ala-Phe-Pro-Phe-p-nitroanilide bound CypA. The bound sample was measured under an excess of substrate yielding a 95% saturation of CypA at 10ºC. Under these conditions contributions from substrate binding and dissociation are negligible; thus the measured relaxation dispersion profiles correspond only to the cis-trans isomerisation and can be fitted by a two-state model (Carver-Richards equation for two-site exchange) (Carver & Richards, 1972). Individual fits of dispersion profiles obtained for substrate bound CypA exhibit similar rate constants permitting a global fit with a single rate constant $k_{ex} = k_{cat}^{ct} + k_{cat}^{tc}$ of value 2730 ± 220s^{-1}. Based on previously obtained populations of ES_{cis} and ES_{trans} the authors were able to separate k_{ex} into $k_{cat}^{ct} \approx 1{,}090\ s^{-1}$ and $k_{cat}^{tc} \approx 1{,}640\ s^{-1}$. For free CypA individual fits of relaxation dispersion profiles cluster into two groups and residues within these groups were fitted globally. The exchange

rate for the larger of the two groups takes a value of 1,140 ± 200 s^{-1} and describes the following exchange process:

$$E_{major} \underset{k_{reverse}}{\overset{k_{forward}}{\rightleftharpoons}} E_{minor} \quad , \tag{47}$$

with $k_{forward} \approx 60\ s^{-1}$ and $k_{reverse} \approx 1{,}080\ s^{-1}$. It is striking that the values obtained for $k_{reverse}$ and k_{cat}^{ct} are almost identical. Taken together with very similar chemical shift difference between E_{major} and E_{minor} and between ES_{cis} and ES_{trans} the obtained results suggest that S_{cis} binds to E_{major} and S_{trans} binds to E_{minor}. From this it follows that the motions present during catalysis are present even in the absence of substrate and upon substrate binding the pre-existing equilibrium is shifted towards ES_{trans}. Additional relaxation dispersion measurements were conducted on several mutants of CypA to show that the motions occurring in CypA are of collective nature (Eisenmesser et al., 2005). The early application of relaxation dispersion NMR to CypA allowed the localisation of residues involved in substrate binding and isomerisation (Eisenmesser et al., 2002). However, a more advanced relaxation dispersion study of CypA was able to reveal that the motions that are characteristic for catalysis are already present in the free enzyme and that conformational exchange rates correspond to catalytic turnover rates. This illustrates that motions necessary for catalysis are intrinsic to the enzyme and can limit the overall turnover (Eisenmesser et al., 2005).

In a similar spirit to the investigations of CypA motions during catalysis (Eisenmesser et al., 2005, 2002) Kern and co-workers also looked at the role of protein dynamics during the enzymatic turnover of adenylate kinase (Henzler-Wildman et al., 2007; Wolf-Watz et al., 2004). Adenylate kinases (Adks) are enzymes that maintain the cellular equilibrium concentration of adenylate nucleotides by catalysing the reversible conversion of ATP and AMP into two ADP molecules (Eq. (48)). They possess two substrate lids that close upon substrate binding, which is an essential step for the phosphoryl transfer catalysed.

$$\begin{array}{ccccccc} E + Mg^{2+} * ATP + AMP & & & & & & E + Mg^{2+} * ADP + ADP \\ k_{off} \uparrow \downarrow k_{on} & & & & & & k_{on} \downarrow \uparrow k_{off} \\ E_{AMP}^{Mg^{2+} * ATP} & \underset{k_{open}}{\overset{k_{close}}{\rightleftharpoons}} & E_{AMP}^{Mg^{2+} * ATP} & \underset{k_{p-transfer}}{\overset{k_{p-transfer}}{\rightleftharpoons}} & E_{ADP}^{Mg^{2+} * ADP} & \underset{k_{close}}{\overset{k_{open}}{\rightleftharpoons}} & E_{ADP}^{Mg^{2+} * ADP} \end{array} \tag{48}$$

For their research Wolf-Watz et al. chose to work with two homologues Adks: the mesophilic *Escherichia coli* (mesoAdk) and the hyperthermophile *Aquifex aeolicus* (thermoAdk). A comparison of enzyme activities and protein dynamics at different temperatures shows that below the degradation temperature of mesoAdk (45ºC) thermoAdk exhibits a lower catalytic activity. However, the observed

temperature curves feature a similar shape, shifted by 40ºC, and show maximal activity at each enzyme's optimal temperature. Backbone dynamics during substrate turnover were measured for both enzymes at 20ºC and for thermoAdk at 50ºC; at 20ºC thermoAdk is nine fold less active than mesoAdk while at 50ºC it has comparable activity to mesoAdk at 20ºC. ^{15}N relaxation dispersion measurements were conducted using a relaxation compensated constant-time CPMG experiment with TROSY selection (Loria et al., 1999a; Tollinger et al., 2001) and quantitative results were obtained by fits to a two-site exchange model (Carver & Richards, 1972) representing the lid opening and closing. In the presence of substrate this model is valid only for the saturated state (used here). Relaxation dispersion data reveal that conformational exchange affects sites throughout the protein and is not localised to the active site. A quantitative analysis of the data yields single rate constants of 1660 ± 90 s^{-1} for mesoAdk and 1615 ± 100 s^{-1} for thermoAdk, both measured at 20ºC. Since the catalysis of thermoAdk is much slower at 20ºC the similar exchange rates raised the question for the nature of the rate limiting step in the reaction. This question was addresses by studying the backbone dynamics of thermoAdk at 20ºC in the presence of AMP and the nonconvertible ATP analogue AMPPNP. Results show dynamical and structural parameters, which are equivalent to those obtained for the true substrates, suggesting that the observed relaxation dispersion profiles are dominated by the opening and closing of the lids. The interpretation of the observed chemical exchange as the lid opening and closing was further supported by the coincidence of the lid opening rates with steady state turnover values and the authors identified the lid-opening rate as the rate-limiting step for catalysis. It was therefore suggested that the reduced rate of catalytic activity found for the hyperthermophilic enzyme is solely caused by a slower lid opening rate (Henzler-Wildman et al., 2007; Wolf-Watz et al., 2004).

Low populated structures in nucleic acids: Relaxation dispersion NMR in biological systems is generally associated with conformational exchange in proteins. The early applications of $R_{1\rho}$ measurements to probe the dynamics of ribozymes (Hoogstraten et al., 2000; Latham, Brown, McCallum, & Pardi, 2005) by Pardi and co-workers and CPMG experiments by Boisbouvier et al.(Boisbouvier et al., 1999) opened up a new avenue for relaxation dispersion experiments. The new applications include the introduction of carbon off-resonance $R_{1\rho}$ measurements (A. L. Hansen et al., 2009) for labelled and unlabelled nucleic acids (see history section above) that allowed the observation of transient Hoogsteen base pairs in canonical duplex DNA (Nikolova et al., 2011) as well as the visualisation of transient low-populated RNA structures (Dethoff, Petzold, Chugh, Casiano-Negroni, & Al-Hashimi, 2012).

The DNA double helix can adapt a range of conformations that maintain the Watson-Crick base pairing and these structural variations are widely known to adopt important roles in DNA recognition, topology, and nucleosome positioning. Nikolova et al. investigated the excistence of excited states in canonical duplex DNA (Figure 17a) using unlabelled and uniformly ^{13}C-^{15}N-labelled DNA in carbon

$R_{1\rho}$ relaxation dispersion measurements. Measurements were conducted at a single field (14.1 T), using selective 1D $R_{1\rho}$ experiments at variable effective spin-lock strength, $\omega_{eff} = 100 - 3{,}500$ Hz (A. L. Hansen et al., 2009). The $R_{1\rho}$ relaxation dispersions revealed a chemical exchange at $A \cdot T$ and $G \cdot C$ base pairs in CA/TG steps (Figure 17b) which are, together with TA steps, the most flexible dinucleotides in DNA. The on-resonance relaxation dispersion profiles depicted in Figure 17b show extensive $R_{1\rho}$ realaxation dispersions at base carbon C8 and sugar carbon C1' of adenenine and guanine residues as well as on the C6 carbon of cytosine. In contrast, no dispersions are observed for thymine carbons, the C2 carbon in the adenine base, and the C1' site of the cytosine sugar. The on-resonance relaxation dispersion were supplemented with off-resonance $R_{1\rho}$ realaxation dispersions, shown in Figure 17c, and were analysed by the two-state model described by Eq. (21). Analysis reveals that the chemical exchange for the $T \cdot A$ base pair is faster than that for the $G \cdot C$ base pair and quantifies the populations of $T \cdot A$ and $G \cdot C$ excited-states at 0.47 % and 0.64 %, respectively (for measurements of A_6-DNA at 26ºC). For the same sites, excited-state life times were determined to be ~0.3 ms for the $T \cdot A$ base pair and ~1.5 ms for the $G \cdot C$ base pair. These releaxation dispersion parameters were clomplemented by the observed downfiled-shifted carbon chemical shifts, which are as folows: $\Delta\omega_{AB(C8)} \sim 2.7 - 3.2$ ppm, $\Delta\omega_{AB(C\prime)} \sim 3.1 - 3.7$ ppm and $\Delta\omega_{AB(C6)} \sim 2.2$ ppm.

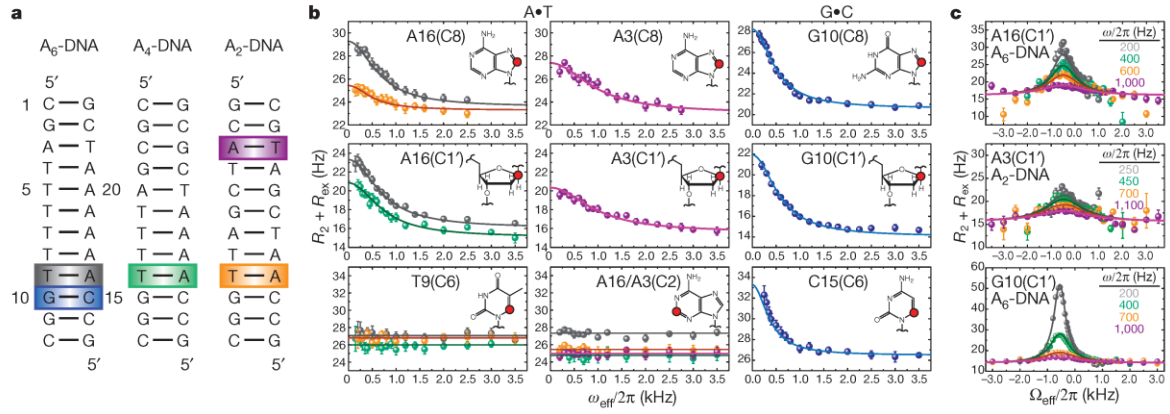

Figure 17: (a) DNA constructs which contain A-tracts of varying length. $A \cdot T$ and $G \cdot C$ at CA/TG steps that show conformational exchange are colour coded. (b) On-resonance ^{13}C $R_{1\rho}$ relaxation dispersion profiles for $A \cdot T$ at 26ºC and for $G \cdot C$ at 30.5ºC. The solid line indicates the best base pair global fit to a two-state asymmetric exchange model. (c) Representative off-resonance relaxation dispersion profiles for C1' sites with solid lines indicating the best global fit. This Figure is reproduced with permission from (Nikolova et al., 2011) (Figure 1).

Having quantified the relaxation parameters the obvious interest of Al-Hashimi and co-workers was to identify the excited-state they observed for CA/TG steps. Previously published results showed that Watson-Crick base pairs can spontaneously break open and access extra-helical conformations. However, the exchange rate observed in their work ($k_{AB} \sim 4 - 20\ s^{-1}$) happened to be within an order of magnitude ($\sim 40 - 400\ s^{-1}$ at 25 ºC) of previously determined rates for base-pair opening with the

excited states populated at least three orders of magnitude higher than previously reported. To shed light on the identity of the excited state Nikolova et al. conducted further carbon $R_{1\rho}$ relaxation dispersion measurements, this time as a function of temperature. These data were subsequently analysed by transition state theory van't Hoff analysis allowing the authors to give a complete thermodynamic and kinetic description of the observed two-state equilibrium. This led to activation free energies and enthalpies, which are comparable to previously reported values for base pair opening, thus implying that the transition to the excited state involves a breakup of the base pair stacking and hydrogen bonding present in a Watson-crick base pair. However, the loss in enthalpy observed in the transition state is remedied once the excited state is formed. In fact, the excited state was shown to be entropically destabilised, which hinted at an excited state that is more rigid than the ground state and therefore unlikely a flexible looped-out state.

Taken all their data and reasoning together, Nikolova et al. summarised that the excited state requires a complete disruption of the Watson-Crick base pairs, while possesing an equivalent thermodynamic stability. From that they inferred that the excited state must be an alternative base pair. Clues on the type of base pair came from the large dispersion observed at purine C8 and C1' and the accompanying downfield chemical shifts, which, when compared to previos studies of carbon chemical shifts and density functional theory (DFT) calculations, suggest an anti-to-syn transition. This transition does result in the creation of a Hoogsteen base-pair, which is optimally stabilised by two-hydrogen bonds (Figure 18). The Hoogsteen base pair even explains the dispersion observed for cytosine C6 as the Hoogsten $C \cdot G$ pair requires the protonation of cystein N3 (Nikolova et al., 2011).

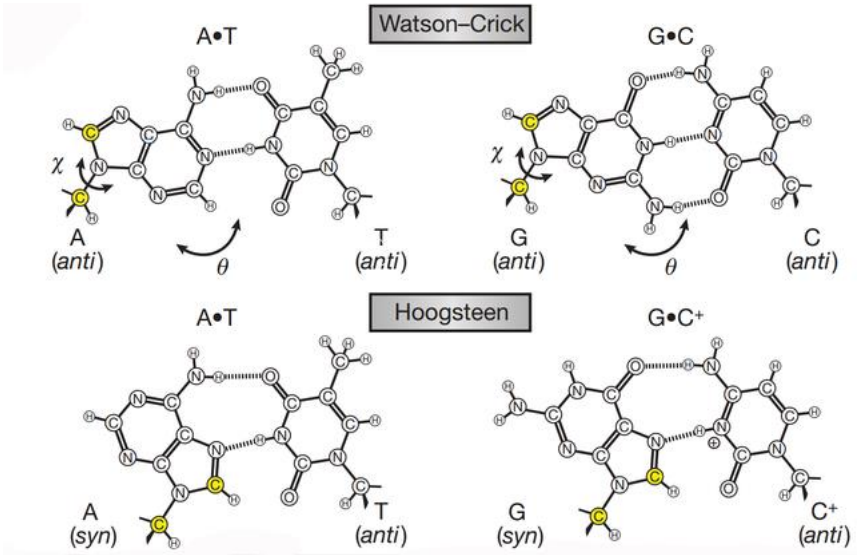

Figure 18 Chemical structures for the Watson-Crick and Hoogsteen $A \cdot T$ and $G \cdot C^+$ base pairs. The geometry of the Hoogsteen base-pairing is achieved by a purine rotation around the glycosidic bond, χ, and by base

flipping around, θ. This action simultaneously affects C8 and C1', which are both highlighted in yellow. This figure has been reproduced with permission from (Nikolova et al., 2011) (Figure 3a).

This beautiful study of conformational exchange revealed that Hoogsteen base pairs, which had previously only been observed in duplex DNA bound to transcription factors and in damaged DNA, do excist as low-populated short-lived states in canonical duplex DNA. An important finding, since it expands the structural complexity of DNA beyond what can be reached by Watson-Crick base-pairing.

Relaxation dispersion NMR in the solid-state: Recently, the measurement of conformational exchange was extended to solid-state NMR (Tollinger, Sivertsen, Meier, Ernst, & Schanda, 2012). In their study Tollinger et al. employ a CPMG relaxation dispersion experiment and measurements of differential multiple quantum coherence decays to demonstrate conformational exchange on microcrystalline ubiquitin. The presented relaxation measurements required long relaxation times and in the solid-state they can only be reached by sample deuteration and fast magic-angle spinning (45-50 kHz). Under those conditions it is often possible to accomplish ^{15}N single quantum lifetimes exceeding 100-200 ms — for the crystalline ubiquitin used here tens of milliseconds were reached. First the authors conducted multiple-quantum exchange experiments to qualitatively access the presence of exchange on the nano- to milliseconds timescale. After exchange was observed for three residues more quantitative results were obtained by relaxation compensated single quantum CPMG (Loria et al., 1999a; Tollinger et al., 2001) and analysed by numerical integration of the Bloch-McConnell equations. Three residues — I23, K27, and T55 — showed large dispersions in the CPMG measurement, which coincides with large ΔR_{MC} and suggests conformational exchange at those sites. All other residues in the protein show flat dispersion profiles and therefore no chemical exchange. Dispersion profiles for I23, K27, and T55 were globally fit to a two-state exchange model revealing that the N-terminal part of the α-helix and the adjacent loop are in exchange with a minor conformation populated at 10%. At 27ºC k_{ex} takes values of about 1400 to 2800 s^{-1}. The presented quantitative results were compared to ubiquitin dynamics in the liquid state and it is striking that the solid-state dynamics are more than one order of magnitude slower. This indicates the significant impact of a crystalline environment on the free energy barrier and the authors demand caution when interpreting soluble proteins in a crystalline preparation (Tollinger et al., 2012).

5 Perspectives

To conclude this review we will shortly summarise the potential of relaxation dispersion NMR to describe biological systems as well as areas, which will need further development before they become routine techniques for biological applications.

Under ideal conditions, relaxation dispersion experiments provide a wide range of chemical shifts of a low-populated state along with chemical exchange parameters, such as, the rate of exchange and the population of the involved states. When such experiments are performed either at different temperatures (Mulder, Mittermaier, et al., 2001) or at different pressure (Korzhnev et al., 2006) the rates and populations derived can be used to derive thermodynamic parameters such at $\Delta H, \Delta S$, and ΔC_p for the chemical exchange under investigation and/or $\Delta H^{\dagger}$ and $\Delta S^{\dagger}$ for the transition state(s) (Korzhnev, Religa, Lundström, Fersht, & Kay, 2007). Recently, it has become possible to calculate the overall average backbone structure of small, rigid proteins solely from chemical shifts using a combination of database approaches (Shen et al., 2009) and advanced computational procedures (Cavalli et al., 2007; Shen et al., 2008). Deriving backbone chemical shifts and vector-orientations of low-populated states from relaxation dispersion experiments now also allow detailed structural models of low-populated states (Korzhnev, Religa, Banachewicz, Fersht, & Kay, 2010; Neudecker et al., 2012; Vallurupalli et al., 2008b) that are transiently populated. Developments in the interpretation of methyl-group chemical shifts in terms of side-chain structure and dynamics (Butterfoss et al., 2010; D. F. Hansen & Kay, 2011; London, Wingad, & Mueller, 2008) have extended the use of CPMG relaxation dispersion to now also probe the hydrophobic core of low-populated states. Thus, we are now in the fortunate situation where kinetic parameters, thermodynamic parameters, and the structure of low-populated states can be assessed, if the population of the state under investigation is larger than ~1% and its' lifetime exceeds ~0.5 ms.

Limited research has been presented using relaxation dispersion to study intrinsically disordered proteins, despite its power to elucidate their coupled folding and binding as discussed above (Sugase et al., 2007). The reason could be highly heterogeneous structural ensembles or that intrinsically disordered proteins sample time-scales that cannot be characterised by the CPMG methods. Relaxation dispersion measurements could potentially, with better sensitivity to a broader time-scale, be used in the future to unravel the molecular mechanisms and diverse biological functions of intrinsically disordered proteins.

On a more methodological outlook where there are still vast improvements possible in the application of relaxation dispersion NMR experiments is in the solid-state. In terms of experimental design such improvements include more efficient coherence transfers by replacing the INEPT transfer with cross-polarisation and optimised proton decoupling and/or levels of protonation to improve sensitivity (Tollinger et al., 2012). The exciting perspectives of probing micro- to millisecond motions in the solid state includes the study of membrane proteins and processes such as allosteric binding, gating, and transport of molecules across membranes.

Bibliography

Allard, P., Helgstrand, M., & Hard, T. (1997). A method for simulation of NOESY, ROESY, and off-resonance ROESY spectra. *Journal of Magnetic Resonance*, *129*(1), 19–29.

Allard, P., Helgstrand, M., & Hard, T. (1998). The complete homogeneous master equation for a heteronuclear two-spin system in the basis of Cartesian product operators. *Journal of Magnetic Resonance*, *134*(1), 7–16.

Allerhand, A., Chen, F., & Gutowsky, H. S. (1965). Spin-Echo NMR Studies of Chemical Exchange. III. Conformational Isomerization of Cyclohexane and d11-Cyclohexane. *The Journal of Chemical Physics*, *42*(9), 3040. doi:10.1063/1.1696376

Allerhand, A., & Gutowsky, H. S. (1964). Spin—Echo NMR Studies of Chemical Exchange. I. Some General Aspects. *The Journal of Chemical Physics*, *41*(7), 2115–2126. doi:10.1063/1.1726215

Allerhand, A., & Gutowsky, H. S. (1965). SpinEcho Studies of Chemical Exchange. II. Closed Formulas for Two Sites. *The Journal of Chemical Physics*, *42*(5), 1587. doi:10.1063/1.1696165

Ando, I., Saito, H., Tabeta, R., Shoji, A., & Ozaki, T. (1984). Conformation-dependent carbon-13 NMR chemical shifts of poly(L-alanine) in the solid state: FPT INDO calculation of N-acetyl-N'-methyl-L-alanine amide as a model compound of poly(L-alanine). *Macromolecules*, *17*(3), 457–461. doi:10.1021/ma00133a036

Auer, R., Neudecker, P., Muhandiram, D. R., Lundström, P., Hansen, D. F., Konrat, R., & Kay, L. E. (2009). Measuring the signs of 1H(alpha) chemical shift differences between ground and excited protein states by off-resonance spin-lock R(1rho) NMR spectroscopy. *Journal of the American Chemical Society*, *131*(31), 10832–3. doi:10.1021/ja904315m

Baldwin, A. J., Hansen, D. F., Vallurupalli, P., & Kay, L. E. (2009). Measurement of methyl axis orientations in invisible, excited states of proteins by relaxation dispersion NMR spectroscopy. *Journal of the American Chemical Society*, *131*(33), 11939–48. doi:10.1021/ja903896p

Baldwin, A. J., Religa, T. L., Hansen, D. F., Bouvignies, G., & Kay, L. E. (2010). 13CHD2 methyl group probes of millisecond time scale exchange in proteins by 1H relaxation dispersion: an application to proteasome gating residue dynamics. *Journal of the American Chemical Society*, *132*(32), 10992–5. doi:10.1021/ja104578n

Bertini, I., Ciurli, S., Dikiy, A., Gasanov, R., Luchinat, C., Martini, G., & Safarov, N. (1999). High-Field NMR Studies of Oxidized Blue Copper Proteins: The Case of Spinach Plastocyanin. *Journal of the American Chemical Society*, *121*(10), 2037–2046. doi:10.1021/ja983833m

Bertini, I., Lucinat, C., & Parigi, G. (2001). *Solution NMR of Paramagnetic MoleculesApplications to metallobiomolecules and models* (pp. 1–372). Elsevier B.V.

Bloch, F., Hansen, W. W., & Packard, M. (1946). Nuclear Induction. *Physical Review*, *69*(3-4), 127–127. doi:10.1103/PhysRev.69.127

Boehr, D. D., Dyson, H. J., & Wright, P. E. (2006). An NMR perspective on enzyme dynamics. *Chemical Reviews*, *106*(8), 3055–79. doi:10.1021/cr050312q

Boehr, D. D., McElheny, D., Dyson, H. J., & Wright, P. E. (2006). The dynamic energy landscape of dihydrofolate reductase catalysis. *Science*, *313*(5793), 1638–42. doi:10.1126/science.1130258

Boisbouvier, J., Brutscher, B., Simorre, J.-P., & Marion, D. (1999). 13C spin relaxation measurements in RNA: sensitivity and resolution improvement using spin-state selective correlation experiments. *Journal of Biomolecular NMR*, *14*(3), 241–252. doi:10.1023/A:1008365712799

Bouvignies, G., Korzhnev, D. M., Neudecker, P., Hansen, D. F., Cordes, M. H. J., & Kay, L. E. (2010). A simple method for measuring signs of (1)H (N) chemical shift differences between ground and excited protein states. *Journal of Biomolecular NMR*, *47*(2), 135–41. doi:10.1007/s10858-010-9418-8

Brown, L. ., & Sanctuary, B. . (1991). Hetero-TOCSY experiments with WALTZ and DIPSI mixing sequences. *Journal of Magnetic Resonance*, *91*(2), 413–421. doi:10.1016/0022-2364(91)90207-A

Butterfoss, G. L., DeRose, E. F., Gabel, S. A., Perera, L., Krahn, J. M., Mueller, G. A., … London, R. E. (2010). Conformational dependence of 13C shielding and coupling constants for methionine methyl groups. *Journal of Biomolecular NMR*, *48*(1), 31–47. doi:10.1007/s10858-010-9436-6

Carr, H. Y., & Purcell, E. M. (1954). Effects of Diffusion on Free Precession in Nuclear Magnetic Resonance Experiments. *Physical Review*, *274*(1953), 630–638. doi:10.1103/PhysRev.94.630

Carver, J. P., & Richards, R. E. (1972). A general two-site solution for the chemial exchange produced dependence of T2 upon the Carr-Purcell pulse separation. *Journal of Magnetic Resonance*, *6*, 89–105.

Cavalli, A., Salvatella, X., Dobson, C. M., & Vendruscolo, M. (2007). Protein structure determination from NMR chemical shifts. *Proceedings of the National Academy of Sciences of the United States of America*, *104*(23), 9615–9620. doi:10.1073/pnas.0610313104

Clore, G. M., Driscoll, P. C., Wingfield, P. T., & Gronenborn, A. M. (1990). Analysis of the backbone dynamics of interleukin-1.beta. using two-dimensional inverse detected heteronuclear nitrogen-15-proton NMR spectroscopy. *Biochemistry*, *29*(32), 7387–7401. doi:10.1021/bi00484a006

Davis, D. G., Perlman, M. E., & London, R. E. (1994). Direct measurement of the dissociation rate constant for inhibitor enzyme complexes via the T1p and T2 (CPMG) methods. *Journal of Magnetic Resonance*, *104*, 266–275.

Dethoff, E. A., Petzold, K., Chugh, J., Casiano-Negroni, A., & Al-Hashimi, H. M. (2012). Visualizing transient low-populated structures of RNA. *Nature*, *491*(7426), 724–8. doi:10.1038/nature11498

Deverell, C., Morgan, R. E., & Strange, J. H. (1970). Studies of chemical exchange by nuclear magnetic relaxation in the rotating frame. *Molecular Physics*, *18*(4), 553–559. doi:10.1080/00268977000100611

Eisenmesser, E. Z., Bosco, D. A., Akke, M., & Kern, D. (2002). Enzyme Dynamics During Catalysis. *Science*, *295*(5559), 1520–1523. doi:10.1126/science.1066176

Eisenmesser, E. Z., Millet, O., Labeikovsky, W., Korzhnev, D. M., Wolf-Watz, M., Bosco, D. A., … Kern, D. (2005). Intrinsic dynamics of an enzyme underlies catalysis. *Nature*, *438*(7064), 117–21. doi:10.1038/nature04105

Evenäs, J., Malmendal, A., & Akke, M. (2001). Dynamics of the transition between open and closed conformations in a calmodulin C-terminal domain mutant. *Structure (London, England : 1993)*, *9*(3), 185–95. Retrieved from http://www.ncbi.nlm.nih.gov/pubmed/11286885

Farber, P. J., Slager, J., & Mittermaier, A. K. (2012). Local Folding and Misfolding in the PBX Homeodomain from a Three-State Analysis of CPMG Relaxation Dispersion NMR Data. *The Journal of Physical Chemistry B*, *116*, 10317–10329. doi:10.1021/jp306127m

Farrow, N. A., Zhang, O., Forman-Kay, J. D., & Kay, L. E. (1994). A heteronuclear correlation experiment for simultaneous determination of 15N longitudinal decay and chemical exchange rates of systems in slow

equilibrium. *Journal of Biomolecular NMR*, *4*(5), 727–34. Retrieved from http://www.ncbi.nlm.nih.gov/pubmed/7919956

Fawzi, N. L., Ying, J., Ghirlando, R., Torchia, D. A., & Clore, G. M. (2011). Atomic-resolution dynamics on the surface of amyloid-β protofibrils probed by solution NMR. *Nature*, *480*(7376), 268–72. doi:10.1038/nature10577

Geen, H., & Freeman, R. (1991). Band-selective radiofrequency pulses. *Journal of Magnetic Resonance*, *93*, 93–141.

Grey, M. J., Wang, C., & Palmer III, A. G. (2003). Disulfide bond isomerization in basic pancreatic trypsin inhibitor: multisite chemical exchange quantified by CPMG relaxation dispersion and chemical shift modeling. *Journal of the American Chemical Society*, *125*(47), 14324–35. doi:10.1021/ja0367389

Hahn, E. (1950). Spin Echoes. *Physical Review*, *80*(4), 580–594. doi:10.1103/PhysRev.80.580

Hansen, A. L., Nikolova, E. N., Casiano-Negroni, A., & Al-Hashimi, H. M. (2009). Extending the range of microsecond-to-millisecond chemical exchange detected in labeled and unlabeled nucleic acids by selective carbon R(1rho) NMR spectroscopy. *Journal of the American Chemical Society*, *131*(11), 3818–9. doi:10.1021/ja8091399

Hansen, D. F., & Kay, L. E. (2007). Improved magnetization alignment schemes for spin-lock relaxation experiments. *Journal of Biomolecular NMR*, *37*, 245–255.

Hansen, D. F., & Kay, L. E. (2011). Determining valine side-chain rotamer conformations in proteins from methyl 13C chemical shifts: application to the 360 kDa half-proteasome. *Journal of the American Chemical Society*, *133*(21), 8272–8281.

Hansen, D. F., & Led, J. J. (2003). Implications of using approximate Bloch–McConnell equations in NMR analyses of chemically exchanging systems: application to the electron self-exchange of plastocyanin. *Journal of Magnetic Resonance*, *163*(2), 215–227. doi:10.1016/S1090-7807(03)00062-4

Hansen, D. F., & Led, J. J. (2006). Determination of the geometric structure of the metal site in a blue copper protein by paramagnetic NMR. *Proceedings of the National Academy of Sciences of the United States of America*, *103*(6), 1738–1743. doi:10.1073/pnas.0507179103

Hansen, D. F., Neudecker, P., & Kay, L. E. (2010). Determination of isoleucine side-chain conformations in ground and excited states of proteins from chemical shifts. *Journal of the American Chemical Society*, *132*(22), 7589–91. doi:10.1021/ja102090z

Hansen, D. F., Neudecker, P., Vallurupalli, P., Mulder, F. A. A., & Kay, L. E. (2010). Determination of Leu side-chain conformations in excited protein states by NMR relaxation dispersion. *Journal of the American Chemical Society*, *132*(1), 42–3. doi:10.1021/ja909294n

Hansen, D. F., Vallurupalli, P., & Kay, L. E. (2008a). An improved 15N relaxation dispersion experiment for the measurement of millisecond time-scale dynamics in proteins. *The Journal of Physical Chemistry B*, *112*(19), 5898–904. doi:10.1021/jp074793o

Hansen, D. F., Vallurupalli, P., & Kay, L. E. (2008b). Quantifying two-bond 1HN-13CO and one-bond 1H(alpha)-13C(alpha) dipolar couplings of invisible protein states by spin-state selective relaxation dispersion NMR spectroscopy. *Journal of the American Chemical Society*, *130*(26), 8397–8405. doi:10.1021/ja801005n

Hansen, D. F., Vallurupalli, P., & Kay, L. E. (2009). Measurement of methyl group motional parameters of invisible, excited protein states by NMR spectroscopy. *Journal of the American Chemical Society*, *131*(35), 12745–12754. doi:10.1021/ja903897e

Hansen, D. F., Vallurupalli, P., Lundström, P., Neudecker, P., & Kay, L. E. (2008). Probing chemical shifts of invisible states of proteins with relaxation dispersion NMR spectroscopy: how well can we do? *Journal of the American Chemical Society*, *130*(8), 2667–75. doi:10.1021/ja078337p

Hansen, D. F., Westler, W., Kunze, M., Markley, J., Weinhold, F., & Led, J. J. (2012). Accurate structure and dynamics of the metal-site of paramagnetic metalloproteins from NMR parameters using natural bond orbitals. *Journal of the American Chemical Society*, *134*(10), 4670–82. Retrieved from http://discovery.ucl.ac.uk/1342864/

Hass, M. A., Hansen, D. F., Christensen, H. E., Led, J. J., & Kay, L. E. (2008). Characterization of conformational exchange of a histidine side chain: protonation, rotamerization, and tautomerization of His61 in plastocyanin from Anabaena variabilis. *Journal of the American Chemical Society*, *130*(26), 8460–8470. doi:10.1021/ja801330h

Henzler-Wildman, K. A., & Kern, D. (2007). Dynamic personalities of proteins. *Nature*, *450*(7172), 964–72. doi:10.1038/nature06522

Henzler-Wildman, K. A., Thai, V., Lei, M., Ott, M., Wolf-Watz, M., Fenn, T., … Kern, D. (2007). Intrinsic motions along an enzymatic reaction trajectory. *Nature*, *450*(7171), 838–44. doi:10.1038/nature06410

Hill, R. B., Bracken, C., DeGrado, W. F., & Palmer III, A. G. (2000). Molecular Motions and Protein Folding: Characterization of the Backbone Dynamics and Folding Equilibrium of α 2 D Using 13 C NMR Spin Relaxation. *Journal of the American Chemical Society*, *122*(47), 11610–11619. doi:10.1021/ja001129b

Hoogstraten, C. G., Wank, J. R., & Pardi, A. (2000). Active Site Dynamics in the Lead-Dependent Ribozyme †. *Biochemistry*, *39*(32), 9951–9958. doi:10.1021/bi0007627

Igumenova, T. I., Brath, U., Akke, M., & Palmer III, A. G. (2007). Characterization of chemical exchange using residual dipolar coupling. *Journal of the American Chemical Society*, *129*(44), 13396–7. doi:10.1021/ja0761636

Ishima, R., Baber, J., Louis, J. M., & Torchia, D. A. (2004). Carbonyl carbon transverse relaxation dispersion measurements and ms-micros timescale motion in a protein hydrogen bond network. *Journal of Biomolecular NMR*, *29*(2), 187–98. doi:10.1023/B:JNMR.0000019249.50306.5d

Ishima, R., & Torchia, D. A. (2003). Extending the range of amide proton relaxation dispersion experiments in proteins using a constant-time relaxation-compensated CPMG approach. *Journal of Biomolecular NMR*, *25*(3), 243–8.

Kay, L. E., Bull, T. ., Nicholson, L. ., Griesinger, C., Schwalbe, H., Bax, A., & Torchia, D. . (1992). The measurement of heteronuclear transverse relaxation times in ax3 spin systems via polarization-transfer techniques. *Journal of Magnetic Resonance*, *100*(3), 538–558. doi:10.1016/0022-2364(92)90058-F

Kay, L. E., Torchia, D. A., & Bax, A. (1989). Backbone dynamics of proteins as studied by nitrogen-15 inverse detected heteronuclear NMR spectroscopy: application to staphylococcal nuclease. *Biochemistry*, *28*(23), 8972–8979. doi:10.1021/bi00449a003

Koerdel, J., Skelton, N. J., Akke, M., Palmer III, A. G., & Chazin, W. J. (1992). Backbone dynamics of calcium-loaded calbindin D9k studied by two-dimensional proton-detected nitrogen-15 NMR spectroscopy. *Biochemistry*, *31*(20), 4856–4866. doi:10.1021/bi00135a017

Kontaxis, G., & Bax, A. (2001). Multiplet component separation for measurement of methyl 13C-1H dipolar couplings in weakly aligned proteins. *Journal of Biomolecular NMR*, *20*(1), 77–82.

Korzhnev, D. M., Bezsonova, I., Evanics, F., Taulier, N., Zhou, Z., Bai, Y., … Kay, L. E. (2006). Probing the transition state ensemble of a protein folding reaction by pressure-dependent NMR relaxation dispersion. *Journal of the American Chemical Society*, *128*(15), 5262–9. doi:10.1021/ja0601540

Korzhnev, D. M., Kloiber, K., & Kay, L. E. (2004). Multiple-quantum relaxation dispersion NMR spectroscopy probing millisecond time-scale dynamics in proteins: theory and application. *Journal of the American Chemical Society*, *126*(23), 7320–9. doi:10.1021/ja049968b

Korzhnev, D. M., Neudecker, P., Mittermaier, A., Orekhov, V. Y., & Kay, L. E. (2005). Multiple-site exchange in proteins studied with a suite of six NMR relaxation dispersion experiments: an application to the folding of a Fyn SH3 domain mutant. *Journal of the American Chemical Society*, *127*(44), 15602–15611. doi:10.1021/ja054550e

Korzhnev, D. M., Orekhov, V. Y., & Kay, L. E. (2005). Off-resonance R(1rho) NMR studies of exchange dynamics in proteins with low spin-lock fields: an application to a Fyn SH3 domain. *Journal of the American Chemical Society*, *127*(2), 713–21. doi:10.1021/ja0446855

Korzhnev, D. M., Religa, T. L., Banachewicz, W., Fersht, A. R., & Kay, L. E. (2010). A transient and low-populated protein-folding intermediate at atomic resolution. *Science*, *329*(5997), 1312–6. doi:10.1126/science.1191723

Korzhnev, D. M., Religa, T. L., Lundström, P., Fersht, A. R., & Kay, L. E. (2007). The Folding Pathway of an FF domain: Characterization of an On-pathway Intermediate State Under Folding Conditions by 15N, 13Cα and 13C-methyl Relaxation Dispersion and 1H/2H-exchange NMR Spectroscopy. *Journal of Molecular Biology*, *372*(2), 497–512. doi:10.1016/j.jmb.2007.06.012

Korzhnev, D. M., Salvatella, X., Vendruscolo, M., Di Nardo, A. A., Davidson, A. R., Dobson, C. M., & Kay, L. E. (2004). Low-populated folding intermediates of Fyn SH3 characterized by relaxation dispersion NMR. *Nature*, *430*(6999), 586–90. doi:10.1038/nature02655

Kristensen, S. M., Siegal, G., Sankar, A., & Driscoll, P. C. (2000). Backbone dynamics of the C-terminal SH2 domain of the p85alpha subunit of phosphoinositide 3-kinase: effect of phosphotyrosine-peptide binding and characterization of slow conformational exchange processes. *Journal of Molecular Biology*, *299*(3), 771–788.

Kupce, E., & Freeman, R. (1995). Adiabatic pulses for wideband inversion and broadband decoupling. *Journal of Magnetic Resonance*, *115*, 273–276.

Latham, M. P., Brown, D. J., McCallum, S. A., & Pardi, A. (2005). NMR methods for studying the structure and dynamics of RNA. *Chembiochem : A European Journal of Chemical Biology*, *6*(9), 1492–505. doi:10.1002/cbic.200500123

Le, H., & Oldfield, E. (1994). Correlation between 15N NMR chemical shifts in proteins and secondary structure. *Journal of Biomolecular NMR*, *4*(3), 341–348.

Lim, K. H., Dyson, H. J., Kelly, J. W., & Wright, P. E. (2013). Localized Structural Fluctuations Promote Amyloidogenic Conformations in Transthyretin. *Journal of Molecular Biology*, *425*(6), 977–988. doi:10.1016/j.jmb.2013.01.008

London, R. E., Wingad, B. D., & Mueller, G. A. (2008). Dependence of amino acid side chain 13C shifts on dihedral angle: application to conformational analysis. *Journal of the American Chemical Society*, *130*(33), 11097–105. doi:10.1021/ja802729t

Loria, J. P., Rance, M., & Palmer III, A. G. (1999a). A Relaxation-Compensated Carr−Purcell−Meiboom−Gill Sequence for Characterizing Chemical Exchange by NMR Spectroscopy. *Journal of the American Chemical Society*, *121*(10), 2331–2332. doi:10.1021/ja983961a

Loria, J. P., Rance, M., & Palmer III, A. G. (1999b). A TROSY CPMG sequence for characterizing chemical exchange in large proteins. *Journal of Biomolecular NMR*, *15*(2), 151–5.

Lundström, P., & Akke, M. (2005). Off-resonance rotating-frame amide proton spin relaxation experiments measuring microsecond chemical exchange in proteins. *Journal of Biomolecular NMR*, *32*(2), 163–73. doi:10.1007/s10858-005-5027-3

Lundström, P., Hansen, D. F., & Kay, L. E. (2008). Measurement of carbonyl chemical shifts of excited protein states by relaxation dispersion NMR spectroscopy: comparison between uniformly and selectively (13)C labeled samples. *Journal of Biomolecular NMR*, *42*(1), 35–47. doi:10.1007/s10858-008-9260-4

Lundström, P., Hansen, D. F., Vallurupalli, P., & Kay, L. E. (2009). Accurate measurement of alpha proton chemical shifts of excited protein states by relaxation dispersion NMR spectroscopy. *Journal of the American Chemical Society*, *131*(5), 1915–26. doi:10.1021/ja807796a

Lundström, P., Teilum, K., Carstensen, T., Bezsonova, I., Wiesner, S., Hansen, D. F., … Kay, L. E. (2007). Fractional 13C enrichment of isolated carbons using [1-13C]- or [2- 13C]-glucose facilitates the accurate measurement of dynamics at backbone Calpha and side-chain methyl positions in proteins. *Journal of Biomolecular NMR*, *38*(3), 199–212. doi:10.1007/s10858-007-9158-6

Lundström, P., Vallurupalli, P., Hansen, D. F., & Kay, L. E. (2009). Isotope labeling methods for studies of excited protein states by relaxation dispersion NMR spectroscopy. *Nature Protocols*, *4*(11), 1641–8. doi:10.1038/nprot.2009.118

Lundström, P., Vallurupalli, P., Religa, T. L., Dahlquist, F. W., & Kay, L. E. (2007). A single-quantum methyl C-13-relaxation dispersion experiment with improved sensitivity. *Journal of Biomolecular NMR*, *38*(1), 79–88. doi:10.1007/s10858-007-9149-7

Luz, Z., & Meiboom, S. (1963). Trimethylammonium Ion in Aqueous Solution — Order of the Reaction with Respect to Solvent. *The Journal of Chemical Physics*, *39*(2), 366–370. doi:10.1063/1.1734254

Massi, F., Grey, M. J., & Palmer III, A. G. (2005). Microsecond timescale backbone conformational dynamics in ubiquitin studied with NMR R-1p relaxation experiments. *Protein Science*, *14*(3), 735–742.

McConnell, H. M. (1958). Reaction Rates by Nuclear Magnetic Resonance. *The Journal of Chemical Physics*, *28*(3), 430. doi:10.1063/1.1744152

Meiboom, S., & Gill, D. (1958). Modified Spin-Echo Method for Measuring Nuclear Relaxation Times. *Review of Scientific Instruments*, *29*(8), 688. doi:10.1063/1.1716296

Meinhold, D. W., & Wright, P. E. (2011). Measurement of protein unfolding/refolding kinetics and structural characterization of hidden intermediates by NMR relaxation dispersion. *Proceedings of the National Academy of Sciences of the United States of America*, *108*(22), 9078–83. doi:10.1073/pnas.1105682108

Morrison, E. A., DeKoster, G. T., Dutta, S., Vafabakhsh, R., Clarkson, M. W., Bahl, A., … Henzler-Wildman, K. A. (2012). Antiparallel EmrE exports drugs by exchanging between asymmetric structures. *Nature*, *481*(7379), 45–50. doi:10.1038/nature10703

Mulder, F. A. A., Mittermaier, A., Hon, B., Dahlquist, F. W., & Kay, L. E. (2001). Studying excited states of proteins by NMR spectroscopy. *Nature Structural Biology*, *8*(11), 932–5. doi:10.1038/nsb1101-932

Mulder, F. A. A., Skrynnikov, N. R., Hon, B., Dahlquist, F. W., & Kay, L. E. (2001). Measurement of slow (micros-ms) time scale dynamics in protein side chains by (15)N relaxation dispersion NMR spectroscopy: application to Asn and Gln residues in a cavity mutant of T4 lysozyme. *Journal of the American Chemical Society*, *123*(5), 967–75.

Mulder, F. A. A., Spronk, C. A., Slijper, M., Kaptein, R., & Boelens, R. (1996). Improved HSQC experiments for the observation of exchange broadened signals. *Journal of Biomolecular NMR*, *8*(2), 223–8. doi:10.1007/BF00211169

Neal, S., Nip, A. M., Zhang, H., & Wishart, D. S. (2003). Rapid and accurate calculation of protein 1H, 13C and 15N chemical shifts. *Journal of Biomolecular NMR*, *26*(3), 215–240.

Neudecker, P., Robustelli, P., Cavalli, A., Walsh, P., Lundström, P., Zarrine-Afsar, A., … Kay, L. E. (2012). Structure of an intermediate state in protein folding and aggregation. *Science*, *336*(6079), 362–6. doi:10.1126/science.1214203

Neudecker, P., Zarrine-Afsar, A., Davidson, A. R., & Kay, L. E. (2007). Phi-value analysis of a three-state protein folding pathway by NMR relaxation dispersion spectroscopy. *Proceedings of the National Academy of Sciences of the United States of America*, *104*(40), 15717–22. doi:10.1073/pnas.0705097104

Nikolova, E. N., Kim, E., Wise, A. A., O'Brien, P. J., Andricioaei, I., & Al-Hashimi, H. M. (2011). Transient Hoogsteen base pairs in canonical duplex DNA. *Nature*, *470*(7335), 498–502. doi:10.1038/nature09775

Orekhov, V. Y., Korzhnev, D. M., & Kay, L. E. (2004). Double- and zero-quantum NMR relaxation dispersion experiments sampling millisecond time scale dynamics in proteins. *Journal of the American Chemical Society*, *126*(6), 1886–91. doi:10.1021/ja038620y

Orekhov, V. Y., Pervushin, K. V., & Arseniev, A. S. (1994). Backbone dynamics of (1-71)bacterioopsin studied by two-dimensional 1H-15N NMR spectroscopy. *European Journal of Biochemistry*, *219*(3), 887–896. doi:10.1111/j.1432-1033.1994.tb18570.x

Ottiger, M., Delaglio, F., & Bax, A. (1998). Measurement of J and dipolar couplings from simplified two-dimensional NMR spectra. *Journal of Magnetic Resonance (San Diego, Calif. : 1997)*, *131*(2), 373–8. doi:10.1006/jmre.1998.1361

Palmer III, A. G., & Massi, F. (2006). Characterization of the dynamics of biomacromolecules using rotating-frame spin relaxation NMR spectroscopy. *Chemical Reviews*, *106*(5), 1700–19. doi:10.1021/cr0404287

Pervushin, K. V., Riek, R., Wider, G., & Wüthrich, K. (1997). Attenuated T2 relaxation by mutual cancellation of dipole-dipole coupling and chemical shift anisotropy indicates an avenue to NMR structures of very large biological macromolecules in solution. *Proceedings of the National Academy of Sciences of the United States of America*, *94*(23), 12366–71.

Purcell, E. M., Torrey, H. C., & Pound, R. V. (1946). Resonance Absorption by Nuclear Magnetic Moments in a Solid. *Physical Review*, *69*(1-2), 37–38. doi:10.1103/PhysRev.69.37

Shen, Y., & Bax, A. (2007). Protein backbone chemical shifts predicted from searching a database for torsion angle and sequence homology. *Journal of Biomolecular NMR*, *38*(4), 289–302. doi:10.1007/s10858-007-9166-6

Shen, Y., Delaglio, F., Cornilescu, G., & Bax, A. (2009). TALOS+: a hybrid method for predicting protein backbone torsion angles from NMR chemical shifts. *Journal of Biomolecular NMR*, *44*(4), 213–223. doi:10.1007/s10858-009-9333-z

Shen, Y., Lange, O., Delaglio, F., Rossi, P., Aramini, J. M., Liu, G., … Bax, A. (2008). Consistent blind protein structure generation from NMR chemical shift data. *Proceedings of the National Academy of Sciences of the United States of America*, *105*(12), 4685–4690. doi:10.1073/pnas.0800256105

Skrynnikov, N. R., Dahlquist, F. W., & Kay, L. E. (2002). Reconstructing NMR spectra of "invisible" excited protein states using HSQC and HMQC experiments. *Journal of the American Chemical Society*, *124*(41), 12352–12360.

Skrynnikov, N. R., Mulder, F. A. A., Hon, B., Dahlquist, F. W., & Kay, L. E. (2001). Probing slow time scale dynamics at methyl-containing side chains in proteins by relaxation dispersion NMR measurements: application to methionine residues in a cavity mutant of T4 lysozyme. *Journal of the American Chemical Society*, *123*(19), 4556–66.

Sorensen, O. W., Eich, G. W., Levitt, M. H., Bodenhausen, G., & Ernst, R. R. (1983). Product operator formalism for the description of NMR pulse experiments. *Progress in NMR Spectroscopy*, *16*, 163–192.

Spera, S., & Bax, A. (1991). Empirical correlation between protein backbone conformation and C.alpha. and C.beta. 13C nuclear magnetic resonance chemical shifts. *Journal of the American Chemical Society*, *113*(14), 5490–5492. doi:10.1021/ja00014a071

Sprangers, R., & Kay, L. E. (2007). Quantitative dynamics and binding studies of the 20S proteasome by NMR. *Nature*, *445*(7128), 618–622. doi:10.1038/nature05512

Stone, M. J., Chandrasekhar, K., Holmgren, A., Wright, P. E., & Dyson, H. J. (1993). Comparison of backbone and tryptophan side-chain dynamics of reduced and oxidized Escherichia coli thioredoxin using nitrogen-15 NMR relaxation measurements. *Biochemistry*, *32*(2), 426–435. doi:10.1021/bi00053a007

Sugase, K., Dyson, H. J., & Wright, P. E. (2007). Mechanism of coupled folding and binding of an intrinsically disordered protein. *Nature*, *447*(7147), 1021–5. doi:10.1038/nature05858

Szyperski, T., Luginbühl, P., Otting, G., Güntert, P., & Wüthrich, K. (1993). Protein dynamics studied by rotating frame 15N spin relaxation times. *Journal of Biomolecular NMR*, *3*(2). doi:10.1007/BF00178259

Tollinger, M., Sivertsen, A. C., Meier, B. H., Ernst, M., & Schanda, P. (2012). Site-resolved measurement of microsecond-to-millisecond conformational-exchange processes in proteins by solid-state NMR spectroscopy. *Journal of the American Chemical Society*, *134*(36), 14800–7. doi:10.1021/ja303591y

Tollinger, M., Skrynnikov, N. R., Mulder, F. A. A., Forman-Kay, J. D., & Kay, L. E. (2001). Slow dynamics in folded and unfolded states of an SH3 domain. *Journal of the American Chemical Society*, *123*(46), 11341–52.

Tzeng, S.-R., & Kalodimos, C. G. (2009). Dynamic activation of an allosteric regulatory protein. *Nature*, *462*(7271), 368–72. doi:10.1038/nature08560

Vallurupalli, P., Bouvignies, G., & Kay, L. E. (2012). Studying "invisible" excited protein states in slow exchange with a major state conformation. *Journal of the American Chemical Society*, *134*(19), 8148–61. doi:10.1021/ja3001419

Vallurupalli, P., Hansen, D. F., & Kay, L. E. (2008a). Probing structure in invisible protein states with anisotropic NMR chemical shifts. *Journal of the American Chemical Society*, *130*(9), 2734–5. doi:10.1021/ja710817g

Vallurupalli, P., Hansen, D. F., & Kay, L. E. (2008b). Structures of invisible, excited protein states by relaxation dispersion NMR spectroscopy. *Proceedings of the National Academy of Sciences of the United States of America*, *105*(33), 11766–71. doi:10.1073/pnas.0804221105

Vallurupalli, P., Hansen, D. F., Lundström, P., & Kay, L. E. (2009). CPMG relaxation dispersion NMR experiments measuring glycine 1H alpha and 13C alpha chemical shifts in the "invisible" excited states of proteins. *Journal of Biomolecular NMR*, *45*(1-2), 45–55. doi:10.1007/s10858-009-9310-6

Vallurupalli, P., Hansen, D. F., Stollar, E., Meirovitch, E., & Kay, L. E. (2007). Measurement of bond vector orientations in invisible excited states of proteins. *Proceedings of the National Academy of Sciences of the United States of America*, *104*(47), 18473–7. doi:10.1073/pnas.0708296104

Vallurupalli, P., & Kay, L. E. (2006). Complementarity of ensemble and single-molecule measures of protein motion: a relaxation dispersion NMR study of an enzyme complex. *Proceedings of the National Academy of Sciences of the United States of America*, *103*(32), 11910–11915. doi:10.1073/pnas.0602310103

Vallurupalli, P., Scott, L., Williamson, J. R., & Kay, L. E. (2007). Strong coupling effects during X-pulse CPMG experiments recorded on heteronuclear ABX spin systems: artifacts and a simple solution. *Journal of Biomolecular NMR*, *38*(1), 41–6. doi:10.1007/s10858-006-9139-1

Wang, C., Grey, M. J., & Palmer III, A. G. (2001). CPMG sequences with enhanced sensitivity to chemical exchange. *Journal of Biomolecular NMR*, *21*(4), 361–6. Retrieved from http://www.ncbi.nlm.nih.gov/pubmed/11824755

Ward, K. M., Aletras, A. H., & Balaban, R. S. (2000). A new class of contrast agents for MRI based on proton chemical exchange dependent saturation transfer (CEST). *Journal of Magnetic Resonance*, *143*(1), 79–87. doi:10.1006/jmre.1999.1956

Wells, E. J., & Gutowsky, H. S. (1965). NMR Spin-Echo Trains for a Coupled Two-Spin System. *The Journal of Chemical Physics*, *43*(9), 3414. doi:10.1063/1.1726421

Wishart, D. S., & Case, D. A. (2001). Use of chemical shifts in macromolecular structure determination. *Methods in Enzymology*, *338*, 3–34.

Wishart, D. S., & Sykes, B. D. (1994). The 13C chemical-shift index: a simple method for the identification of protein secondary structure using 13C chemical-shift data. *Journal of Biomolecular Nmr*, *4*, 171–180.

Wolf-Watz, M., Thai, V., Henzler-Wildman, K. A., Hadjipavlou, G., Eisenmesser, E. Z., & Kern, D. (2004). Linkage between dynamics and catalysis in a thermophilic-mesophilic enzyme pair. *Nature Structural & Molecular Biology*, *11*(10), 945–9. doi:10.1038/nsmb821

Xu, X.-P., & Case, D. A. (2002). Probing multiple effects on 15N, 13C alpha, 13C beta, and 13C' chemical shifts in peptides using density functional theory. *Biopolymers*, *65*(6), 408–23. doi:10.1002/bip.10276

Zuiderweg, E. R. . (1990). Analysis of multiple-pulse-based heteronuclear J cross polarization in liquids. *Journal of Magnetic Resonance*, *89*(3), 533–542. doi:10.1016/0022-2364(90)90336-8